** Not Completed*

10 RADAR AND TROPICAL CYCLONES

10.1 Introduction

When a tropical cyclone was first "seen" by radar in 1944, it was immediately recognized that a powerful new tool for the detection and tracking of these storms had been found. Today, radar is considered to be an indispensable tool for any tropical cyclone warning service and many specially designed sets are now in use around the world for this purpose. Although there are books on radar and radar meteorology, the aspects of the subject particular to tropical cyclones are given only cursory treatment and it is my experience that many meteorologists and others are uncertain of the value and limitations of radar for detecting and tracking these storms. The correct interpretation of radar presentations of tropical cyclones is of paramount importance in the preparation of wind, surge and flood warnings to individual communities. Accordingly, I have thought it desirable to give the subject a more detailed treatment than one might expect to find in a primarily meteorological text.

In some ways it can be said that the idea of detecting objects with radio waves is as old as their discovery, for when Heinrich Hertz first clearly generated these waves in 1884 (following their prediction, from theoretical considerations, by James Clerk Maxwell in 1862) he showed that they could also be reflected and refracted by certain objects, as Maxwell had predicted. Subsequently, methods were devised to use this reflecting or "echo-sounding" property to detect objects and to measure their distance from the transmitter. These methods were at first known by such names as "radio location" and "radio detection" but in 1942 the U.S. Navy coined the immediately popular acronym "radar" from the term "Radio Direction and Ranging".

It is very seldom that a committee produces anything original but it is a remarkable fact that radar in the form most commonly used by meteorologists today derives from a committee set up in England in 1934 for the Scientific Survey of Air Defence. Sir Robert Watson-Watt was a pioneer in this field which followed on from his work in the British Meteorological Office (and from 1921 in the Department of Scientific and Industrial Research) on the radio location of thunderstorms. The principle of this form of radar is that powerful pulses of radio waves of short duration, are transmitted and on encountering a scattering or reflecting object some small fraction of the energy in each pulse will be returned by the object or "target"as an "echo" which, if strong enough, can be detected by sensitive receivers. The direction of arrival of the returned pulse gives the direction to the target and its distance away can be determined from the time it takes the pulse to travel to the object

and thence to the receiver in straight lines at the speed of light which is assumed to be constant. The currently accepted value of the speed of light in a vacuum is 299 792 458 m/s with an uncertainty of $\pm$ 1.2 m/s but for most practical meteorological purposes a velocity of 3×10^8 m/s is assumed.

By using large parabolic aerials and radio waves with a wavelength of less than 1 m, known as microwaves, it is possible to produce a highly directional radio beam with which it is possible to scan, as with a searchlight, until a "return" or "echo" is obtained from some target. The returned pulse is usually received by the same aerial as is used for transmission, an automatic switch closing off the receiver during the short time interval used for transmitting. The angle of "elevation" above the horizontal of the beam and its "azimuth" or bearing from north, indicate the direction of the target. This information and the distance to the target can be displayed on a variety of direct reading indicators but for our purposes we need to consider only two.

The movable aerial is most frequently oriented so that its beam is approximately horizontal and is rotated about a vertical axis. During the rotation frequent pulses of radio energy are transmitted. Any echoes that are received can be located in azimuth and distance on a plan position indicator (PPI). This is a cathode-ray tube, similar to those used for the screens of television sets, in which a received echo is made to brighten the screen to produce a spot or "blip" at a distance from the centre of the tube proportional to the distance to the target and on a bearing from the centre corresponding to that of the target. Distances are readily estimated from range markers which appear as concentric circles (Fig. 10.3 (i)). The brightness of the target as seen on the PPI varies, to a limited degree, according to the intensity of the received echo. A strong echo is shown as a brighter return than a weak one. Such a PPI presentation, being a projection on the horizontal plane through the radar, of echoes received from all points of the compass, is rather like a map and, indeed, such indicators are used on ships and aircraft to display coastlines and other features to assist in navigation. The origin can be shifted from the centre of

the display if it is desired to confine attention to echoes from a particular sector (Fig. ~~10.31~~ 10.7(6)).

It will be clear that if the target is a high flying aircraft it could be above the radar beam and would not appear on a PPI. Such high targets can be detected by elevating the radar beam above the horizontal until the target is seen on the PPI. However, to enable the heights of targets to be determined the aerial is first stopped from rotating and is then "nodded", up and down, about a horizontal axis so that the beam sweeps through a sector in a vertical plane. All targets in this plane are then displayed at their correct height and range on a "range height indicator" (RHI). This is also a cathode ray tube but with the origin (radar location) at the bottom left-hand side of the screen; Targets appear further towards the right as their slant-range increases and higher up on the display as their height increases so that the slant-range to the target and its elevation are immediately indicated. Slant-range markers appear as vertical lines on an RHI. Height markers are electronically produced and are usually curved so that, at all ranges, the height indicated is that above the curved surface of the earth (Fig. ~~10.25~~ 10.6(4)). In order to facilitate the determination of heights, the scale in the vertical is usually made greater than that in the horizontal thereby distorting the shape of echoes by stretching them along the vertical.

The radars used in Great Britain to detect approaching aircraft during the early part of World War II used very large fixed aerials and radio wavelengths of 10 - 15 m. The invention of the magnetron in the same country in 1940 enabled powerful pulses of microwaves to be generated so permitting the radio energy to be focussed into sharp beams by relatively small, moveable aerials. Table 10.1(1) lists the frequency and wavelength bands used for radars of various kinds. The bands are given letters for easy identification. Radars used to detect rain, snow and hail are usually known as "meteorological" or "weather" radars and usually have wavelengths between 30 and 250 mm. In what follows the world "radar" should be taken to refer to these radars unless it is specifically stated otherwise.

Table 10.1.(1) Radio Waves used by Meteorological Radars

Band	Frequency range MHz			Wavelength range mm		
P	220	–	300	1 360	–	1 000
UHF	300	–	1 000	1 000	–	300
L	1 000	–	2 000	300	–	150
S	2 000	–	4 000	150	–	75
C	4 000	–	8 000	75	–	37.5
X	8 000	–	12 500	37.5	–	24.0
Ku	12 500	–	18 000	24.0	–	16.7
K	18 000	–	26 500	16.7	–	11.3
Ka	26 500	–	40 000	11.3	–	7.5

Whilst microwave radars were being developed, Ryde (1941) was making theoretical studies to determine whether their performance would be affected by the scattering or absorption effects of fog, clouds, rain, snow, hail and dust storms. In this classical work he predicted that, under certain conditions, microwave radars would detect areas of rain. On the 20 February 1941, some months after this prediction, a rain shower was detected and tracked to a distance of 13 km off the coast of England using a radar working on a wavelength of 100 mm (for brevity called 100 mm radar). Some years later, on 14 September 1944, a radar of the U.S. Navy at Lakehurst, New Jersey detected the spiral rainbands of a hurricane (Maynard 1945) and on 18 December in the same year a typhoon was similarly detected on a ship of the U.S. Navy in the Philippine Sea. The question arises as to how these echoes from atmospheric phenomena are formed?

10.2 Scattering

Scattering occurs when a radio wave, or other electromagnetic wave, passes over a stationary object whose dielectric properties differ from those of the surrounding medium. In these circumstances some of the energy is absorbed and appears as heat and some is re-radiated in all directions, without change of wavelength. A change of wavelength occurs if the body is moving relative to the transmitter and this case is considered in Sect. 10.8.4. The scattering arises because the radio wave induces oscillating electric and magnetic multipoles within the object which re-radiate in all directions some of the incident energy. (Ryde 1941) That part of the scattered energy which is radiated back along the beam towards the radar is called the "back-scattered power" and it is this power alone which can be said to be reflected by the object. However, most objects absorb some of the incident radiation and do not re-radiate the remainder equally in all directions. To distinguish between the back-scattering capabilities of different targets a concept known as the "back-scattering cross-section" $\bar{\sigma}$ is introduced. This is defined as the equivalent area of an isotopic scatterer which, radiating equally in all directions, would return to the receiver an amount of power equal to that actually returned by the target. The back-scattering cross-section $\bar{\sigma}$ is therefore a measure of the amount of power scattered in a backward direction towards the radar compared with the amount of power falling on the object. $\bar{\sigma}$ depends on the size, shape, aspect and electrical properties of the target and on the wavelength.

When the target is very large compared with a wavelength and of simple form e.g. a sphere, $\bar{\sigma}$ can be calculated from the same geometrical laws of reflection as apply to light. However, if the object is of complicated form then $\bar{\sigma}$ has to be measured experimentally at different aspects and wavelengths. Typical values are listed in Table 10.2(1).

Table 10.2 (1) Approximate Values of Radar Back-Scattering Cross-Section - σ

Object	σ		Wavelength
	Broadside	Head on	
	m^2	m^2	mm
Raindrops diameter 1 mm	3.5×10^{-10}	3.5×10^{-10}	30
diameter 5 mm	5.5×10^{-6}	5.5×10^{-6}	30
House Sparrow	5×10^{-4}	0.3×10^{-4}	30
Starling	11×10^{-4}	2×10^{-4}	30
Pigeon	30×10^{-4}	1.5×10^{-4}	30
Raindrops diameter 1 mm	2.84×10^{-12}	2.84×10^{-12}	100
diameter 5 mm	4.4×10^{-8}	4.4×10^{-8}	100
Starling	34×10^{-4}	-	100
Metal Sphere diameter 300 mm	7×10^{-2}	7×10^{-2}	100 and 30
Light Aircraft	10	5	100 and 30
Jet Liner	100	25	100 and 30

10.2.1 Small spherical particles

In 1871 Lord Rayleigh derived a formula for the scattering of light by particles smaller than one wavelength of the incident light. He found that the intensity of the light scattered by such small particles in the atmosphere was proportional to the sixth power of their diameter and inversely proportional to the fourth power of the wavelength. He showed that this effect caused the sky to appear blue because this component of sunlight has a shorter wavelength than the red and is scattered about 10 times more by particles and molecules in the atmosphere so giving the sky its blue colour. In space where there are few scattering particles the sky appears black. At sunrise and sunset, the sun's rays pass through a long atmospheric path and much of the blue component of sunlight is lost en-route leaving predominantly red light to produce the red sun and red cloud effects.

For Rayleigh scattering the back-scattering cross-section of a particle of diameter D, small compared with the wavelength λ, is given by

$$\sigma = \pi^5 \cdot \frac{|e - 1|^2}{|e + 2|} \cdot \frac{D^6}{\lambda^4} \qquad -(10.\text{?}(1))$$

where both λ and D are expressed in metres and e is a property of the material of which the particle is composed and is known as the complex dielectric constant. The equation is accurate to within 10% of the true value when D is less than one twentieth of λ and still holds approximately when D is as large as one fifth of the wavelength, Fig. 10.?.(1) If the sphere is of metal then the square of the expression in brackets is replaced by a factor 1.60.

If the scattering particles have a diameter greater than one fifth of a wavelength then the more general and complex Mie theory of scattering applies and the value of σ oscillates between wide limits as the particle size increases and resonance effects occur. Fig. 10.? (1) shows how the resonance depends on the ratio of the circumference of the particles to the wavelength; the first peak (greatest σ) occurs when the circumference equals the wavelength. Thereafter σ oscillates and approaches the optical or surface scattering value as the circumference increases to about ten times the wavelength. The back-scattering cross-section of a metal sphere approaches its geometrical cross section $\pi D^2/4$ whereas a water drop attains only 0.63 (0.56 at L band) of this value. The largest raindrops have diameters of about 5.5 mm. Equation (10.?(1)) can therefore be used to calculate the σ of rain and cloud drops at wavelengths of 30 mm or more, but Mie theory has to be used in the case of large hailstones.

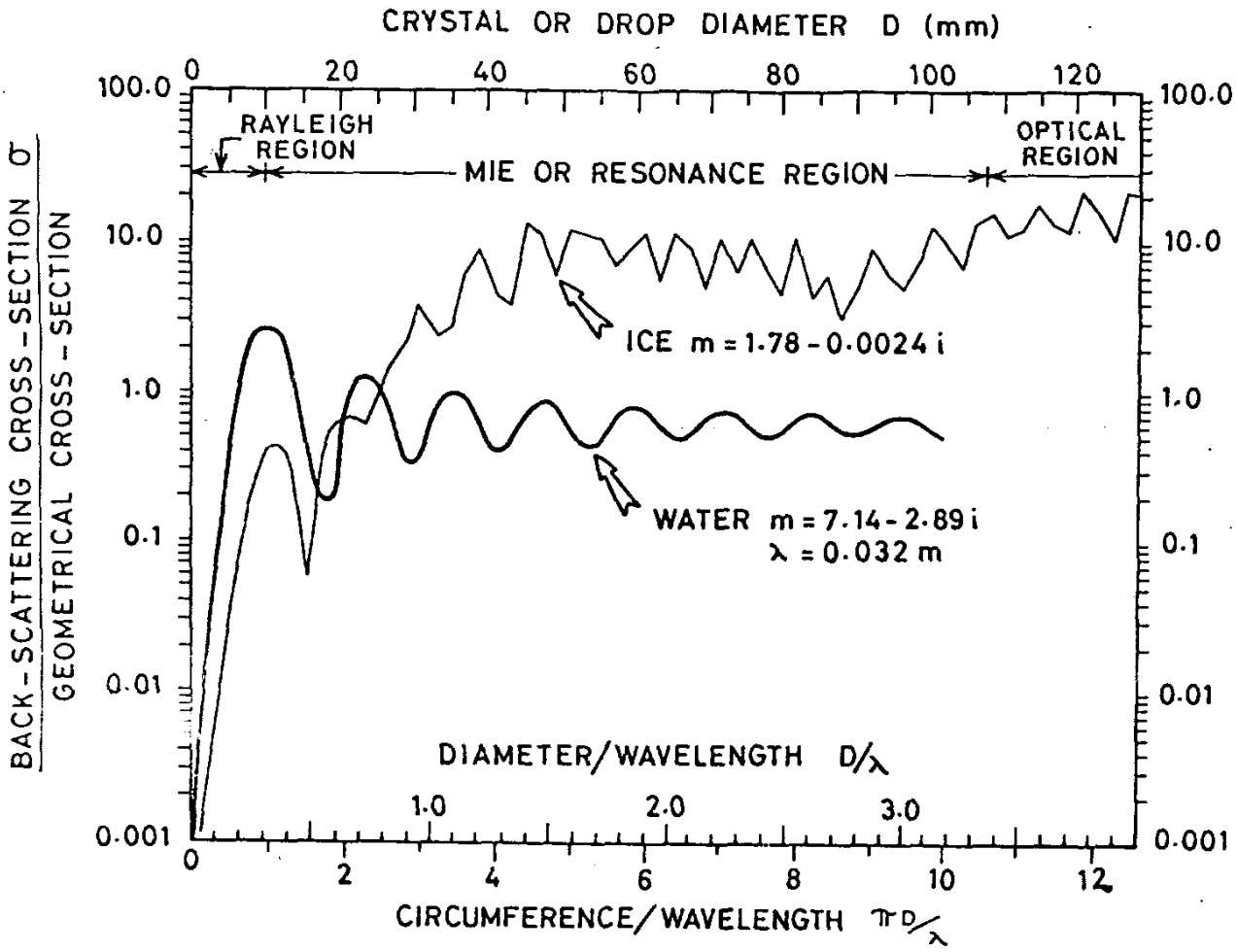

Fig. 10.2(1) Calculated values of the back-scattering cross-section shown as a fraction of the geometrical cross-section for water drops at a wavelength of 32 mm and a temperature of 0°C and for ice at all wavelengths from 10 to 600 mm. m is the complex refractive index and λ the wavelength. (Adapted from Herman & Battan 1961).

Large targets return an amount of energy proportional to their cross-sectional area whereas, for small targets in the Rayleigh region, the amount returned is proportional to the third power of the area (D^6). At a wavelength of 100 mm doubling the size of an aircraft would double its back scattered power but doubling the diameter of a raindrop from 1 mm to 2 mm increases the back scattered power 64 times.

The dielectric constant of water varies with temperature and wavelength; at $0^{\circ}C$ it ranges from about 40 to 80 over wavelengths from 30 to 100 mm but for ice the value remains fairly constant at 3.17 for the same range of wavelengths. The ratio of the speed of radar waves in free space (vacuum) to their speed in a medium, is known as the refractive index of the medium and for most media considered it can be taken as equal to the square root of the dielectric constant. For practical purposes therefore the refractive index of ice is constant at 1.78 while for water it varies with both temperature and wavelength. For example, at $0^{\circ}C$, it is 8.99 and 7.14 at wavelengths of 100 and 30 mm respectively. The value of the square of the expression in brackets in eqn (10.2(1)) does not vary much, and for meteorological purposes it can be taken as being 0.93 for water and 0.176 for ice of density 917 kg/m^3. Drops of water therefore back scatter radar energy about five times better than ice spheres of the same size. The refractive index of ice particles varies with their density, the value of the square of the expression in brackets in eqn (10.2(1)) can therefore be much less than 0.176 for snowflakes with entrapped air or as high as 0.197 for ice with the density of water (1 000 kg/m^3) - a concept sometimes useful when dealing with ice particles which will melt to form raindrops. In the range of wavelengths considered, eqn (10.2(1)) can be re-written for spherical water drops as:

$$\sigma = 284 \frac{D^6}{\lambda^4} \qquad - (10.2(2)) .$$

Kerker et al (1951), showed that small melting ice spheres ($D \ll \lambda$) surrounded by a film of water of thickness greater than one fifth of their original radius will scatter as well as water spheres of the same mass.

An exception to the rule that water spheres back scatter more energy than ice spheres of the same size occurs when their diameters equal or exceed the wavelength. Under such conditiions an ice sphere behaves as a dielectric lens focussing the incident rays onto the inside rear of the

stone where they are partially reflected as in cats' eyes. Fig. 10.2(c) shows that such stones can return more than 10 times the energy returned by water spheres of the same size. By contrast, reflection from large water spheres is almost entirely from the convex front surface, because of the high refractive index of water, and is divergent. Such rays as do enter the drop are strongly refracted towards the axis and leave before reaching the rear surface.

10.2.2 Small non-spherical scatterers

We have so far considered only spheres but, ice crystals, small hailstones and large raindrops ($D > 280\,\mu m$) can depart considerably from spherical form and, if oriented so that their major axes are parallel to the direction of polarisation of the incident waves, they back scatter more effectively than spheres of the same volume. Conversely they back scatter less effectively than spheres if their minor axes are parallel to the direction of polarisation. In particular, Atlas et al (1953) showed that a randomly oriented collection of small oblate and prolate water spheroids (major axes $\leq \lambda/4$) back scattered more energy than water spheres of the same volume. These effects are less marked for ice particles than for water drops and are even weaker in the case of dry snowflakes because of their low dielectric constant. Indeed, as far as their back scattering performance is concerned, dry snowflakes may be considered as ice spheres of the same mass.

Atlas et al (1953) also showed that small randomly-oriented oblate and prolate water spheres whose major axis was 10 times the diameter could scatter about 10 and 25 times more than spheres of the same volume, respectively. However, in nature, although raindrops do tend to oscillate about a preferred oblate shape they generally suffer only small distortions with maximum axial ratios of about 1.5 (Mason 1971) and thus, the corresponding increase in returned power is negligible. Dry ice spheroids, even with axial ratios as large as 10, back scatter a little less than twice as well as spheres. However, the shape effect is important in two cases: firstly, when non-spherical hailstones melt and acquire a water coating enabling them to back scatter as though they were water drops of the same size and shape, and secondly, when snowflakes begin to melt and acquire a covering of water. The irregular, variable shape and low density of snowflakes makes it difficult to assess their back scattering performance quantitatively but it is probable that, when wet, they scatter incident energy as if they were constituted entirely of water. A snowflake which becomes wet therefore, gives an enhanced return because of both its effective change of state and its non-spherical shape. These effects contribute to the causes of the bright band, or enhanced returns, seen just below the level at which the temperature is $0^{\circ}C$ in rain which is being formed by the Wegener-Bergeron process (Fig. 3.13).

10.2.3 Polarisation

Most meteorological radars radiate plane polarised waves and best detect those with the same polarisation, we must therefore consider what effect different scatterers have on the plane of polarisation. On scattering by solid or liquid perfect spheres the plane of polarisation of radar waves is preserved. However in the case of drops or particles which are non-spherical the plane of polarisation remains unchanged only when it includes the major or minor axis of the scatterers (assumed to have an ellipsoidal shape); for other aspects some of the returned energy will be polarised at right angles to the incident waves and therefore, will not be detected by the receiver. Some air traffic control radars can transmit circularly polarised waves, that is, radiation in which the direction of vibration of the waves rotates about the axis of propagation as the waves progress without change of amplitude. Wave crests, in this case, simultaneouly advance and rotate along a helical path. When reflected by a sheet of metal or scattered by a spherical drop, circularly polarised waves change their direction of rotation and so cannot be detected on returning to the radar. However, aircraft return some radar waves after they have been reflected more than once. At each reflection on different parts of the aircraft, the direction of polarisation is changed so that those waves which undergo two, or any even number of reflections, return with circular polarisation of a sense compatible with the receiver which can then detect them. It is therefore possible to receive some returns from an aircraft whilst those from raindrops are not detected. In this way aircraft may be seen on the PPI even when enveloped in heavy rainstorms. The power received from raindrops can be reduced 100 times (-20 dB)* by using circularly polarised radiation but the method is less effective when used against non-spherical drops, such as wet snowflakes, when reductions of only 30 times (-15 dB) or so, are possible. In returns from heavy rain there will be a small component of depolarised power due to multiple scattering by larger raindrops.

Before we can determine which targets will return sufficient power to a radar to be detected we must first consider the radar beam and the propagation of radar waves in the atmosphere.

*dB is an abreviation for decibel, a measure of relative power on a logarithmic scale given by the relation 10 Log (p_2/p_1). For example, if p_2 is twice p_1, the power ratio in decibels will be 10 Log 2 = 3dB or again, if p_2 is one hundredth of p_1 the ratio is 10 Log (0.01) = 10(-2) = -20 dB.

10.3 The Radar Beam

10.3.1 Formation

A radar transmitter produces bursts or pulses of radio energy of high intensity and short duration. Typically, each pulse will be transmitted with a power of between 20 kW and 1 MW and will have a duration of one or two microseconds. The length of a pulse is obtained by multiplying its duration by the velocity of light; a 1 μs pulse is therefore approximately 300 m long. Pulses are emitted at a constant rate known as the "pulse repetition frequency" (p r f) which has to be lower in long-range radars than in those of short range because more time is required in the former for the distant echoes to return to the transmitter before the next pulse is dispatched. Typically, for a radar with an operational range of 460 km, the p r f will be about 275 per second representing an interval between pulses of 3 636 μs, (time for the waves to travel out 545 km and return).

The pulses of radio waves in most meteorological radars are carried from the transmitter, in a waveguide, to the focus of a circular "dish" aerial and are there formed into a slightly divergent beam whose intensity is strongest along the axis of the aerial and falls off with distance from the axis. The beam "width" in any plane is expressed as the angle between those directions in which the intensity of the beam is one half of the intensity on the axis - the "half-power points". The rate of decrease of power further off the axis than the half-power points is usually very great so that for many practical purposes the total radar energy can be considered as being within the beam as defined. However, there are also some much weaker beams which are found at greater angles to the main beam axis than the half-power points, these off-centre beams are called "side lobes" and they must be considered when dealing with strongly-echoing targets at close range.

A circular aerial of parabolic form and diameter D will, at a wavelength λ, produce a conical beam approximately 1.2 λ/D radians wide. At 100 mm wavelength, a 2° beam of circular section is produced by an aerial having a diameter of 3.5 m whereas, at a wavelength of 30 mm, the same beam width is produced by an aerial with diameter of only 1 m. The area of the aerial is called its "aperture" but its "effective aperture" when transmitting or intercepting radiation is somewhat less, usually by about a half, depending on its design which will determine the efficiency of the feed and the uniformity of aerial illumination.

Because the aerial beam diverges, the power illuminating a given point target is inversely proportional to the square of its range, so that doubling the distance to a target reduces the power incident upon it by a factor 1/4.

10.3.2 Propagation

If microwaves traversed the atmosphere in straight lines, the distance to which a radar could detect a target at a given height above the earth's surface, would be limited by the optical horizon. Beyond this limited distance the target would be below the line of sight because of the curvature of the earth. For rectilinear propagation the maximum range from a radar at sea level to a target at a height z_1(km) above the ground is $113\sqrt{z_1}$ km. By siting the radar on a hill top at a height z_2 the maximum range for detection can be increased by a further $113\sqrt{z_2}$ km. With straight line propagation a radar near sea level could detect a target at an altitude of 10 km to a distance of 360 km. However, in the atmosphere, some bending of radar rays usually takes place.

The refractive index of the atmosphere decreases with decreasing density and decreasing water vapour pressure and for these reasons it usually decreases with height. Microwaves will therefore travel slower near the ground than higher up so causing a slight downward curvature of all except vertical rays. The refractive index near the surface is typically about 1.0003 and falls off linearly with height usually at a rate of 4×10^{-8} per meter - these typical values are used to define "standard conditions" in which the curvature of the beam is about three quarters of that of the earth's surface. This downward curvature of the rays slightly extends the distance to the horizon to $132\sqrt{z_1}$ km - about 17% greater than for rectilinear propagation. The maximum range r_{max} is then given by

$$r_{max} = 132(\sqrt{z_1} + \sqrt{z_2}) \quad \text{km} \qquad (10.3(1)) \ (\text{~~10.2a~~})$$

If the rate of decrease of refractive index with height increases by as little as 10.9 parts in a hundred million - to 14.9×10^{-8} per meter - then the downward curvature of initially horizontal rays becomes equal to that of the earth's surface. Under such circumstances there is no horizon and the rays bend round the earth close to the surface. A gradient of refractive index of this magnitude can be caused by an increase of temperature with height (inversion) or, more frequently, by a more than usual rate of decrease in the amount of water vapour present, or both. Non-standard distributions of refractive index in the atmosphere give rise to "anomalous propagation".

Abnormal downward bending is called "super-refraction". The distributions of temperature and humidity that give rise to super-refraction usually occur in shallow layers about 1-200 m deep and constitute a "duct" in which the rays are trapped. If the rays leave the radar at angles of elevation of 2^{o} or more their path through the duct is usually too short to permit of their being curved into a trapped configuration. When super-refraction takes place echoes can be seen from coast lines or hills which are normally not "seen" because of the earth's curvature. In Fig.10.3(2), for example, the NE corner of Hainan Island and the Luichow Peninsula are normally not seen on radar because they are below the radar horizon.

Echoes may be returned from targets at such great distances as to be outside the ranges shown on the PPI display. Under these circumstances a pulse will return after the succeeding pulse has been transmitted and the target will appear at some incorrect range on the PPI. This is illustrated in Fig. 10.2(1) where Luzon and the Vietnam coast are beyond the normal maximum 445 km range but appear - misplaced - on the succeeding scan of the PPI. In the time interval between successive pulses (3 636 μs) radar waves can travel out approximately 545 km and, if reflected, return to the radars. The indicated range of the anomalous echoes in the figure should be increased by 545 km to obtain their true range. Care is therefore necessary to identify occasions when super-refraction is taking place so that "second scan" or "second trip" echoes are not mistaken for echoes from targets within normal range. If they are moving with a component of motion in azimuth these echoes will usually appear to be moving more slowly than other echoes nearby. If they are from stationary targets their lack of movement may appear to be anomalous. It is also possible for second scan echoes to be superimposed on nearer echoes to give a false impression of echo intensity. For example, the island of Taiwan on second scan appears just to the east of Hong Kong and enhances permanent echoes there. Second scan echoes are characterised by their narrow azimuthal extent.

On occasions when more than one duct exists radar rays may take different paths of different lengths so that a single target, such as a ship or small island, appears on a PPI as a group of echoes on the same bearing but at slightly different ranges (Fig. 10.8(2) ~~10.34~~). Returns due to anomalous propagation disappear if the radar beam is elevated a few degrees. This characteristic can be used to differentiate

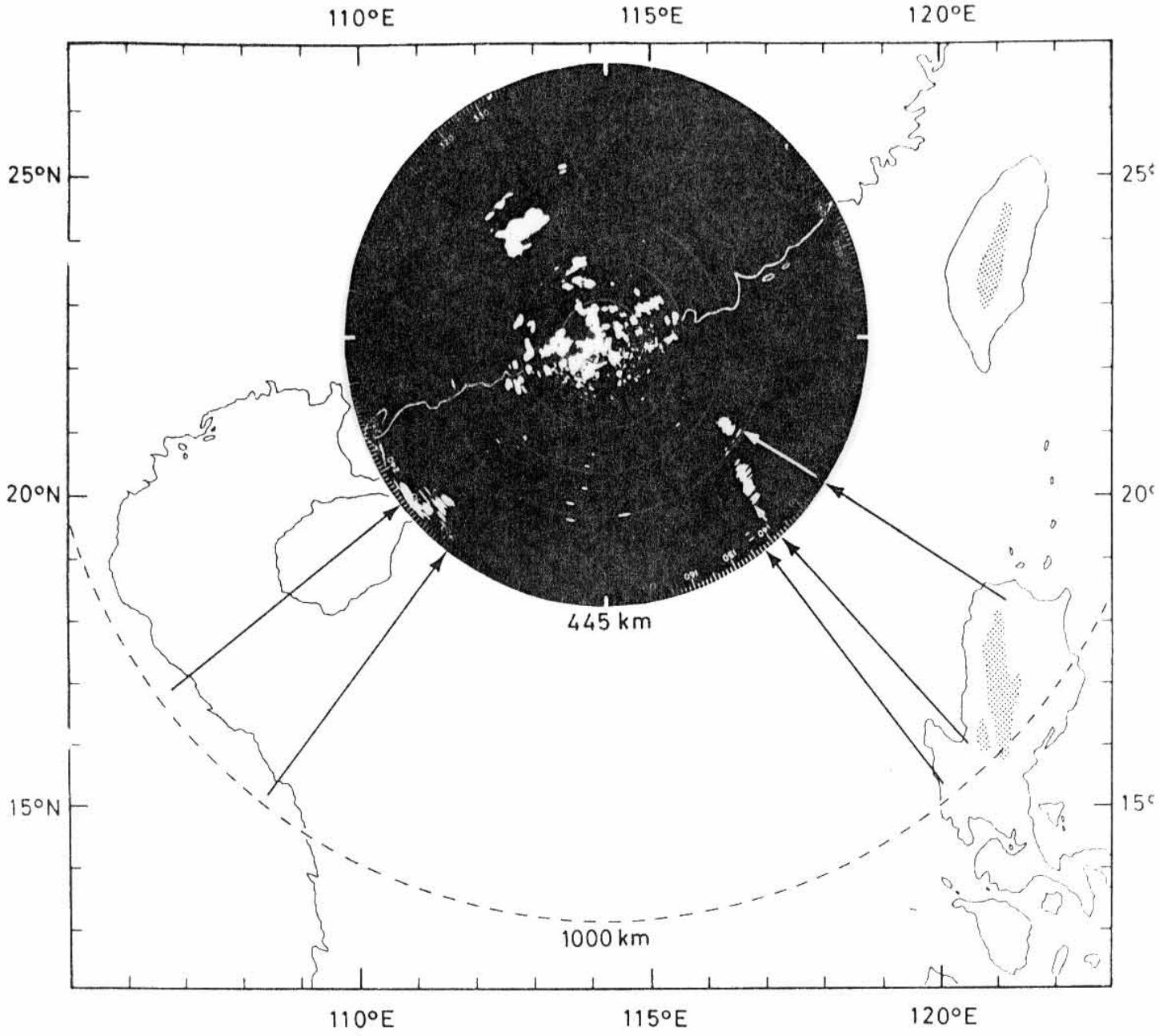

10.3(1)

Fig. ~~10.2~~ The PPI of the Hong Kong Plessey 43S, 100 mm radar photographed at 0815 GMT on 16 March 1967 during super-refractive conditions. The range rings are at intervals of 74 km.

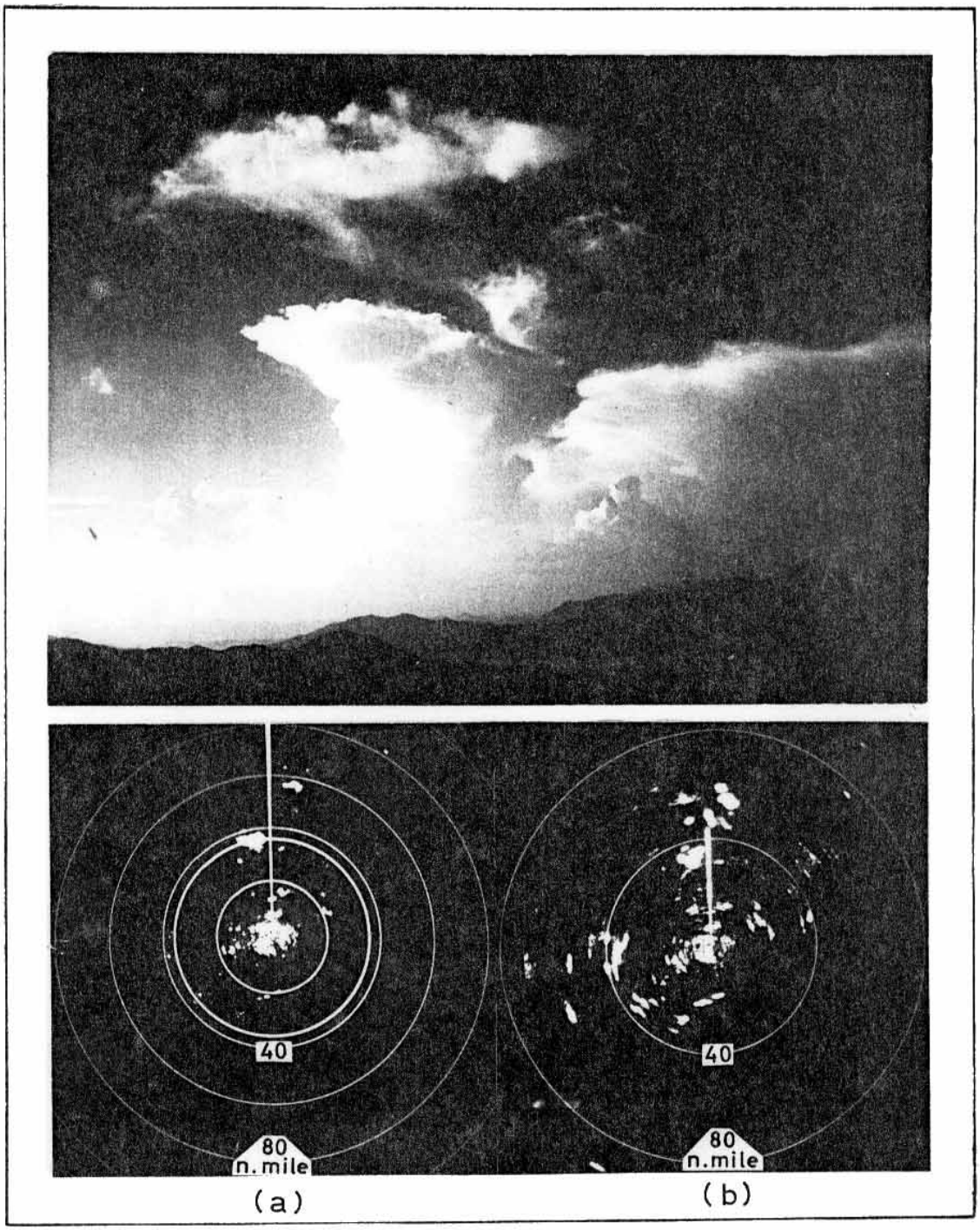

Fig. 10.3 (z) Cumulonimbus clouds over China 36 n.mile (67 km) and 56 n.mile (104 km) north of Hong Kong at 1835 h local time (0935Z) on 13th May, 1974; their echoes as seen on (a) a 32 mm radar and (b) a 107 mm radar. The characteristics of the radars are (a) 20kW, beam width 0.75^{o} (horizontal) by 2.8^{o} (vertical) and (b) 650kW beam width 2^{o}.

them from almost all returns due to precipitation.

Occasions when the radar range is reduced, either by super-refraction causing the beam to strike the earth's surface before reaching normal maximum range or by upward bending, are more frequent than occasions of extended range. Anomalous propagation near tropical cyclones is discussed in sects 10.8.1 and 10.8.2.

10.3.3 Attenuation

As waves in the radar beam travel through the atmosphere they are attenuated in three ways. Firstly, cloud droplets, rain, snow, hail and other particles scatter energy out of the beam; secondly, these same particles absorb some energy which appears as heat and, finally, the atmospheric gases - primarily oxygen and water vapour - also absorb some energy. These processes lead to a rapid (exponential) decrease of energy in the beam as the total distance travelled - out and back - increases. Attenuation from each of these causes is insignificant at the longer wavelengths (100 to 200 mm), but increases markedly as the wavelength decreases. In quantitative terms, the attenuation of 100 mm radiation in rainfall having a rate of R mm/h and a typical drop-size distribution is, at 18°C, $R.3x10^{-4}$ dB/km, but at 30 mm wavelength it is $R^{1.3}.74x10^{-4}$ dB/km. When R = 100 mm/h, these equations yield attenuation rates of 0.7 per cent/km and 97 per cent/km respectively. For 30 and 50 mm radars the attenuation of the beam during the penetration of tropical rainstorms is often so great as to prevent the detection of more distant severe storms as shown in Fig. 10.3(a). Although the 32 mm radar shows the small echo about 60 n. mile to the NNE it cannot detect the rain clouds seen in (b) at ranges of about 50 and 55 n. mile beyond the large cloud just west of north.

10.4 The Radar Equation

10.4.1 Discrete targets

By considering the geometrical relationships between the diverging outgoing and returning radar beams, the back-scattering cross-section of the target σ and the aerial size and efficiency it can be shown that the power received p_r from a target of back-scattering cross-section σ at a range r is

$$p_r = \frac{p_t \, A_e^2}{4\pi\lambda^2 r^4} . \sigma \qquad - (10.4(1))$$

where p_t is the transmitted power and A_e is the effective aperture of the aerial*. For a typical typhoon tracking radar such as the Plessey 43S, conservative values of the symbols are λ = 0.107 m (equivalent to 2800 MHz), p_t = 650 kW (at waveguide outlet) and A_e = 5.15 m^2 (0.48 x area). Equation (10.3) can then be written for this radar as

$$P_r = 120 \times 10^6 . \frac{\sigma}{r^4} \qquad - (10.4(2))$$

The power received at the radar must exceed a certain minimum value if it is to be distinguished from the random fluctuations or "noise" inherent in receiver circuits, or from stray radiations picked up by the aerial. The minimum detectable power for the typical radar under consideration is about 6×10^{-14} W.+ If the power received from a target is equal to this value or greater it will be detected. Equation (10.4(2)) can be re-arranged and with p_r set at the minimum detectable power it will give the maximum range r_{max} for detection of a target of cross-section σ:

$$r^4_{max} = 2 \times 10^{21} . \sigma \qquad - (10.4(3))$$

If values of σ from Table 10.2(1) are substituted in eqn (10.4(3)), it will be found that a 5 mm raindrop and a metal sphere of diameter 300 mm are detectable at ranges of less than 3 and 110 km respectively. Aircraft, if high enough, will be detectable out to the maximum range (approx. 450 km) of the radar.

* Equation (10.3) can also be expressed in terms of G the "gain" of the aerial - a measure of its directional efficiency - by writing $A_e = \frac{G\lambda^2}{4\pi}$. The 43S radar aerial has a power gain of 37.5 dB or 5 623 times (at λ = 100 mm) and effective aperture A_e = 5.15 m^2.

+ If the minimum detectable signal-to-noise ratio at the receiver is S/N, then Pr = S and N = kTB when K is boltzman's constant, T is the absolute temperature and B is the band width of the system. Pr in eqn (10.4) can be replaced by (S/N) kTB .

10.4.2 Assemblies of raindrops

From the previous section it is easily calculated that even powerful radars cannot detect a single raindrop - be it the largest possible - beyond a few kilometres. Small raindrops at ranges beyond 1 km return an amount of energy well below the minimum detectable. However, raindrops occur most frequently in concentrations of between 100 and 1 000/m^3 so that many of them contribute to the power back-scattered to the radar. In the case of the Plessey 438 radar the beam is approximately 2^o wide and the pulses have a duration of 2 μs corresponding to a length of approximately 600 m. At a range of 60 km the beam will be 2 km wide and will illuminate a volume of 2 x 10^9 m^3. If the concentration of raindrops therein is a typical 500/m^3, then 10^{12} drops will back scatter energy. However, only those in half the volume illuminated scatter waves which arrive simultaneously at the receiver. This arises because the power back scattered from the front of a pulse by drops at a range of r plus a half pulse length, will return to the radar at the same time as energy back scattered from the rear of the pulse by particles at range r - and so on. Therefore, the number of drops simultaneously returning power will be one half of 10^{12} or 5 x 10^{11} and, if they are all 1 mm in diameter, each will back scatter an undetectable 26 x 10^{-24}W (from eqn (10.4)(2)) However, the total power returned by all 5 x 10^{11} drops would be 13 x 10^{-12}W which is readily detectable.

In practice the back-scattered power from randomly distributed raindrops is found to fluctuate from one pulse to the next. This is a result of the re-arrangement of the particles as they move relative to each other and to the radar, producing returns which sometimes reinforce and sometimes cancel each other, so giving rise to what is called "incoherent scattering". It takes time for an arrangement of drops to change and it is found that the power of one returned pulse correlates well with the next, but less well with the next-but-one, and so on until, after intervals of the order of 5 to 20 ms (for λ = 100 mm) the intensity of the returns are independent of each other. Because of this fluctuating nature of the returns from an assembly of raindrops, it is necessary to consider the average power received over several pulses $\bar{p}_r$ as being representative of the back-scattering capabilities of the target, rather than that returned by any one pulse.

To determine the average power received from an assembly of raindrops eqn(10.4(1)) has to be modified to allow for the fact that there are many scatterers of different sizes. Also the rainstorm may not entirely fill the beam and that even when it does, ~~do so~~ the beam is not uniform in intensity so that the efficiency of the aerial for both transmitting and receiving is not equal for all the scatterers in any pulse volume. It is also necessary to consider the attenuation of the beam as it passes through storms and clouds closer to the radar. When all these factors are taken into account the basic radar equation giving the average power received from precipitation targets becomes:-

$$\bar{p}_r = \frac{p_t A_e h}{8\pi r^2} \cdot \left[\frac{\pi^2}{32\ 1n2}\right] \cdot FK \sum_{vol} \sigma \qquad \text{10.4(4) - (10.6)}$$

Where h is the pulse length, K is an attenuation factor, F is the fraction of the beam filled by the assembly of scattering particles and $\sum_{vol} \sigma$ ~~means~~ is the sum of the back-scattering cross-sections of all the particles in unit volume. ~~and~~ This is known as the "reflectivity" and is represented by the symbol η .

Prior to 1962, eqn(10.6) 10.4(4) was used without the factor in square brackets and in that form it overestimated the average returned power by a factor of between 2 and 5 when compared with that found experimentally. In a more rigorous derivation Probert-Jones (1962) showed that the earlier equation was in error in two ways; it overestimated the cone of received power by a factor $2\ln 2 = 1.386$, and it overestimated the effectiveness of the aerial by a factor $16/\pi^2 = 1.62$. These correcting factors are included in the square bracket and have the effect of reducing the average returned power by a factor of 0.445.

If the scattering particles are spherical raindrops their back-scattering cross-sections σ are given by eqn(10.2) (2) which can be used to replace σ in eqn(10.6) 10.4(4), Furthermore, if the storm fills the beam and there is no attenuation, then $F = K = 1$. After making these substitutions and combining all the constants eqn(10.6) 10.4(4) can be written as

$$\bar{p}_r = 5.03 \frac{p_t A_e h}{\lambda^4} \frac{\sum D^6 N}{r^2} \qquad \text{10.4(5) - (10.7)}$$

where $\sum_1^N D^6$ means the sum of the sixth power of the diameter of every drop in unit volume. It will be noticed that the power received by a given radar from an extended target of many scatters varies inversely as the square of the range r whereas, for the case of discrete targets (eqn (10.4)) it varies inversely as the fourth power of the range. It will also be noted that if other factors remain constant the returned power is inversely proportional to the fourth power of the wavelength i.e. the smaller the wavelength the greater the power returned. However, in practice, the increased attenuation at smaller wavelengths makes it desirable to use a wavelength of 100 mm or more in the tropics, for most meteorological purposes. If values appropriate to the Plessey 43S are substituted for the symbols in eqn (10.4(5)) we find that

$$\bar{p}_r = 7.77 \times 10^{13} \cdot \frac{\sum N D^6}{r^2} \qquad - (10.4(6))$$

and if the minimum detectable signal is taken as 6×10^{-14} W then the maximum range at which a rainstorm will be detected will be

$$r_{max} = 3.6 \times 10^{13} \sqrt{\sum D^6 N} \qquad - (10.4(7))$$

A rainstorm, meeting the conditions under which eqn (10.4(7)) was derived, and having only 4 drops, of diameter 1 mm, in each cubic metre would be detectable out to a distance of about 72 km.

10.4.3 Detection of clouds

The diameters of the drops comprising water clouds cover a wide spectrum from about 5 to 200 μm and their concentrations in any given cloud vary with its type and location. The average concentration of drops in normal tropical maritime cumulus is about 75 x $10^6/m^3$ with a maximum of about 500 x $10^6/m^3$. Such clouds contain drops ranging in diameter from about 5 to 50 μm with those of about 25 μm being most frequent. The number of drops larger than 25 μm decreases rapidly with increasing size. If we assume a cloud in which all the drops have diameters of 25 μm with a concentration of 100 x 10^6 per cubic metre (more than average) then such a cloud would have a high water content of 0.8 g/m^3 and would back scatter much more strongly than an average tropical cumulus. Nevertheless, if these extreme values for cumulus drop-size and concentrations are substituted in eqn (10.9) 10.4(1) it will be found that the cloud would not be detectable beyond 6 km. In nature, cloud drop-size distributions are such that normal meteorological radars detect only those clouds which contain droplets large enough to fall as precipitation. Ice scatters only one-fifth as well as water so that normal cirrus clouds are usually undetected at all ranges. However, in some circumstances, cirrus ice crystals can be large enough to yield a detectable signal on normal meteorological radars. Radars operating on shorter wavelengths of about 10 mm will readily detect non-precipitating cloud droplets and cirrus ice crystals and can be used to determine the vertical extent of such clouds.

10.4.4 Detection of rainfall

We have noted that a typical meteorological radar could detect a hypothetical cloud at a range of 70 km if it contained four 1 mm raindrops in each cubic metre. The fall speed of drops of 1 mm diameter is about 4 m/s so that the cloud would yield a rate of rainfall of about 0.03 mm/h. This immediately suggests the possibility that radar could measure rainfall over large areas. For many purposes this would be much more useful than the information obtained from standard gauges which sample very small areas of the order 10^{-8} km^2. Unfortunately, there are many complicating factors, the most severe being that there is no unique relationship between reflectively and rate of rainfall, the latter depends on the volume of the drops (proportional to D^3) and their rate of fall (proportional to $D^{\frac{1}{2}}$) but the returned power is proportional to the sixth power of the drop diameters (D^6). Large drops therefore make a greater contribution to reflectivity than to rainfall. For example, the power returned by the four 1 mm drops in each cubic metre of our hypothetical cloud would be equal to that returned by 256 drops of half the diameter in the same volume. The water content in the latter case is eight times the former but the rainfall rate is only four times as great because the small drops fall more slowly than the larger ones. This example shows that the two rain clouds returning equal power to the radar could yield rainfall rates differing by a factor of four. Although there is no unique drop-size distribution for a given rate-of-rainfall, rain clouds of the same type at the same stage of development and in the same environmental conditions do tend to produce raindrops in a similar spectrum of sizes. Empirical relationships between rainfall and reflectivity under given conditions can therefore be developed. These relationships enable worthwhile measurements to be made in certain cases and so we will discuss the principles, limitations and some applications of the technique to tropical cyclone rainfall.

An extended assembly of raindrops returns an amount of power proportional to the sum of the many products ND^6 where N is the number of raindrops of diameter D in unit volume as given in eqn (10.8). This sum is called the "reflectivity factor" and is denoted by the letter Z, so that

$$Z = \sum ND^6 \qquad - (10.10)$$

and eqn (10.8) can be written as:- 10.4(6)

$$\bar{p}_r = C \frac{Z}{r^2} \qquad - (10.11) \quad 10.4(9).$$

where C is specific to a particular radar and can be determined. It should be noted that the reflectivity factor Z, differs from the reflectivity η (sect 10.4.2) because the latter varies with wavelength (eqn 10.2) 10.2(2) whereas Z is dependent only on the distribution of drop sizes. When raindrop diameters are expressed in mm and their concentration is given as the number per m^3 then the units of Z are mm^6/m^3. However, it is sometimes useful to express Z relative to $Z_o = 1\ mm^6/m^3$, the ratio being expressed in decibels (see footnote p.8) such that $dBZ = 10 \log_{10}(Z/1)$. In this way a reflectivity factor of $10^5 mm^6/m^3$ can also be expressed as 50 dBZ .

If the conditions used to determine eqn (10.11) 10.4(9) are fulfilled then, the reflectivity factor Z of a raincloud can be determined by measuring the average power received $\bar{p}_r$ and the distance to the storm r. The distance is shown directly on the PPI: $\bar{p}_r$ is more difficult to measure with precision. In routine operations $\bar{p}_r$ is often determined by observing by how much it exceeds the known minimum detectable signal for the radar, p_{min}. One method of doing this is to progressively attenuate the received signal with an adjustable, calibrated control to the point at which the storm ceases to be detectable on a correctly adjusted PPI screen. The attenuation required can be expressed as a direct ratio $\bar{p}_r$ to p_{min} or more usually, in decibels. This method may lead to significant overestimates of the true average power, especially at short range, and more sophisticated signal averaging methods are used when greater accuracy is required.

Most radar receivers can be set so that received signals are amplified by an amount which increases as the square of the range. Storms with equal reflectivity factor then appear equally bright on the PPI at all ranges and disappear at equal settings of attenuation. This facility, known as "swept gain"+ enables the reflectivity of storms above a certain intensity to be compared directly without the need to make adjustments for their range; its application is usually restricted to ranges within about 200 km. If the minimum detectable reflectivity

+ This is called "sensitivity-time control" or STC in American usage.

factor for a target in this range is Z_{min} and if the reflectivity of a particular target is x dB greater than Z min, then the reflectivity of this target expressed in dBZ is equal to $x + 10 \log_{10} Z_{min}$. For the Plessey 43S radar, eqn (10.4(7)) indicates that Z_{min} at the full swept gain range of 200 km is 30.86 mm^6/m^3. The expression $10 \log_{10} Z_{min}$ is in this case equal to 15 so the reflectivity of a target in dBZ will be obtained by adding 15 to the attenuation required to extinguish the return.

Having determined the reflectivity factor Z for an area of rain the corresponding rate of rainfall R can only be obtained if the appropriate relationship between Z or dBZ and R is known.

10.4.5 Z - R relationships

In a short and classic paper, Marshall and Palmer (1948) presented the average distribution of raindrop sizes in rain of different intensities. The measurements were made at Ottawa in rain formed from snow flakes in stratiform clouds. As shown in Fig. 10.4 (1)(a) the drop sizes are distributed in an approximately exponential form such that there are more small drops in unit volume than large ones and the numbers of both increase with rainfall intensity. Drop-size spectra are highly variable in space and time and individual samples vary considerably from the idealised exponential form (the straight lines in Fig. 10.4(1)(a)). However, averages of a large number of samples from many areas and storm types have been found to fit fairly well the Marshall and Palmer (M-P) distribution represented by the formula:

$$N_D = N_o \exp(-\Lambda D) \qquad (10.4(10))$$

where D is the drop diameter, $N_D\,dD$ is the number of drops between D and D + dD per unit volume of space and N_o is the value of N_D for D = 0. For any intensity of rainfall the equation can be written as:

$$N_D = 8000 \exp(-\Lambda D) \quad m^{-3}\,mm^{-1} \qquad (10.4(11))$$

$$\text{where} \quad \Lambda = 4.1R^{-0.21} \quad mm^{-1} \qquad (10.4(12))$$

and D is expressed in mm, N_D in drops per m^3 per mm and R is the short-period rainfall in mm/h. Substituting these values in eqn (10.4(8)) - which gives the reflectivity factor Z in terms of drop-size spectra - and integrating over all drop sizes from zero to infinity yields the relation $Z = 296R^{1.47}$. Although in nature drop sizes seldom exceed 6 mm and eqn (10.4(10)) overestimates the number of drops with D less than 1.5 mm and although the basic data refer to rain formed by the ice process (sect 3.6.1) nevertheless, this relation between Z and R is close to those obtained in a number of experiments in the humid tropics as shown in Table 10.4(1). Marshall and Palmer also calculated Z and R from actual drop sizes and this data fitted the regression line $Z = 220R^{1.6}$ later revised to

$$Z = 200R^{1.6} \qquad (10.4(13))$$

which has come to be used not only as the standard relationship for rain from stratiform cloud but also as a formula for general application when more specific relationships are not known.

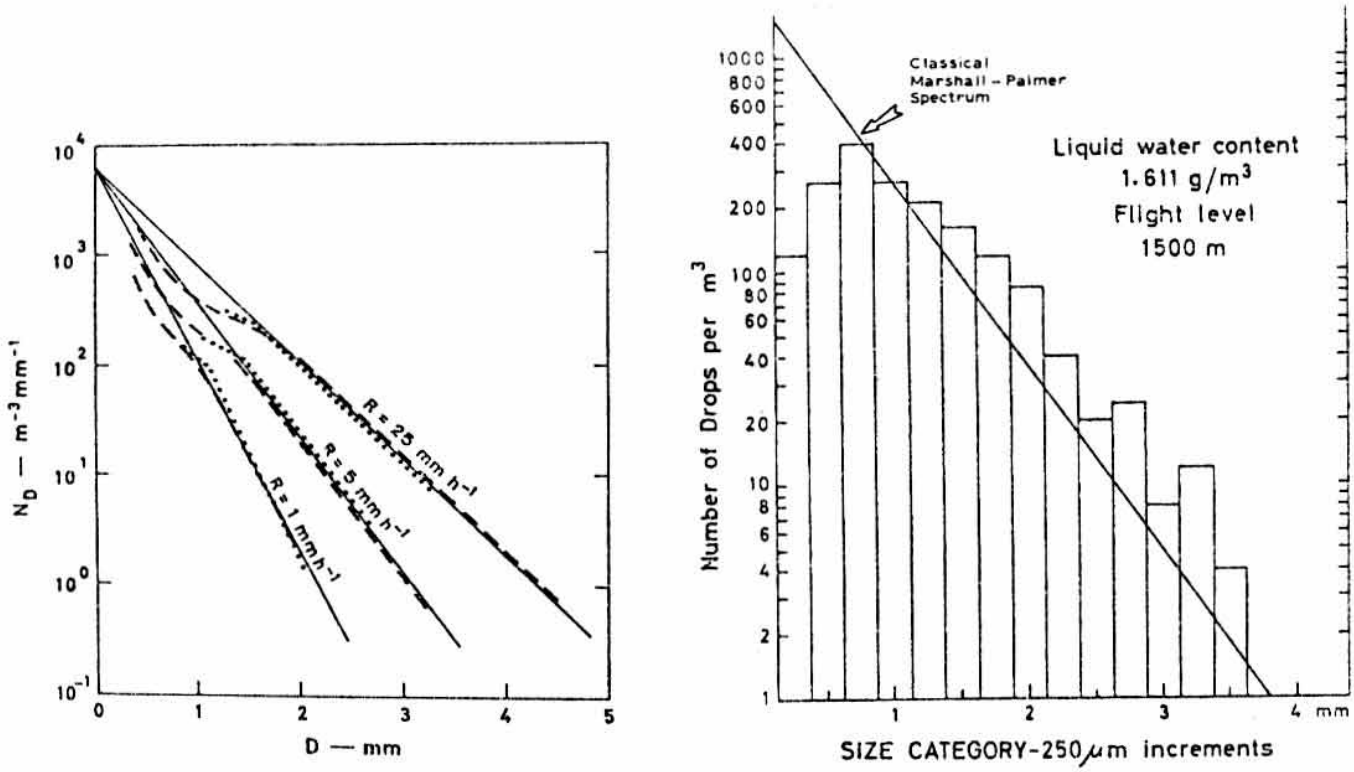

(a) (b)

Fig. 10.4 (a) Marshall and Palmer distribution function for drop sizes (solid lines) compared with Ottawa observations (dotted) and Laws and Parsons results (dashed).
(b) Drop-size distributions from hurricane Ginger 1971.
((a) from Marshall and Palmer 1948 (b) from Merceret 1974a)

Following Marshall and Palmer very many experiments have been made to determine the constants a and b in the general equation

$$Z = aR^b \qquad (10.14)\ 10.4(14)$$

and widely different values for the constants have been found. These experiments used a variety of methods to determine R and Z and they were carried out on rain from different types of cloud in different stages of development and in different geographical regions and environments. Atlas (1964), Mason (1971) and Battan (1973) have provided excellent summaries and assessments of the findings of these experiments which indicate that drop-size spectra vary greatly in space and time and with storm type. Stout and Mueller (1968) show that differences in excess of 500% in rainfall rate for given reflectivity can occur. These differences are primarily associated with differences in geographic region but smaller variations of the order of 150% can be attributed to different types of rain or synoptic conditions. The data now available show that it is no longer appropriate to use eqn (10.4(13)) for all rainfall but that other values of a and b should be chosen to better match the storm type and geographical region. Some values of the constants found at stations in the humid tropics and in the hurricane and typhoon areas are shown in Table 10.4(1).

In Fig. 10.5 (10.4(2)) a rain parameter diagram is shown to illustrate the dependence of the relation between Z and R on some physical characteristics of rain clouds. The diagram is not of universal application because it is based on two assumptions. However the assumptions are realistic so that the diagram shows typical magnitudes for the variables and gives an insight to the physical processes involved. For example, warm oreigenic rain (line b) comprised mostly of small drops (indicated by small value of D_o, the diameter of the drops with median volume) which fall with low velocity, need to be present in greater concentrations (as indicated by the liquid water content W) and yield a smaller reflectivity factor than do the larger drops in a shower (line c) which produces the same rate of rainfall.

If a Z - R relationship of the form of eqn (10.14) (10.4(14)) is known to be valid in given circumstances then it can be combined with eqn (10.11) (10.4(9)) to yield

$$\bar{P}_r = C \frac{a}{r^2} R^b \qquad (10.15)\ 10.4(13)$$

This equation which relates the average power $\bar{P}_r$ returned by raindrops at distance r to the rate of rainfall R, is the basis of the method normally used to measure rainfall by radar.

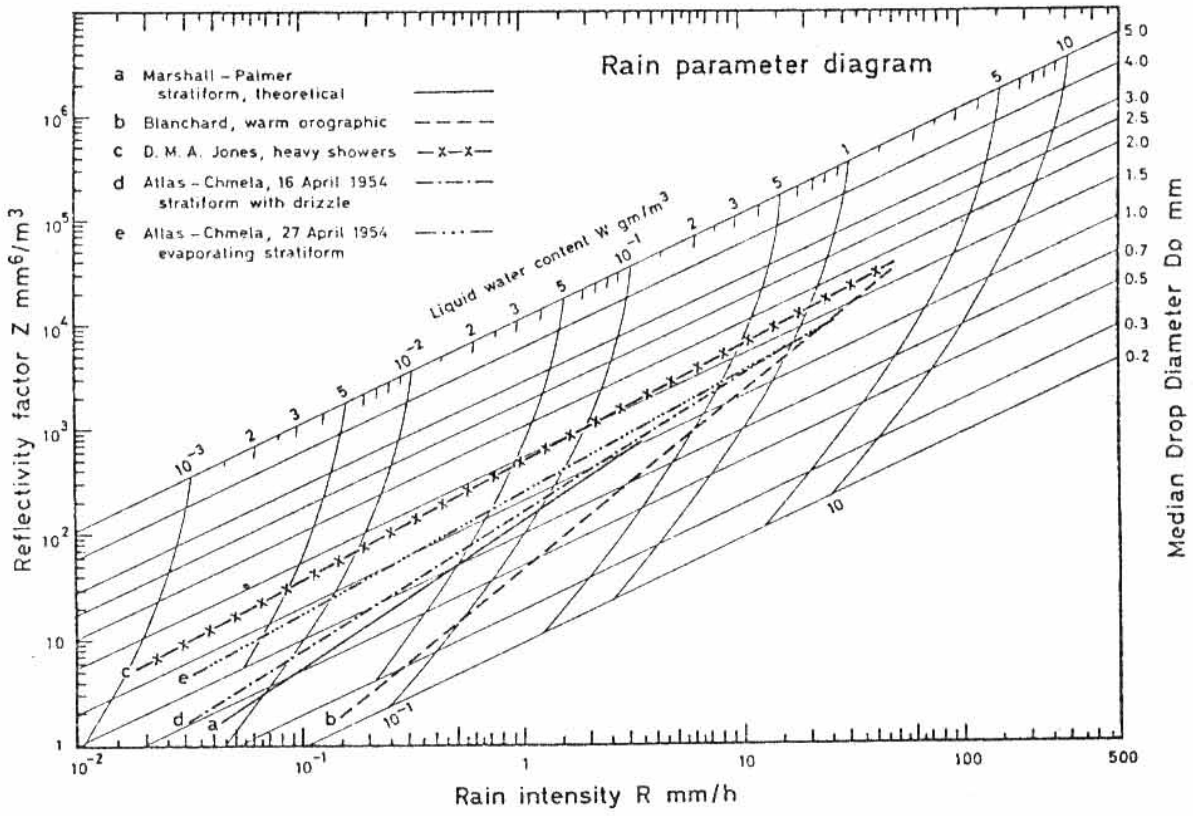

Fig. 10. 4 (2) A rain parameter diagram based on the two assumptions that the total mass W of raindrops in unit volume falls with the velocity of the median volume drops (of diameter D_o) and that a statistic of the size of the spectrum of drop diameters has a commonly found value of 1.5. The diagram is valid for normal surface pressure and temperature. Some experimentally derived relations between R and W are shown. (After Atlas and Chmela 1957).

10.4 (1)

Table 10.3 Radar reflectivity / rainfall rate relationships from drop-size spectra made at tropical locations and in tropical cyclones

Investigators	$Z = aR^b$ a	b	Remarks
NON TROPICAL CYCLONE			
Ground observations			
Diem (1966)	278	1.30	Entebbe, Uganda
	240	1.30	Lwiro, Congo
Mueller and Sims (1966a,b)	311	1.44	Indonesia
	286	1.43	Florida
	221	1.32	Marshall Islands, freezing level approx. 5 100 m
Stout and Mueller (1968)	296	1.35	Easterly wave Florida
	196	1.38	Easterly wave Marshall Islands
	196	1.38	Intertropical C.Z. Marshall Islands
Woodley (1970)	300	1.40	Known as the Miami Z-R relationship. Average for tropical systems including thunderstorms.
Austin et al (1976)	230	1.25	Combination of ship and aircraft data from the tropical Atlantic (GATE area).
Aircraft observations			
Cunning (1976)	365	1.41	Measured just below cloud base in Florida cumulus.
Cunning & Sax (1977)	170	1.52	Measured at cloud base level (100-1 200 m) in all rain over the tropical Atlantic (GATE area). Maximum R = 50 mm/h.
TROPICAL CYCLONE			
Ground observations			
Kessler and Atlas (1956)	296	1.47	Hurricane Edna 1954 Maximum R = 74 mm/h
Wilson and Pollock (1974)	350	1.35	Hurricane Agnes 1972 near Lake Ontario and with a freezing level between 3 200 m and 4 000 m.
Hong Kong (1978)	20	2.09	Several tropical cyclones (See Fig.10.) Maximum R = 282 mm/h
Tone River ..., Japan (1975)			From radar/raingage readings in Tone river basin in typhoons Mary and Polly 1974.
	100	1.1	For $R_{1h} < 25$ mm/h
	6	2.0	For $R_{1h} \geq 25$ mm/h
			Maximum R (over 1 h) = 49 mm/h
Aircraft observations			
Scott and Dossett (1972)	300	1.24	In tropical storm Felice 1970.
	260	1.35	In hurricane Debbie 1969.
Jorgensen (1977)			In the eye wall and just below cloud base in hurricanes:-
(Personal communication)	80	1.61	1) Ellen 1971, 1 000 km ENE of Bermuda (about 35°N) Max. R = 70 mm/h.
	420	1.10	2) Eloise 1975 in the Gulf of Mexico. Max. R = 40 mm/h.

10.4.6 Z-R relationships in typhoons

Information on Z-R relationships in tropical cyclones would not only be of scientific interest but would also be of great practical importance in improving radar-rainfall estimates used for the preparation of flood and landslide warnings. However, such observations as are available in this field are disparate (see Table 10.4(1) ~~10.3~~) and there are phenomena awaiting explanation. For example, it is my experience that heavy typhoon rainfall over Hong Kong is considerably underestimated by the use of a 100 mm radar and the $Z = 200R^{1.6}$ relationship (Bell 1969). Stout and Mueller (1963) reported a similar underestimate of hurricane rainfall and, incidentally, in rainfall in the Marshall Islands (Table 10.4(1)) ~~10.3~~). Lewis et al (1976) found that rainfall over the Florida panhandle in hurricane Eloise 1975, as determined by a 100 mm radar and the equation $Z = 300R^{1.24}$, was in close agreement with the readings at raingauge stations for light to moderate rain. However, at stations where rain amounts of 30 mm or more per hour were recorded the radar estimates were substantially lower. A number of Japanese scientists have also reported that radar underestimates the enhanced typhoon rainfall which occurs in the vicinity of mountains in Japan. Their results are discussed in sect 6. . The balance of available evidence therefore seems to indicate that the equation $Z = 200R^{1.6}$ underestimates the heavy rainfall in tropical cyclones over both flat and mountainous terrain.

The great variation in the values of the constants a and b in tropical cyclone rainfall arise because the basic observations have been made in a variety of ways and in a variety of conditions. Those in hurricane Agnes 1972 were made far from the coast, after the storm had lost its tropical characteristics; others have been made in storms with and without oreigenic effects, the importance of which were stressed in sect 6. Some measurements have been made in mature hurricanes over warm water and others in weakening storms over cooler seas. In addition, while most relationships have been derived from drop-size spectra measured from aircraft at varying heights above the ground others have been measured at ground level and yet others have been derived from radar measurements of Z and rain-gauge readings. In addition, problems associated with sampling are involved when comparing Z-R relationships derived from drop-size spectra and radar. The former relate to volumes of the order of 1 m^3

and sampling time of a few seconds while the radar samples are of average conditions in volumes typically of a few cubic kilometres and over periods which vary from minutes to hours. It is not generally realized that the period and method used to determine time averages greatly influence the values found for a and b(sect 10.4.8).

The first simultaneous observations of drop sizes, rates of rainfall and radar returns in a tropical cyclone were made by Kessler and Atlas (1956) in hurricane Edna 1954. Drop-size spectra in rates of rainfall up to 74 mm/h were observed and found to roughly approximate the M - P distribution of eqn (10.4(10)). The smallest and largest ($\geq$ 2 mm) drops were more abundant, and those between 0.5 and 1.5 mm were less abundant than in an M - P distribution. Over the range of rates of rainfall observed (approximately 1 - 100 mm/h) the relations $Z = 200R^{1.6}$ and $Z = 296R^{1.47}$ were close to one another (Fig. 10.4(3)) and the rainfall rate deduced from the latter relationship was in all cases within a factor of 2 of the true rate. The median volume drop size diameter D_o and the liquid water content W ranged up to 2.6 mm and 3.17 g/m^3 respectively. The maximum drop size observed was 4.3 mm.

In hurricane Agnes 1972 Wilson and Pollock (1974) found that the average relationship $Z = 350R^{1.35}$ was fairly constant during the storm. However, at that time Agnes was near Lake Ontario and had been inland for several days, the freezing level was down in the range 3 200 m to 4 000 m, and the storm would have lost many of its tropical characteristics.

Measurements made in typhoons Mary and Polly 1974 with the Tone river radar pluviometer (see sect 10.4.7) indicated that different equations were necessary to estimate separately the light and heavy rainfall. This is in accordance with the findings of Lewis et al (1976) in hurricane Eloise. For rain yielding more than 25 mm in one hour the Japanese results were best fitted by the equation $Z = 6R^{2.0}$. Table 10.4(2) shows rainfall rates corresponding to some reflectivity factors and selected Z-R relationships. At low reflectivities rainfall estimates from the appropriate equations are not greatly different. For high reflectivity factors the widely used equation $Z = 200R^{1.6}$ yields the lowest rainfall rates. Table 10.4(2) and the foregoing discussion suggest that at high rates of rainfall there may be proportionately less large drops in tropical cyclone rain than in a M - P distribution.

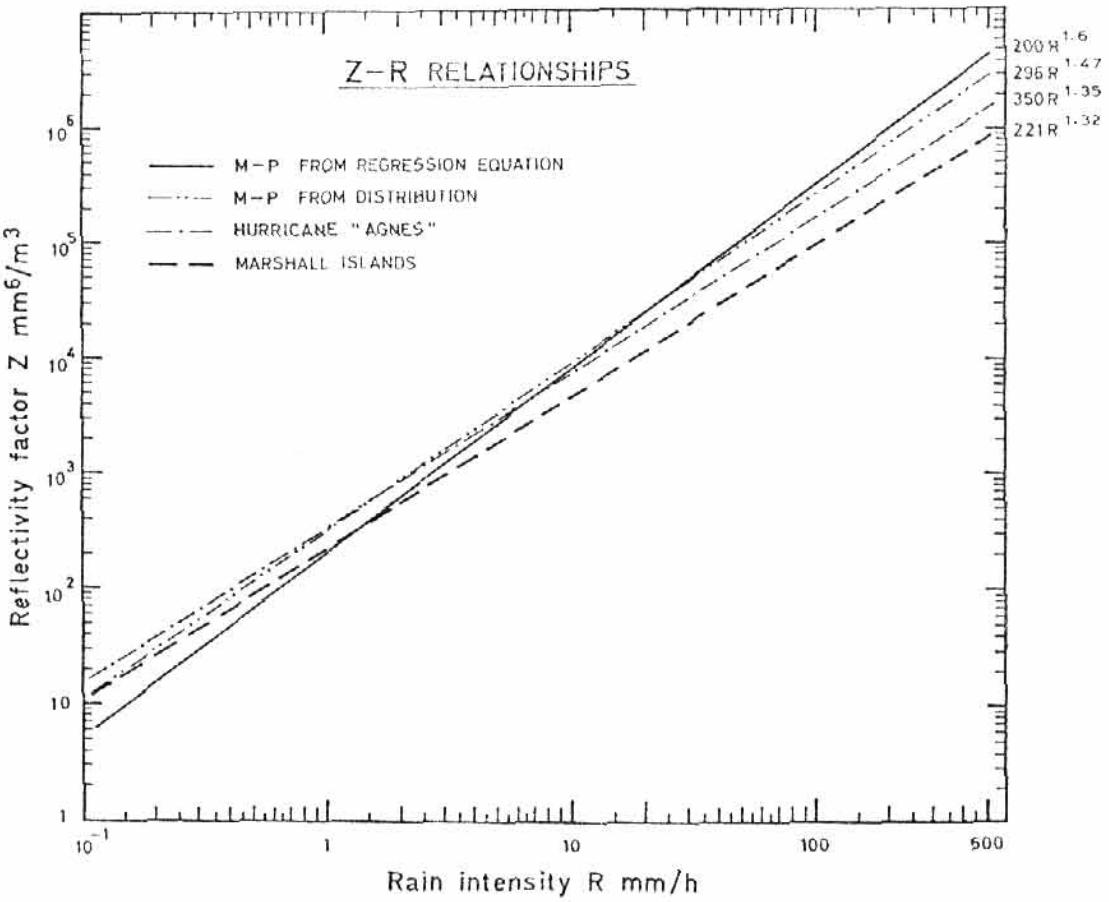

Fig. ~~10.6(3)~~ 10.4(3) Plots of some empirical relationships between Z and R.

Table 10.4 (2) Radar reflectivity factor Z and equivalent rainfall rate R for different Z-R relationships

Z mm^6/m^3	dBZ	$6R^2$	$20R^2$	$200R^{1.6}$	$170R^{1.52}$	$300R^{1.4}$	$221R^{1.32}$	$230R^{1.25}$
					R mm/h			
10^6	60	408	224	205	302	328	588	814
3.16×10^5	55	229	126	100	142	144	246	324
10^5	50	129	71	49	66	63	103	129
10^4	40	41	22	12	15	12	18	20
10^3	30	13	7	2.7	3.2	2.4	3.1	3.2
10^2	20	4.1	2.2	0.6	0.7	0.5	0.5	0.5
10	10	1.3	0.7	0.15	0.16	0.09	0.10	0.08
1	0	0.4	0.2	0.04	0.03	0.02	0.02	0.01
10^{-1}	-10	0.1	----------		D R I Z Z L E		----------	

Two main types of rainfall can be identified in tropical cyclones namely, light to moderate, steady, background rain formed in high and medium level clouds and amounting to 25 mm or less in one hour and, the heavier rain associated with strong convection in the eye wall and spiral rainbands and which can yield 100 mm or more in one hour. (See Fig. 6. Chap ( ) The former originates just below the 0^{o}C level (about 5 km) from melting snow with drop sizes appropriate to a M-P distribution. The heavier rain is formed, in varying degrees, by the warm coalescence process in strong convection. A bright melting band may or may not be present according as to whether the upcurrents near the 0^{o}C level are less or greater than 1 m/s. As rain from either process falls, the drop-size distribution will change according to the depth, water content and updrafts in the lower clouds and the presence or absence of oreigenic cloud and rain. The processes involved in changing the spectra will include (a) coalescence of raindrops of different sizes (b) the growth of raindrops by accretion with cloud droplets; (c) the differential rates of evaporation of drops of different sizes when falling between cloud base and ground and (d) the disruption of large drops in turbulence and collisions. These processes have been simulated in mathematical models and in laboratory experiments but we are not yet in a position to predict ground level spectra in heavy tropical cyclone rainfall.

Mason and Ramanadham (1954) showed that when a flux of raindrops, having an initial M-P distribution, falls through 1 km of cloud with liquid water content of 0.2 g/m^3 the rate of rainfall and the number of larger drops are increased while the smaller drops are depleted. However, in heavy typhoon rain the fall distance will be several kilometres and the water content an order of magnitude greater than assumed in the model. Studies on the collision, coalescence and breakup of large drops at terminal velocities in wind tunnels by McTaggart-Cowan and List (1975), Cotton and Gokhale (1967) and others have shown how collisions in heavy rain lead to the breakup and depletion of large drops. List and Gillespie (1976) modelled the evolution of raindrop spectra by collision-induced breakup and concluded that drops with diameters larger than 2-3 mm, falling in a population of smaller drops typical of natural rain, break up in 1-5 minutes in rainfalls of 100 mm/h. Large drops (4-6 mm) should therefore be scarce in steady state warm rain because they break up in collisions and rarely reach diameters larger than 2.5 mm.

Under such conditions drops could not attain the so-called critical diameter of 5-6 mm at which they are supposed to break up because of aerodynamic instability. In a subsequent discussion with Willis and Merceret (1977), List and Gillespie conclude that drops in the size range 0.5 to 1.0 mm may control the speed of the breakup process and, further, that 1) sufficiently homogeneous warm rain generally consists of relatively small drops and 2) the occurrence of large drops in the range 4-6 mm points to their origin from the cold rain process. Small drops are formed by both processes. Takahashi (1978) used a warm cloud model to show that the inclusion of drop breakup by collision sharply decreased the large raindrop size range and produced a secondary maximum of drop concentration in the normal raindrop size. This peak is consistent with that found in natural warm cloud rainfall and is larger than that derived by similar models which do not include the collision breakup process. Finally, Kessler and Atlas (1956) suggested that intense low-level, mechanical turbulence in tropical cyclones may breakup bigger drops before they reach the critical 5-6 mm size. These processes which deplete the larger drops by breakup processes reduce the reflectivity factor Z corresponding to given rainfall rates.

Observations of drop-size spectra at ground level in heavy (≥80 mm/h) tropical cyclone rainfall are not yet available in sufficient quantity to reliably resolve these issues. Merceret (1974a) analysed drop sizes observed from aircraft flying at 1 500 m, where the temperature was about 17°C, in hurricane Ginger 1971. He found them to be surprisingly well represented by eqn (10.4(10)) both in rainbands and in the eye wall but, as found also by Kessler and Atlas (1956), there were somewhat fewer drops of diameters less than 1 mm than are indicated by the formula. Figure 10.4(1)(b) ~~10.4(b)~~ shows a typical spectrum from these flights. The volume mean diameter of the droplets was of the order 1 mm with the volume median diameter D_o being about 1.5 mm. Merceret (1974b) also examined the distributions of rainfall in hurricane Felice 1970 as observed by aircraft flying in cloud at 4 000 m, and 150 m below cloud base at 450 m. Of the high level samples, 92% had correlation coefficients of 0.9 or more with the classical exponential distribution. Below cloud, only 50% showed such a good correlation. The mean-volume droplet diameter in cloud was 1.03 mm whilst that below cloud was 1.45 mm. The liquid water content remained near constant at 0.935 g/m^3 in cloud and 0.930 g/m^3 below. His results indicate that while the distribution of drops in cloud at 4 000 m in Felice well approximated a M-P distribution, considerable changes in the spectra took place during the fall in cloud and below cloud base in the manner predicted by Mason and Ramanadham (1954). Willis and Merceret (1977) report that in tropical storm Felice there were substantial numbers of drops >3 mm in diameter at levels from below the 500 m cloud base to near the 0°C level at 4.5 km. In the spectra from which Fig. 10.4(4) ~~10.7~~ has been derived many contained significant numbers of drops > 2.5 mm in diameter. Willis and Merceret (1977) consider that Fig. 10.4(4) ~~10.7~~ suggests that there are two groupings of spectra which might reflect whether active convective updrafts were involved in the rain formation or whether the drops grew largely under the influence of gentle or no updraft.

More experimental work is required before we can decide in which circumstances to use which particular Z-R relationship to estimate typhoon rainfall. However, in many regions, it is of great practical importance that heavy typhoon rains are not underestimated. Therefore, when strong radar echoes are observed in typhoons it would seem prudent either to use one of the equations appropriate to strong convective conditions e.g. the Miami $Z = 300R^{1.4}$ or the Marshall Islands $Z = 221R^{1.32}$ - or to determine an appropriate relationship, in real time, as is described in sect 10.4.8.

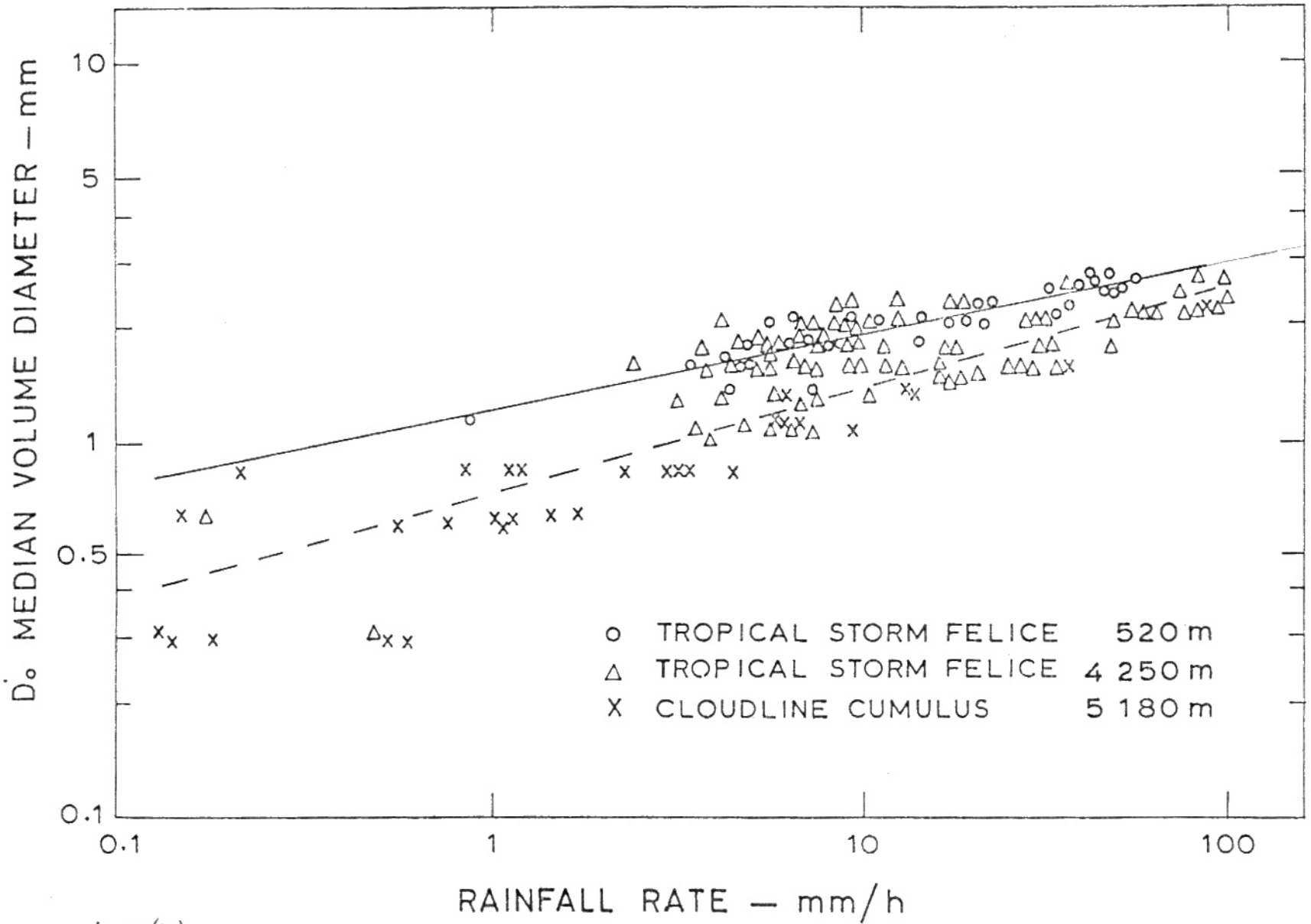

10.4(4)

Fig. ~~10.7~~ Median volume drop diameter D_o versus rainfall intensity from drop-size spectra taken onboard aircraft in tropical storm Felice (5 Sept. 1973) and cloud line cumulus. (After Willis and Merceret 1977.)

10.4.7 Iso-echo contours

Atlas (1947) was the first to show that circuits can be added to a radar receiver so that echoes having intensities within certain limits show on a PPI display at one level of brightness. Several such intensity ranges can be selected and each made to correspond to a different shade on the display. In this way a contour effect can be produced in rain clouds such that edges of the shaded regions correspond to lines known as "iso-echo contours" which correspond to some pre-set intensity. If the Z-R relationship is uniform throughout the storm then these lines correspond to "isohyets" showing the distribution of rainfall intensity.

In Fig. 10.4(5)(a) typhoon Dot 1973 is shown centred inland over South China about 65 km northeast of the Hong Kong radar. In Fig. 10.4(5)(b) the same typhoon is shown using iso-echo circuity. In this particular case the intensity ranges were chosen on the assumption that $Z = 200R^{1.6}$. Rainfall rates below about 1 mm/h appear black, the second brightest shade corresponds to a rate of rainfall of between 1 and 12.5 mm/h, the brightest shade to 12.5 to 25 mm/h and the third brightest shade to rates between 25 to 100 mm/h. Rainfall rates greater than about 100 mm/h appear black again. It is, of course, the intensity of the returned echo which determines the shade. The exact rates of rainfall associated with the contours are unknown unless calibrated against rain-gauges or disdrometers. Note that even the conservative rainfall rates, which derive from the use of $Z = 200R^{1.6}$ still yield black areas ($R \geq 100$ mm/h) in most rainbands.

In this figure the ground echoes have an intensity which is greater than that which corresponds to a rainfall rate of 100 mm/h. They therefore appear black on the PPI as do the returns from light rain with an intensity of less than 1 mm/h. The second brightest shade (1 to 12.5 mm/h) should appear on the outside edge of the brightest echoes but it is not clearly seen because strong convective showers have sharp edges with steep gradients of rainfall rate. The third brightest shade (25 to 100 mm/h) can be seen next to the black core (greater than 100 mm/h) of the large rainband about 40 n miles (74 km) southwest of the radar. When the centre of typhoon Dot, with a minimum pressure of 975 mb, crossed the Royal Observatory the peak rate of rainfall recorded on the Jardi gauge was 218 mm/h (about a 15 s mean) in the northwest part of the eye wall. On the southwest side of the eye, about one hour before the photograph in Fig. 10.4(5)(b) was taken, the

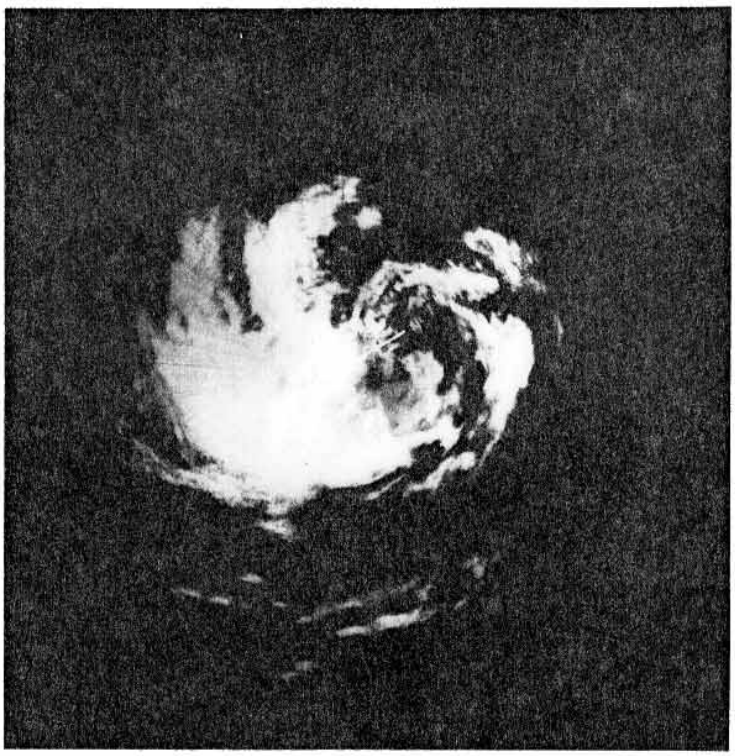

(a)

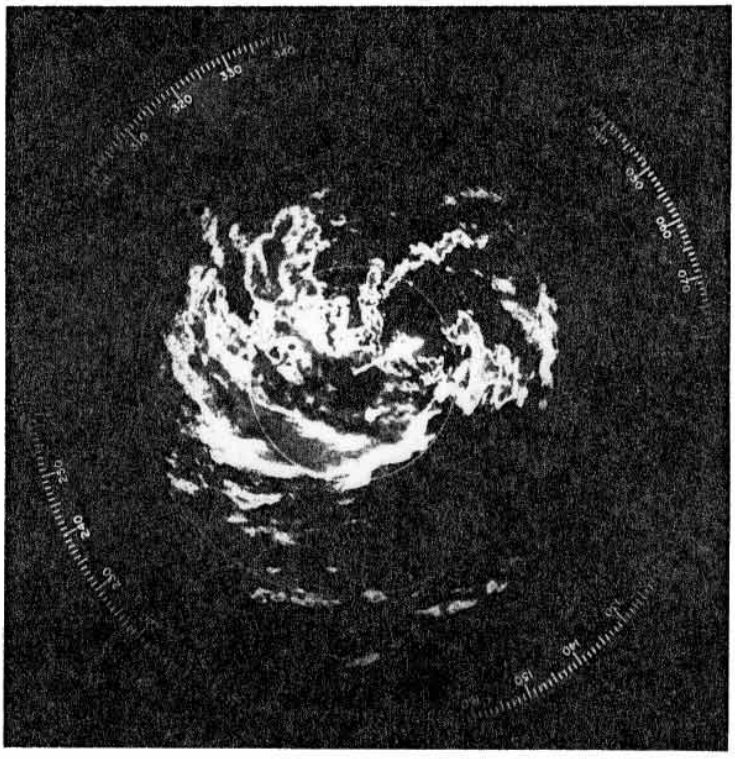

(b)

10.4(5) moving towards the NNE

Fig. ~~10.8 (a)~~ Typhoon Dot ^ at 2340 GMT on July 16th 1973 centred inland about 35 n miles (65 km) northeast of Hong Kong. (b) The same as (a) but with the iso-echo facility switched in. See the text for details. Range rings are at intervals of 40 n miles (74 km).

Jardi gauge at the radar station recorded a peak reading of 170 mm/h.

Several advantages arise from the occasional use of iso-echo displays when tracking tropical cyclone. It gives an immediate indication of areas having high rates of rainfall, it facilitates the identification of rainbands (and associated squalls) embedded in light general rain and, if the higher intensity returns are made to correspond to zero brightness (black) then it minimises ground clutter - and, unfortunately, any rain returns in the same area (but see Sect. 10-2.). These advantages often enable the centre of a cyclone to be more readily identified as illustrated in Fig. ~~10.8 (a) and (b).~~ 10.4(b).

10.4.8 Measurement of rainfall over an area

The simple methods of measuring Z by radar, described in sect 10.4.4 and 10.4.7, can be used with a recommended convective Z-R equation to identify areas of heavy rainfall in typhoons with an accuracy quite adequate for the purposes of preparing warnings of flash floods and landslides. However, for reservoir control, river control, the warning of floods from river basins and other important hydrological uses involving time and area integration of rainfall, more sophisticated techniques are required. It is fortunate that, although there are many sources of error affecting radar estimates of the rainfall at a point on the ground, the accuracy of the measurements increases when they are averaged over extended areas of space and longer periods of time. The main problems and developments in this field, and their relevance to typhoon conditions will be discussed in this section.

The errors inherent in the measurement of rainfall by radar can be large and are due to meteorological and radar-propagation effects and to instrumental errors of measurement. Furthermore, there are difficulties associated with the processing and validation of the observations. The instrumental errors arise primarily from the difficulty of maintaining the stability of calibration of the transmitter power and of the sensitivity of the receiver. It is now generally considered that good practice can keep this error to within $\pm$ 3dB - corresponding to + 33% and -25% in rainfall rates. However, it is known that sufficiently careful maintenance is often lacking so that many radars operate 10 or more dB below specification and some are never calibrated (sect 10.5.4).

In addition to errors caused by maintenance deficiencies there are inaccuracies in measuring the average received power by most commonly used techniques.

Power from the main beam and from the side lobes is usually returned to the radar from the ground in varying degrees. The amount returned depends on the nature and topography of the terrain and its moisture content, the weather, atmospheric propagation conditions and on the bearing and elevation of the aerial. It is not unusual for the power returned from the ground within 30 km of a radar to vary by 5dB (more than 3 times) between one fine day and another (Tone River Office 1975).

Rain lying between a storm under examination and the radar will attenuate the radar beam during both its outward and return journey. This will result in a decrease in power received and lead to an underestimate of Z. It is difficult to accurately compensate for this effect because it depends on the unknown drop-size spectra along the path. At wavelengths, shorter than 100 mm, the effect is severe and is ~~compound~~ made worse by the two-way losses caused by water on the radome. If longer wavelengths are used to alleviate this problem - as is essential in typhoon conditions - it is necessary to use larger aerials to keep the beam width as small as possible to minimize unwanted ground returns and increase the likelihood of a storm filling the beam.

There are many meteorological effects which give rise to errors in rainfall measurements. The problem of determining the appropriate Z-R relationship is one and Table 10.4 (2) suggests that this can be a prime source of error in tropical cyclone conditions. Several drop-size spectra can coexist within the volume of a storm sampled by a radar beam. Large errors in the measurement of Z arise if the rainstorm does not entirely fill the beam or if there are strong gradients of Z within the sampled volume. The presence of a melting band in the sampled volume may also give rise to errors. If updrafts are strong, raindrops in storms observed on the radar PPI may not be falling; they can remain suspended in the air for some time and be carried some kilometres away. Raindrops may continue to grow in their fall below the radar beam, especially when this is high above the ground as is the case with distant storms. When falling through clear air drops may evaporate between cloud base and ground. Size sorting of the drops can

occur in wind shear. Vertical air currents cause the radar-derived value of R to differ from that near the ground where vertical currents are negligible. Moreover, and especially in high wind conditions, there can be large displacements between the place where the radar sees rain and the place where these drops subsequently reach ground. Figure 10.4(6) illustrates some of these meteorological effects. The assembly of raindrops associated with the vigorous convective updraft of the extreme right of (a) rises rapidly to above the $0^{o}C$ level (b) and then begins to fall. However, the drops do not reach the ground in (c) - probably because of upcurrents or evaporation - and in (d) and (e) it is probable that updrafts are preventing them from falling at normal velocities. The raindrops fall slowly from (b) to (e) and finally reach the ground in (f) - some 22 km from where they originated 70 minutes earlier. The trajectory of the assembly of raindrops is shown in (e). Suspended rain like that shown in Fig.10.4(6) is often seen. It may be associated with the cessation of a strong burst of convection, with the shearing of a tall convective tower or with rain formation in medium-level clouds.

In storms in the humid tropics in general and in tropical cyclones in particular some of the meteorological factors adversely affecting the accuracy of rainfall measurement are minimized. This is especially so in measurements of significant rains in excess of 25 mm/h. The melting band is found at a height of 4 km or more and should not interfere with measurements of Z. In addition the atmosphere between cloud base and ground maintains a relatively steady temperature and high humidity and should minimize extreme variations in the rate of evaporation; the power returned to the radar from these tropical storms is large compared to extraneous returns and their size ensures that beam filling problems are less. Against these advantages must be set the effects of strong updrafts and displacement of falling rain by strong winds in typhoons.

Since much of the variability in the Z-R relationship is due to updrafts, wind sorting, displacement and similar time - or space - dependent phenomena, the accuracy of rainfall measurements by radar can be greatly improved by averaging in space and time. Wilson and Pollock (1974) carried out a comprehensive experiment in rainfall measurement over several days in the remnants of hurricane Agnes 1972. They used three radars with special instrumentation for averaging received signals, many rain-gauges and a disdrometer to measure raindrop sizes. After correcting for all known sources of error, the uncertainties resulting

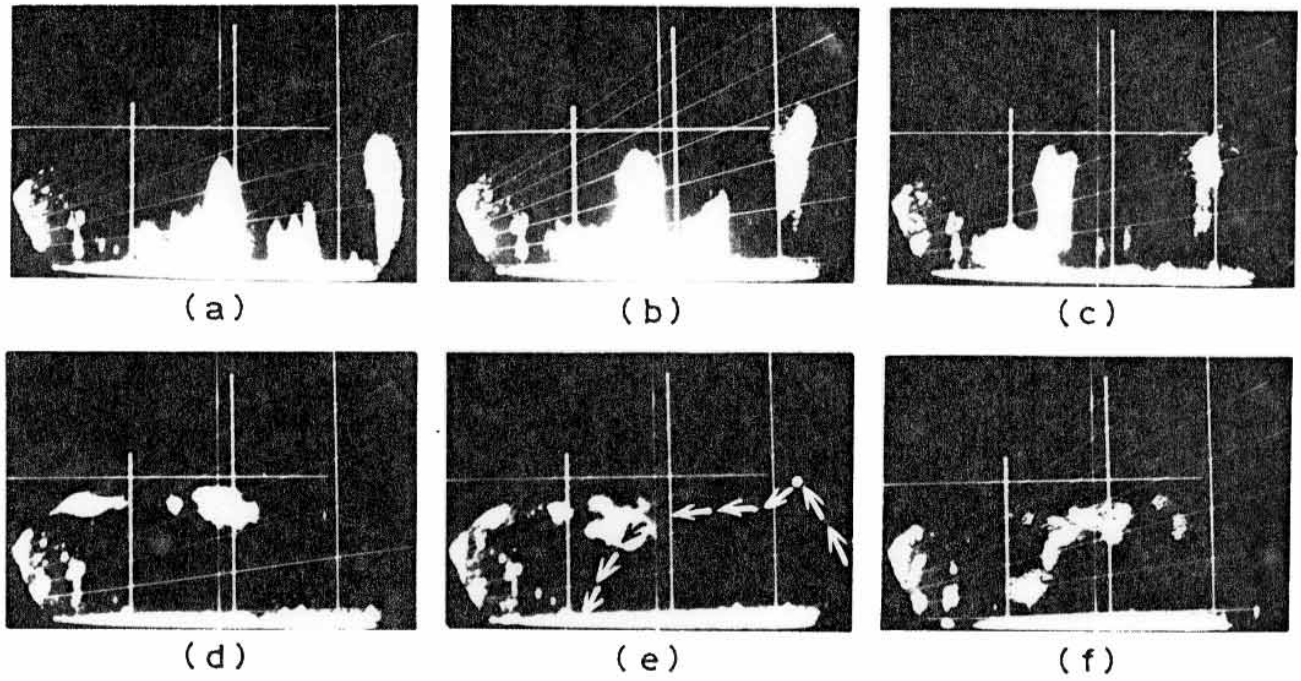

Fig. 10.4(6). Frames at approximately 14 min intervals from a 16 mm time-lapse film of the RHI of the Hong Kong 100 mm radar. Range markers (vertical) are at intervals of 5 n.mile (9.3 km) and elevation markers every 5°. The horizontal height marker is at 6 km. The level of the 0°C isotherm was near 5 100 m. The radar was directed along a bearing of 107° on the 18th July 1969 from about 0358 to 0508 GMT at which time a weak circulation was centred about 460 km to the southeast.

from meteorological effects were much greater than those in measuring Z. Rainfall rates indicated by the radars were more highly correlated with each other than with rain-gauge readings while the Z-R relationship, determined from the disdrometer records, remained essentially constant at $Z = 350R^{1.35}$. The inaccuracies increased and tended towards greater underestimates as the height of the radar beam above the ground increased; beyond about 130 km the magnitude of the radar underestimate increased rapidly. When the radar beam was less than 1.8 km above the ground, 99% of the hourly radar estimates were within 30% of the rain-gauge measurements. This effect places a practical limit on the range at which useful radar rainfall estimates can be made. The results of this experiment are given in Table ~~10.5~~ 10.4(3) and show that, although the ratio of radar to rain-gauge rainfall varied from 0.4 to 2.9 for averages over 8 to 17 hours the total storm averages, from both radars were good.

The accuracy of rainfall estimates over a catchment not in a hilly or mountainous area may be improved by continuously adjusting the radar estimates of rainfall over one or more raingauges to agree with the gauge readings. For this purpose the rain-gauge measurements are telemetred to the radar station. Calibrating factors obtained by comparison are then applied to the radar estimates over the catchment as a whole. A computer is usually used to determine the calibrating factors at gauge locations, to make averages over space and time, to minimise the effects of permanent echoes by removing the echoes and replacing them by an average of any peripheral rain signals, to allow for the displacements of rain by wind and in some measure, for 100 mm radars, to correct for attenuation. Some correction can also be made for ground returns but this is subject to error as already explained. Care must be taken to ensure that the calibrating rain-gauges are sited so as to give readings representative of the whole area otherwise, the non-representative reading will affect all the other estimates in the catchment. The accuracy of this method improves with increasing area out to the limits imposed by beam height.

A sophisticated radar rain-gauge system, sometimes called a radar pluviometer, was established in 1967 over the Tone river basin by the Japanese Ministry of Construction (Tone River Office 1975). The rainfall measurements were used to assist in the control of reservoir

Table 10.4(3) Comparison of the average rainfall over a raingauge network as determined by two radars and raingauges near Lake Ontario in hurricane Agnes 1972

Date/hour (GMT)	Averaging Period h	Network raingauges average mm	Buffalo radar (λ = 105mm) mm	Oswego radar (λ = 54mm) mm
21 June/00 - 21 June/17	17	4.6	7.4 (1.6)*	13.5 (2.9)
21 June/18 - 22 June/10	16	15.5	20.1 (1.3)	31.0 (2.0)
22 June/11 - 22 June/21	10	17.0	7.6 (0.5)	6.9 (0.4)
22 June/22 - 23 June/06	8	33.3	16.8 (0.5)	17.5 (0.5)
23 June/13 - 24 June/06	17	12.9	18.3 (1.4)	14.5 (1.1)
21 June/00 - 24 June/06	78	83.3	71.6 (0.9)	83.1 (1.0)

* Radar/raingauge ratios are given in brackets.
(Adapted from Wilson and Pollock (1974))

levels during heavy rain. The system is comprised of 30 rain-gauges which telemeter their readings to a computer and a 53 mm radar sited on a hill top. The radar measures the average power in each of approximately 4 000 meshes defined by the intersection of circles - 3 km apart and centred on the radar - and 128 sectors of angle 2.81^{o}. The meshes extend out to 102 km and the power received from each is digitised, totalled and averaged over a 5-minute period. The rain-gauges were sited more than 10 meshes (30 km) away from the radar so that their readings could be compared with the power returned from the appropriate meshes without contributions from ground returns. The choice of the 5-minute averaging period was shown to be crucial for the success of radar methods of measuring rainfall. This arises because the rate of rainfall R and the reflectivity factor Z can vary greatly within longer periods. This fact, and the ~~non-linear~~ power-law relationship between Z and R make the use of longer period averages in the equation inappropriate. It was shown that if long period averages of Z and R were used they led to widely varying values for both a and b.

Initially, the power returned from each mesh was to be corrected in the computer for ground returns and then converted to Z. This in turn was converted to R using values of a and b derived from a best fit to the appropriate control-gauge readings. These values of a and b were then used to derive the rainfall rate in the other meshes which, in turn were used to compute corrections for attenuation to be applied to the rainfall rate in all meshes. The resulting rainfall distribution was then compared with that derived from the 30 rain-gauges. However, many problems were encountered in practice. The variables of rainfall rate, power returned, distance and a and b related by equation (10.4(11)) ~~(10.13)~~ were found not to be correlated.

The true ground return at any time was unknown and energy scattered in different directions from side lobes by the ground or from the main beam by hills illuminated raindrops and so added to the energy they returned to the radar. The correction for attenuation which also has an exponential form, could at times be grossly in error. The computations would have required a big computer sited alongside the radar if the results with all their errors, were to be timely.

The procedure subsequently adopted was to fix the Z-R relation at $Z = 100R^{1.1}$ for light rain and $Z = 80R^2$ for rainfall greater than 25 mm/h. These values were found to give best results for use with 5-minute averages in the conditions appropriate to the experiments. In addition, the power received was reduced by a "geographic correction" which was assumed constant for each mesh. It represents the contribution to the received power from ground returns of various kinds including indirect returns. The geographic correction was based on experimental results and on the nature of the topography. With these adjustments the system was used to determine rainfall totals at selected rain-gauges during the passages of typhoons Mary and Polly in 1974. 76% of the hourly totals were within 20% of the gauge readings and the ratio of all the 3-hour radar measurements to the corresponding gauge readings were within the range 0.7 to 1.2. Perfect agreement is not to be expected because of the difficulty of relating the radar measurements for an area with those of a rain-gauge which refer, effectively, to a point.

The attenuation of microwaves of wavelengths near 10 mm is almost linearly related to wavelength (Ryde 1947). It is therefore possible to use such waves to obtain the integrated rainfall rate over a transmission path. Atlas et al (1977) make proposals for making such measurements and recommend, inter alia, that an one-way path between transmitter and receiver is the most suitable for measuring high rates of rainfall because an out-and-return radar beam will be totally attenuated over a path of 30 km at rainfall rates in excess of about 15 mm/h. The non-sphericity of falling raindrops and their preferred orientation causes attenuation to be greater for horizontal polarisation than for vertical polarisation (Oguchi and Hosoya 1974). Measurements should therefore be taken at both polarisations to achieve greater accuracy. Indeed, the conventional methods of making rainfall measurements by radar, as described earlier, can be improved by measuring the intensity of rainfall returns using both horizontal and vertical polarisation. Big drops are flattened more than small ones so that the ratio of the two measurements can be used to give some information on drop size distributions - in particular D_o, the diameter of the median volume drop - and corresponding rainfall rates (Seliga and Bringi 1976). Very few meteorological radars have the facility for changing their polarisation setting. The use of polarisation techniques is therefore limited at the present time but holds promise of being of value in tropical cyclone conditions.

It is clear that rainfall rates and rainfall totals in tropical cyclones can now be measured with an accuracy sufficient to make them of inestimable value to meteorologists and hydrologists alike. Notwithstanding the complexity of the subject and the many sources of errors, good radar practice can yield acceptable results out to about 100 km. Depiction of the instantaneous, relative rainfall distribution over a river basin, even if the absolute values are in error by a factor of two or so, is a great advance over the information available from conventional networks of rain-gauges. For example, it is not unknown for tropical thunderstorms and tropical cyclone rainbands to cause flooding in a basin without any rain-gauge there having recorded rain.

10.5 Radars for Tracking Tropical Cyclones

10.5.1 Specification

To locate and track a tropical cyclone for operational purposes a radar should be able to show the eye wall of the storm at a range of 300 km or more and be able to continue operating in the severe weather conditions which occur when the eye is at close range. A radar which cannot delineate the eye at a range of 300 km will often be unable to provide information in time to enable adequate warning to be given. Indeed, it is probable that gale force winds will already have occurred at the radar station (see Fig. 4.). Similarly, a radar which breaks down or has its efficiency impaired by heavy rain, lightning, flooding or gusts of hurricane force, all of which can occur long before the passage of the eye of a mature typhoon, will cause the loss of information which is vital for the tracking of the centre and the preparation of wind, flood and storm-surge warnings.

For the eye of a typhoon to be displayed on radar it is necessary to detect the rain in the eye wall even if the whole distance between eye and the radar is filled with heavy rain. This latter criterion implies that the radar wavelength must be in the S or L bands (100 to 230 mm). The poor performance of radars operating at shorter wavelengths in heavy rain is illustrated by the curves in Fig. 10.5(1) and in Fig. 10.3(2) the example. If the wavelength is fixed then eqn (10.4(4)) indicates that the average power of the returned signal $\bar{p}_r$ will increase as the size of the aerial, the transmitted power and the pulse length are increased. The ability of the radar to detect distant light rain will also be enhanced if the receiver sensitivity is increased so that weaker signals can be detected. In practice, the choice of radar parameters is a compromise between conflicting factors one of which is cost.

The pulse length must not be so long as to significantly impair resolution; for two objects to be seen as separate targets they must be separated by a distance of a half a pulse length or more. A 5 μs pulse has a length of 1.5 km and will resolve targets separated by 750 m; a lower resolution than this would not be desirable. If a wavelength

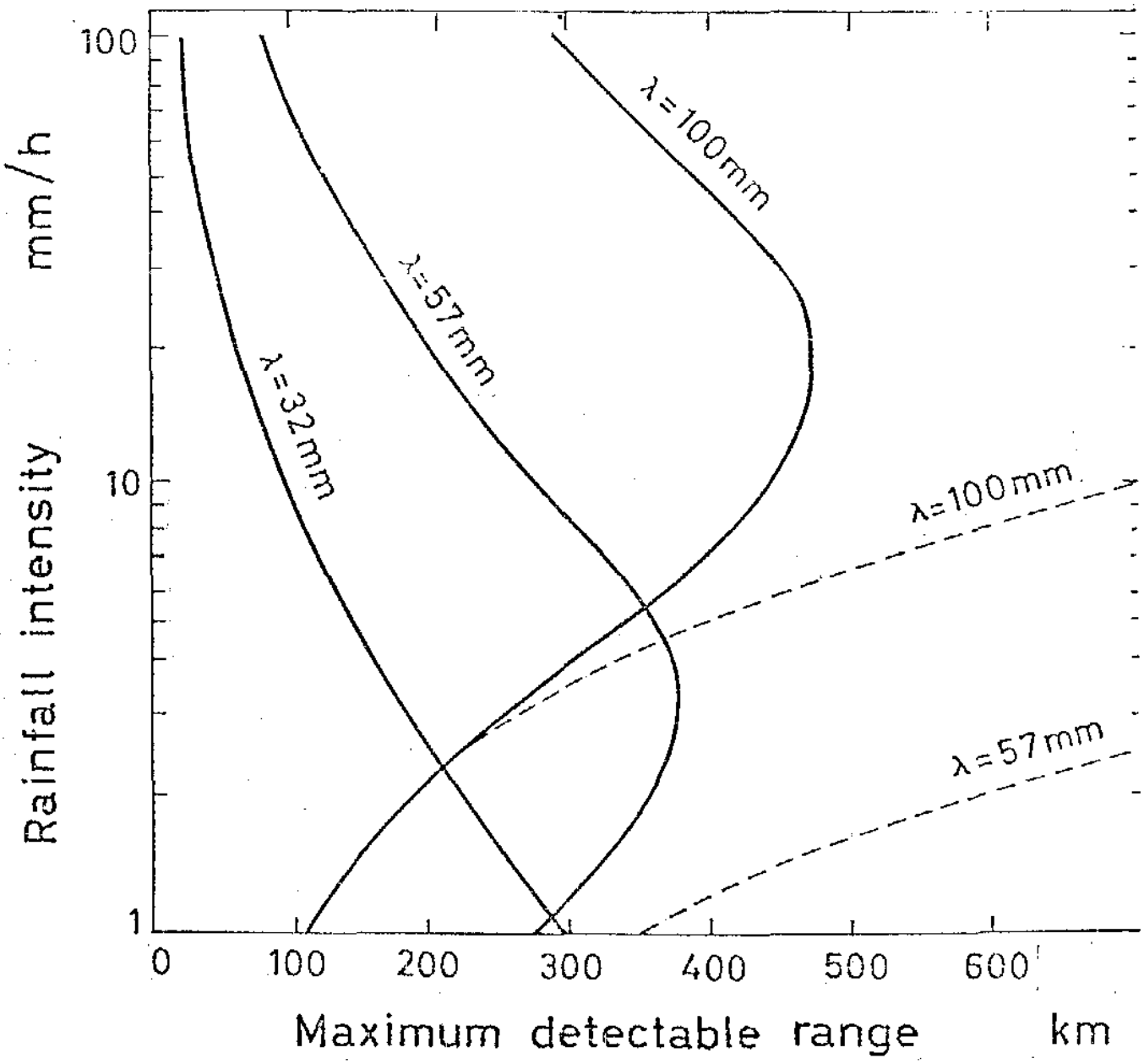

10.5(6)

Fig. ~~10.10~~ Comparison of the capabilities of radars using different wavelengths for detecting distant rainfall. The full line is for a path filled with rainfall of indicated intensity and the dashed line is for a path to this storm through clear air. The radars have a power of 300 kW, an aerial of diameter 3 m and a receiver sensitivity of 10^{-13} W. The range is the radial distance to the storm. (After Kashimoto and Udea 1967).

of 230 mm is chosen for the radar then eqn 10.4(4) shows that, relative to a radar working at a wavelength of 100 mm, the power transmitted p_t and/or the effective aerial aperture A_e must be larger to achieve the same received signal $\bar{p}_r$. High-power transmitters and large aerials are expensive both to purchase and to maintain. Accordingly, a wavelength of 100 mm is normally preferred to one of 230 mm. Furthermore, the performance of the radar at the chosen wavelength and pulse length will be determined by the receiver sensitivity on the one hand and the aerial efficiency and transmitted power on the other. It is again less expensive to build and operate sensitive receivers than to build and operate large aerials and powerful transmitters. It is therefore usual to use a receiver which is as sensitive as possible without recourse to sophisticated and expensive amplifiers which need to be cooled to low temperatures. The transmitter power and aerial size are then designed to be large enough to enable extensive storms with rainfall rates of about 1 mm/h to be detected at maximum range. Most current meteorological radar receivers use amplifiers known as "travelling wave tubes" but the more sensitive "parametric" amplifiers are now being introduced.

In Fig. 10.5(2) the PPI presentation of typhoon Iris 1970 by (a) a 650 kW, 100 mm radar with an aerial aperture of 2.9 m^2 is compared with that in (b) of a 230 mm radar having more than 3 times the power and an aerial of about 12 times the aperture. From eqn 10.4(4) the latter radar should receive approximately 1.2 times the average power received from the same target by the 100 mm radar. The 230 mm radar has the additional advantages of being sited 390 m higher and having a more sensitive receiver. There is seen to be a one to one correspondence of most of the rain echoes in Fig. 10.5(2) except that the higher and more powerful radar sees slightly more of the rain band which lies along a bearing of about 225° at ranges between 100 and 150 n miles and on the 230 mm radar two echoes are visible at 130°, 130 n miles and at 155°, 165 n miles which do not appear on the 100 mm radar display. The reasons for the lack of sea clutter and returns from mountains on the 230 mm display are discussed in sect 10.8.4.

In order to get as many pulses back from a target as possible the pulse repetition frequency (prf) should be as high as is permitted by the requirement for a pulse to make the journey to maximum range and back before the next pulse is transmitted. For a range of 450 km, a prf of less than 300 per second would allow at least 3.33 ms for the two-way trip.

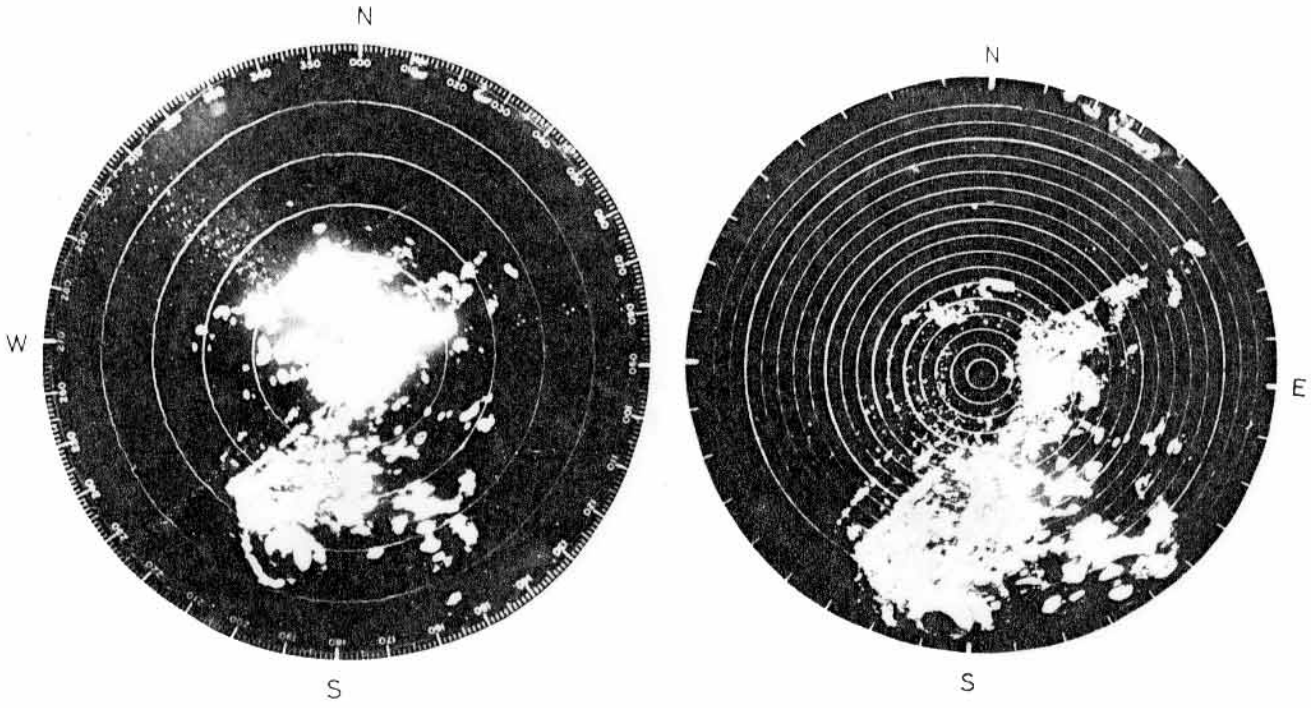

(a) (b)

10.5(2)

Fig. ~~10-13~~ Typhoon Iris 1970 with minimum central pressure of 960 mb and maximum winds of 45 m/s, as seen on 6th October at 0340 GMT by (a) a 100 mm 650 kW radar at Hong Kong and (b) a 230 mm 2 MW radar on a nearby hill. Range rings are at 40 n mile intervals in (a) and 10 n mile intervals in (b). The radars are sited at 568 m (a) and 958 m (b) above mean sea level.

In summary, the ideal radar for tracking tropical cyclones will operate on a wavelength of 100 mm (polarization is discussed in sect 10.8.1) and will have a pulse length of 2 to 5 μs preferably with an option to switch from long (say 4 μs) to short (say 1 μs) when high resolution is required. The receiver will be as sensitive as is practically possible and the peak transmitted power and aerial size will be large enough to enable the eye of a mature typhoon to be detected at a range of at least 300 km. Specifications of some meteorological radars which are used for tracking tropical cyclones are shown in Table ~~10.6~~ 10.5(1). The characteristics of two radars which operate on shorter wavelengths are also given for comparison. Their value for tracking typhoons, however, is limited to occasions when there is much less than the average amount of rain between the radar and the eye wall or when the storm is weak and contains only light rain. I have observed the complete eye wall of a tropical storm about 30 km east of Hong Kong, using a 20 kW 32 mm radar when it could not be seen using an adjacent 650 kW 100 mm set. Similarly, after seeding the eye wall of hurricane Esther 1961, it could no longer be seen with 100 mm radar but remained visible at 30 mm. Simpson et al (1963) attributed this fact to large drops freezing or being replaced by smaller ones. However, for detecting the more destructive typhoons at long range, wavelengths of 100 mm or more are necessary.

10.5.2 Siting

To get the best possible performance from a given radar in the tropical cyclone detection role it is of prime importance that the radar should be well sited, preferably close to the coast and on high ground - ideally a high plateau - so as to get a good "view" of distant rain-bearing clouds which may be below the radar horizon for sets situated at lower levels. Apart from its advantages as an observing location, a radar on a remote mountain site is less likely to have its beam obstructed by future buildings than at lower levels. However, if the radar is on a tower or mountain, then unwanted returns will be received from land and sea surface out to a greater range than for sets at lower altitudes. These unwanted returns from buildings and hills are known as "permanent echoes" and when considered along with returns from the sea are known as "clutter". Towers should be used to give a radar an unobstructed horizon to seaward, but their value for increasing range is limited and should be weighted against the increase in clutter which will result. A 30 m tower increases range by only 20 km (i.e. $113\sqrt{z_2}$ km)

10.5(1)

Table ~~10.6~~. Characteristics of Some Radar Sets Used for Tracking Tropical Cyclones

		MOUNT FUJI	PLESSEY 43S	RAYTHEON WSR-57	TOSHIBA 3173A	MITSUBISHI RC-5	AN/ CPS-9
Transmitted Power Pr	KW	1,500	650	500	600	300	250
Wavelength λ	mm	100	100	100	100	57	32
Aerial Diameter	m	5	3.7	3.7	4	4	2.4
Beam Width	deg	1.5	2.0	1.8	1.9	1.7	1.0
Pulse Duration	μs	4	2	4	2	2	5
Pulse Rep. Frequency	s^{-1}	160	275	200	220	260	186
Min. Detectable Sig. (Approx)	W	6×10^{-15}	5×10^{-14}	10^{-13} to 10^{-15}	1×10^{-13}	2×10^{-14}	2×10^{-14}

At Hong Kong, the Royal Observatory's Plessey 438 100 mm radar is located on a hill top at an elevation of 568 m (Fig. ~~10.12~~ 10.5(3)) and can delineate the eyes of mature typhoons at the maximum range of 460 km (Figs. ~~10.13~~ 10.5(4) and ~~10.29~~ 10.7(4)). The Japanese Meteorological Agencies' high power Mitsubishi radar is sited on top of Mount Fuji at an altitude of 3776 m (Fig. ~~10.14~~ 10.5(5)), and can see typhoons at a distance of 660 km (Fig. 10.5(6)) if the rain-bearing clouds in the eye wall extend to a height of 10 km or more as in Fig. ~~10.32~~ 10.7(7).

When a radar is sited on a hill top it is usual to duplicate the display in the town or airport forecast office, the necessary information being transmitted over a "microwave link" which usually operates on a wavelength of about 40 mm. During the approach of tropical cyclones it is desirable to monitor the displays both at the mountain site and in the forecast centre in case the link should fail. The chosen site should not be susceptible to flooding or landslides caused by torrential typhoon rains and it should afford an unobstructed view to the horizon in directions from which tropical cyclones could approach. The locations of 49 meteorological radars which are used to track typhoons in the Far East are shown in Fig. ~~10.16~~ 10.5(7) together with an indication of their coverage.

10.5.3 Causes of failure

Radars have failed at critical phases during the tracking of tropical cyclones due to such causes as disruption of the public electricity supply, damage from high winds to the aerial, its turning gear or exposed waveguides, damage from lightning or the penetration of rain water into the electronic compartments and waveguides. At 60 m/s rain flies as if discharged from a high pressure hose and it is difficult to stop it from penetrating joints. However, protection from wind and rain can be achieved by the use of a sufficiently strong radome. At a wavelength of 100 mm, or more, the loss of signal strength in the two-way transmission through a well designed dome is small - about 1.5 dB in 100 mm/h rainfall - and quite acceptable. However, at shorter wavelengths the attenuation caused by a wet dome is ~~severe~~ greater and is yet another reason for choosing wavelengths of 100 mm or more. Radomes must be regularly inspected and maintained because their fibreglass panels deteriorate in the strong ultra-violet radiation in tropical sunlight and from repeated stressing in high winds. The domes should be designed to withstand extreme winds - with a return period of 100 years or more - at that particular site. The dome at Hong Kong was built

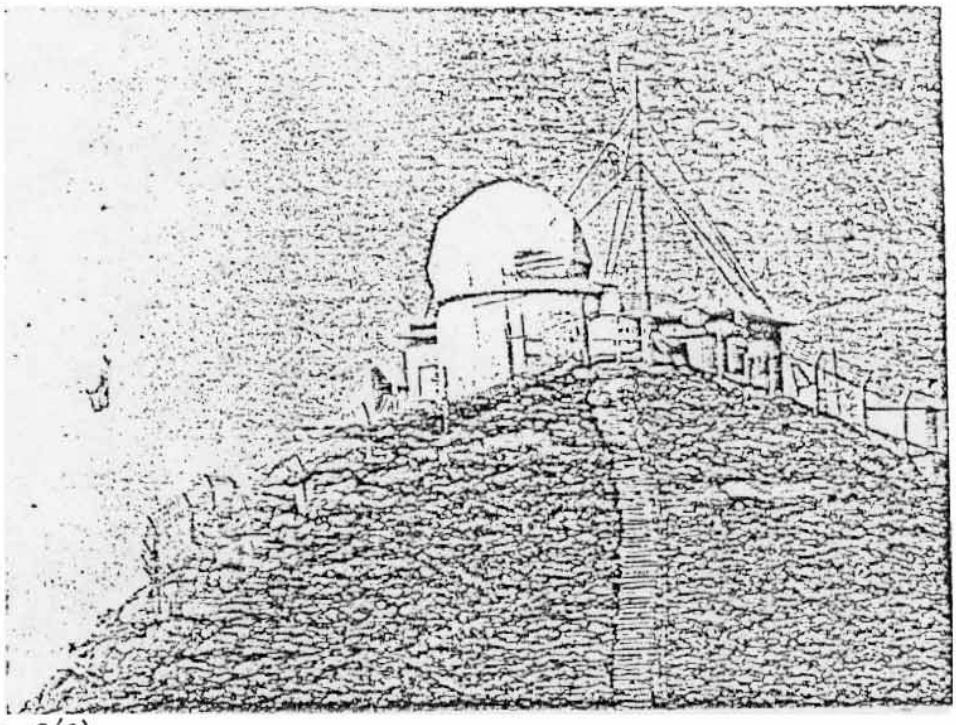

10.5(3)
Fig. ~~10.12~~. The Plessey 43S 100 mm weather radar of the Royal Observatory, Hong Kong sited on Tate's Cairn 568 m above sea level. The radar aerial is protected by a fibreglass dome. The adjacent Decca Type 41, 32 mm radar and the microwave link - on left - can also be seen.

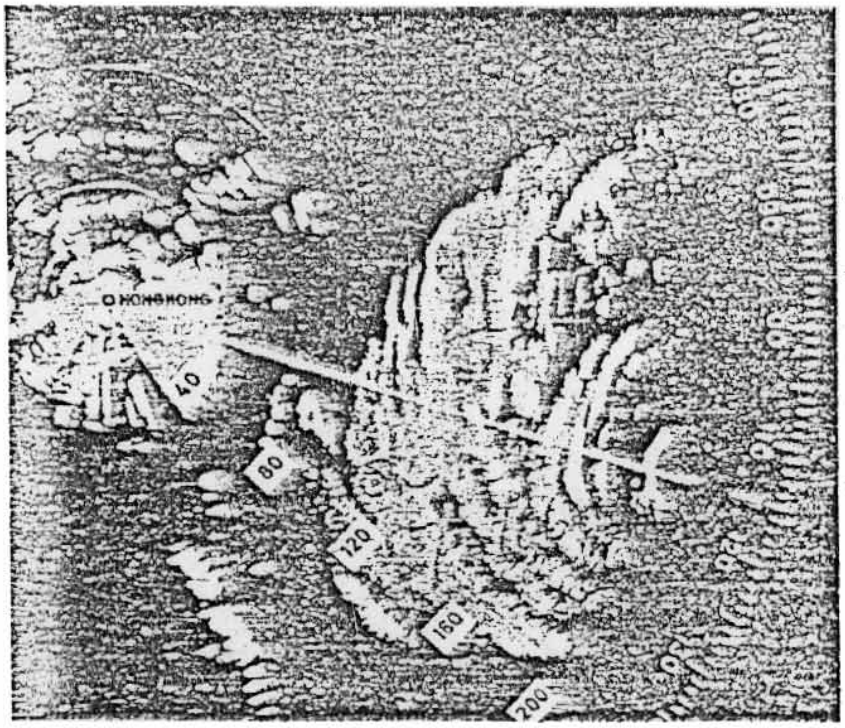

10.5(4)
Fig. ~~10.13~~. Typhoon Elsie, as seen on the PPI of the radar shown in Fig. 10.~~12~~ 5(3) at 0045 GMT on 15th September 1966. The eye is centred 215 n miles (399 km) on a bearing of 115° from the radar. Three hours later a reconnaissance aircraft reported the eye diameter to be 17 n miles (31 km), minimum SLP 943 mb and 700 mb wind 100 knots.

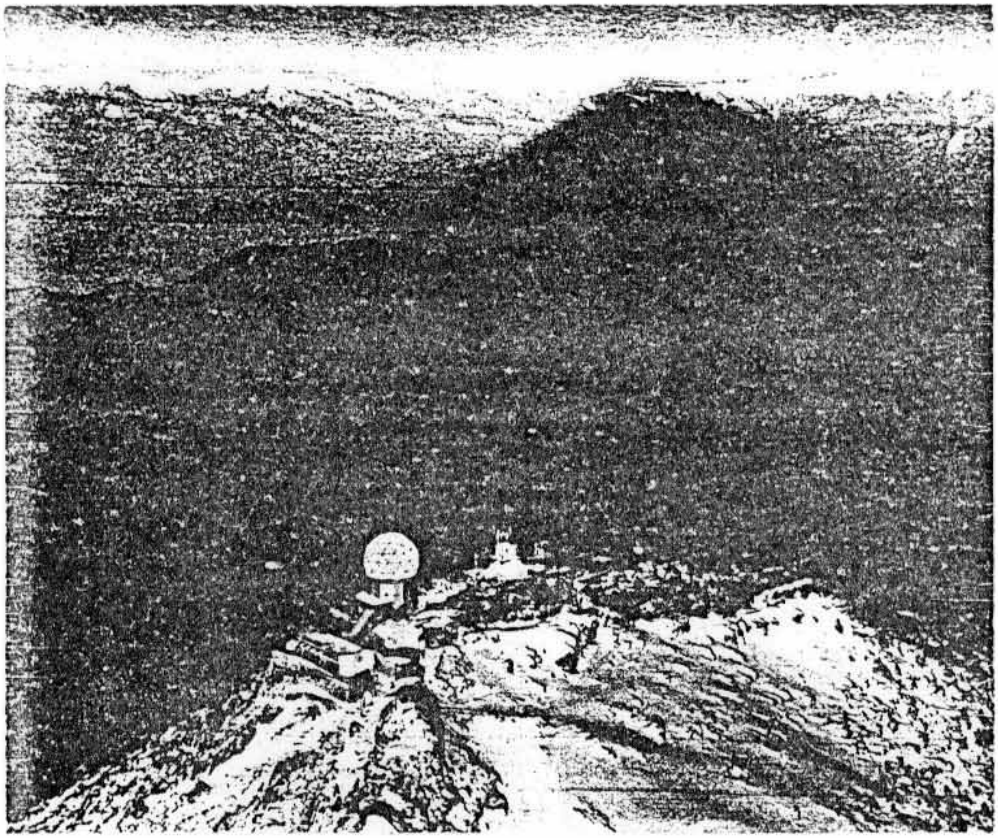

10.5(5)

Fig. ~~10.14~~. The meteorological observatory and high power weather radar at an elevation of 3 776 m above sea level on Mount Fuji, Japan. The shadow of this conical mountain can be seen in the top right of the photograph. (Courtesy the Mainichi Newspaper Tokyo).

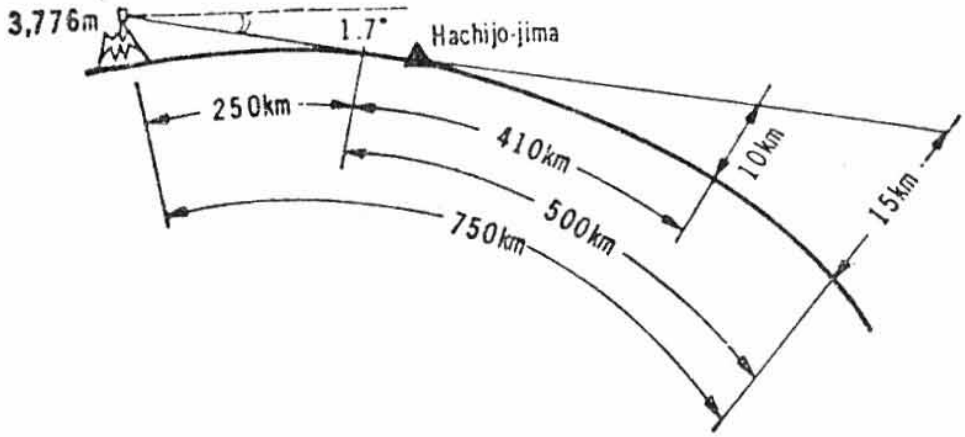

Fig. ~~10.15~~ 10.5(6). Normal propagation of the radar beam from Mount Fuji (3 776 m). The radar horizon is at 250 km. (After Kashimoto and Euda 1967).

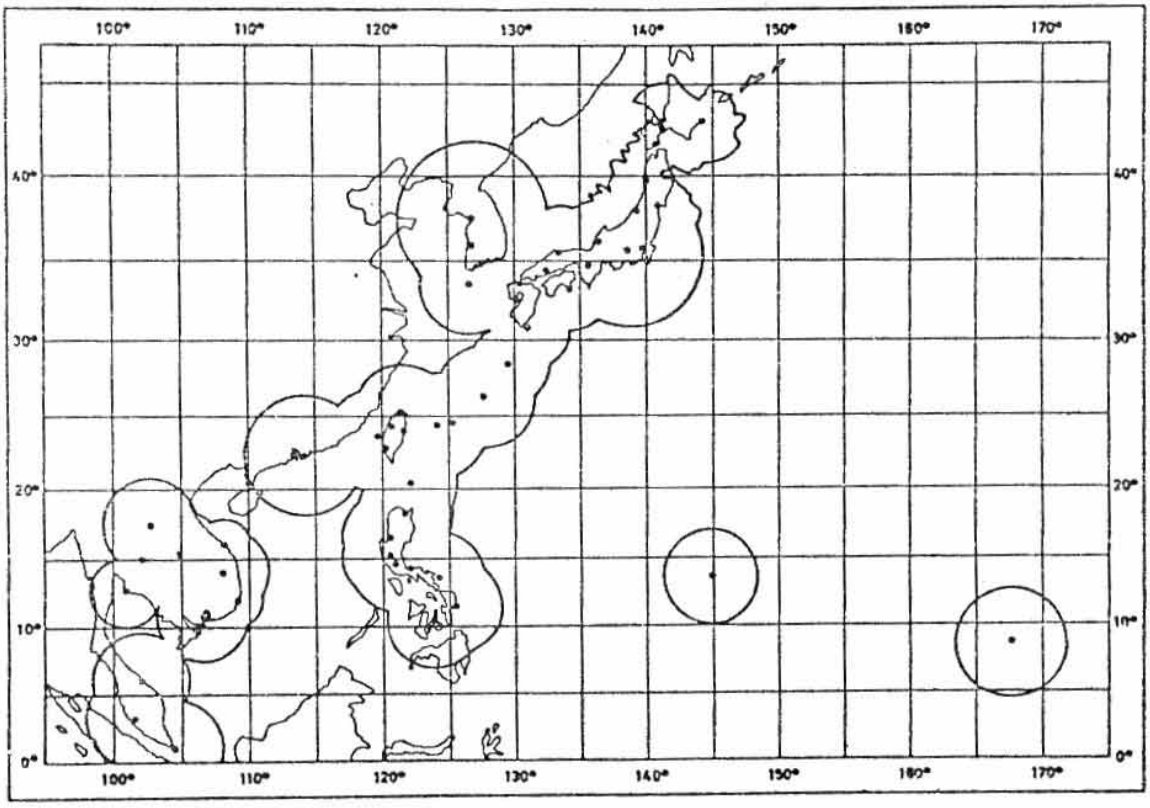

Fig. ~~10.16~~ 10.5(7). The locations of 49 meteorological radars in 1975 and their approximate area of coverage. The list is not exhaustive and does not include radars in Mainland China or in the U.S.S.R.

in 1965 to withstand a 10 second mean wind of 93 m/s (180 knots). In addition, the failure of public electricity supplies during typhoons is often caused by damage to the supply system resulting from lightning, wind, flooding or landslides. Emergency electricity generators should therefore be provided and should be designed to start automatically when the public supply fails. An efficient system to protect the dome and equipment from lightning strikes should also be provided.

If the radar is sited on a tower as is frequently the case then, of course, the tower must be strong enough to withstand extreme wind forces without vibrating unduly and the foundations must be free from the risk of undermining by flood water. Fig. ~~10.17~~ 10.5(8) shows a Raytheon WSR 64 M radar mounted on a tower at Hua Lien in Taiwan. The radar was damaged on 18th November 1967 following failure of the radome in typhoon Gilda during which peak gust speeds at the top of the 30 m radar tower reached approximately 78 m/s (151 knots). This approximation arises because the pen of the anemometer recorder hit the stops at 70 m/s (136 knots) as shown in Fig. ~~10.18.~~ 10.5(9) The panels of low-pressure, laminated fibreglass of which the dome was made had been cracked in the previous July during the passage of typhoon Clara and could not be replaced before the arrival of Gilda. The winds due to Clara were not measured on site but readings from a nearby anemometer suggest that they were less than 60 m/s (113 knots). In Gilda the radome failed and then the radar pedestal was pulled from its concrete mounting and blown off the top of the tower. Fig. ~~10.19~~ 10.5(10) shows the pattern of discoloration that was left in the concrete after the pedestal and reinforcing bars had pulled away. The tower vibrated considerably before the radome was finally lifted off its moorings and blown away with the aerial (Fig. ~~10.20~~ 10.5(11)). Wind gusts in typhoon Gilda exceeded those for which the dome had been designed (Bocks 1967).

10.5(8)
Fig. ~~10.17~~ The 30 m tower at Hua Lien on the east coast of Taiwan with a Raytheon WSR 64 M 100 mm weather radar. The dome and radar were blown off the tower in typhoon Gilda 18th November 1967. (Photo by Bocks 1967)

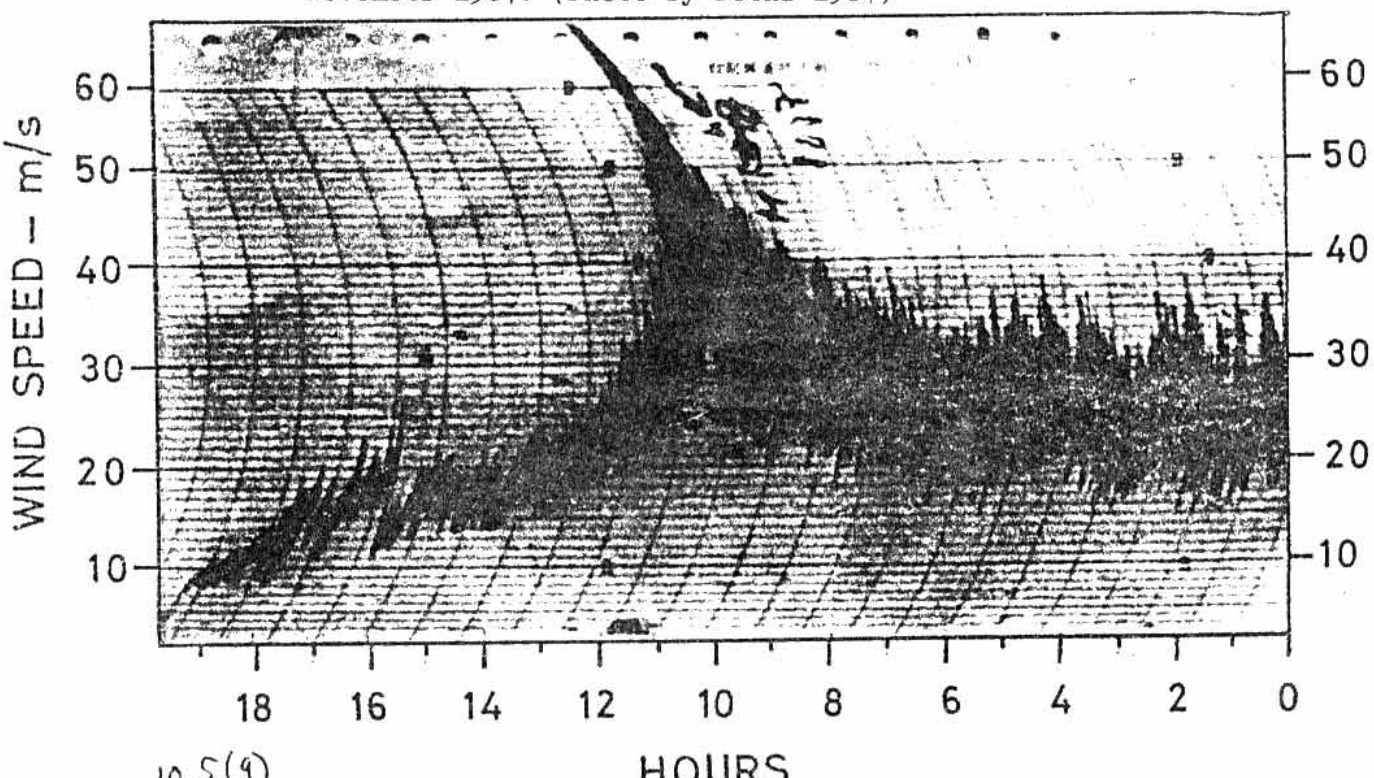

10.5(9)
Fig. ~~10.18~~ Trace from the Hua Lien four cup anemometer which was mounted at the 30 m level. The pen repeatedly hit the stop which corresponds to about 70 m/s. The propellor anemometer at 10 m level registered a peak gust speed of 63.5 m/s. (Photo by Bocks 1967)

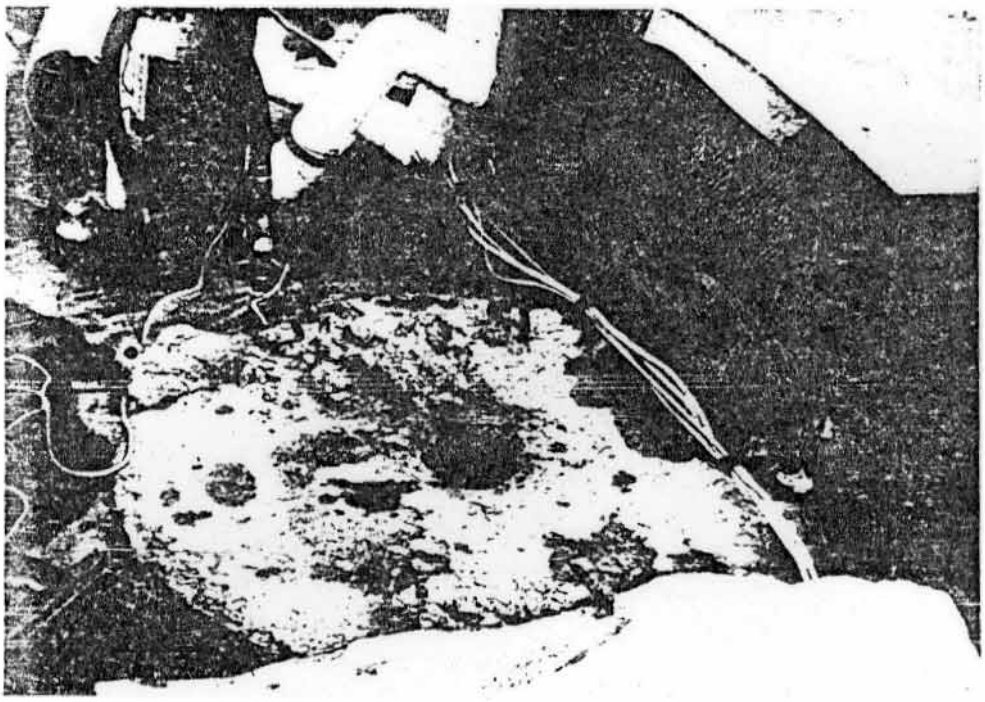

10.5(10)
Fig. ~~10.19~~ Scars on the concrete tower platform at Hua Lien left when the raised circular concrete radar anchorage tore away. Note that four of the six re-enforcement hooks remain in the platform which developed a coloured pattern. (Photo by Bocks 1967)

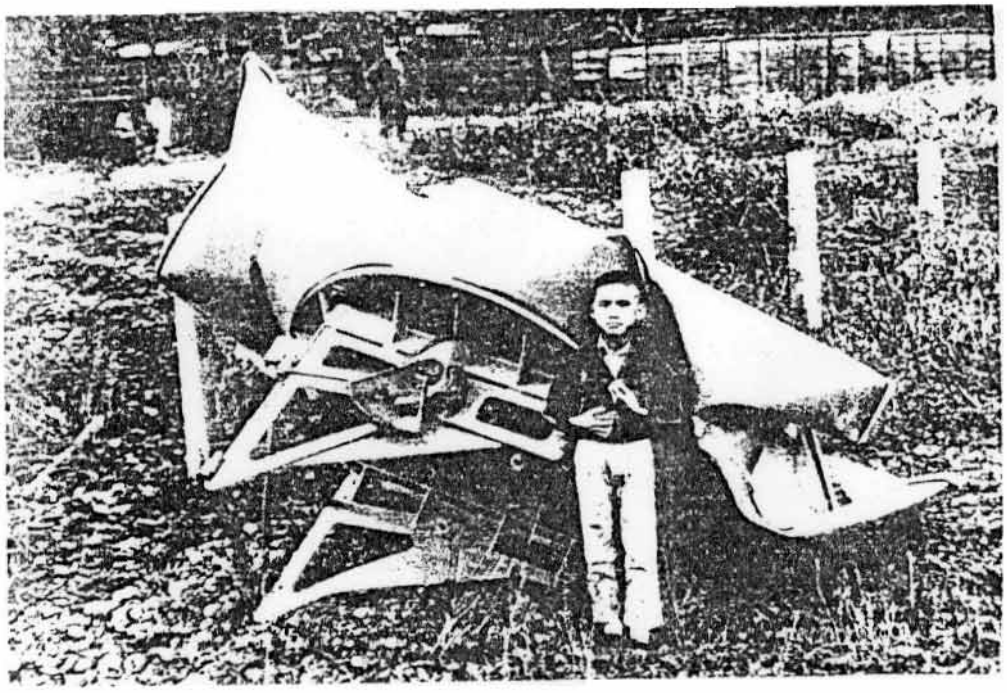

10.5(11)
Fig. ~~10. 20~~ The radar aerial dish after being blown from the top of the Hua Lien radar tower. (Photo by Bocks 1967)

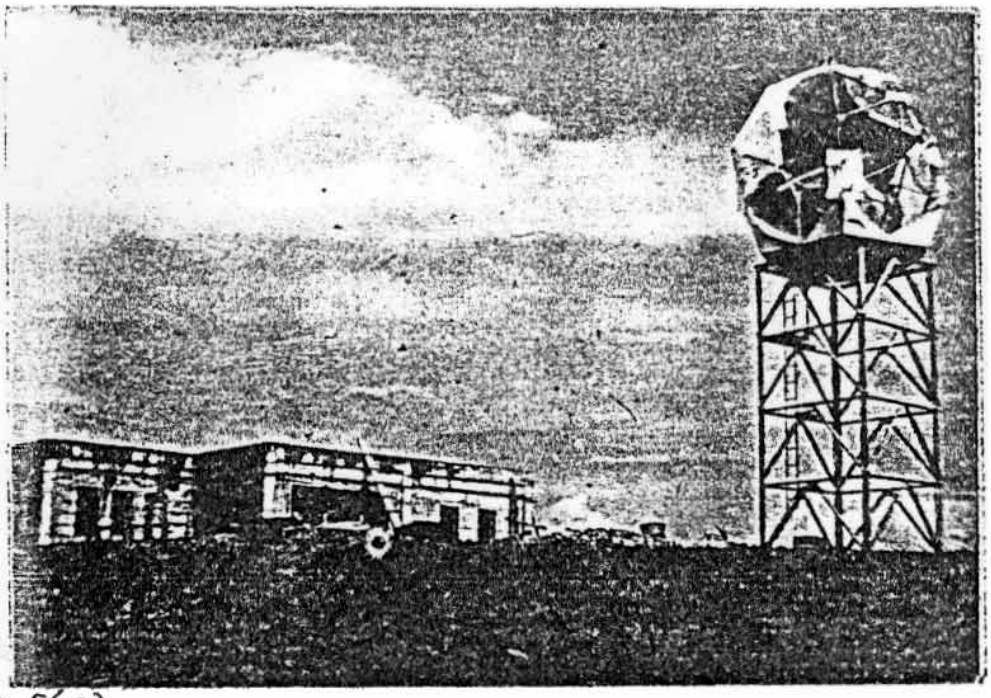

Fig. ~~10.21~~ 10.5(12). The Basco Island fibre-glass radar dome and WSR-57M weather radar after being damaged by typhoon Elsie 1975. (Photograph from PAGASA).

Before it went into full service the weather radar at Basco Island (20.45°N, 121.97°E) was severely damaged by the winds in typhoon Elsie in October 1975 (Fig. ~~10.21~~ 10.5(12)). It is probable that the failure of the dome was in part due to the trap door (1 m x 0.75 m) in the base of the dome being left open. This would permit the air pressure inside to be reduced at times, so increasing the loading on the dome panels already receiving the full dynamic pressure of the wind externally. A station 3 km away reported a minimum pressure of 945.7 mb and peak gust speeds of over 60 m/s. Reports from a reconnaissance aircraft near this time indicated that the central pressure of the typhoon was 913 mb with one minute mean winds of about 65 m/s. Radar photographs of typhoon Elsie and its track are shown in Figs. 10.7(2), 10.7(3) and 10.7(5).

There are many other cases of typhoons having caused damage to weather radars, most of which were unprotected by domes. Historically noteworthy failures were those which occurred to the exposed waveguide on the Virac, Catanduanes (13.5°N 124.3°E) 100 mm radar during the passage of the typhoon Joan (900 mb) which struck Manila in October 1970; and the failure of the aerial turning gear of the Cox's Bazar 100 mm radar during the passage of the infamous November 1970 cyclone which caused about 200 000 deaths. In the latter case the aerial was protected by a dome and gear failure occurred when the wind speed at the radar site was about 20 m/s.

During the approach and passage across Darwin of the devasting cyclone Tracy on Christmas Day 1974 the Plessey WF44 radar there provided excellent surviellance. When the storm was moving away at 0430 CST (Fig. 5.) the emergency generator suffered a mechanical breakdown (not cyclone induced) and operation of the radar ceased. The case is of interest because the radar aerial which was mounted on a 10 m tower was not protected by a dome yet it continued to operate in winds with peak gust speeds exceeding 60 m/s. Some damage to the quadrant gears was experienced but the radar remained serviceable. Nevertheless, a protective dome is recommended particularly in areas where tropical cyclone gales are frequent.

10.5.4 Maintenance and calibration

The importance of good maintenance and accurate calibration of meteorological radars has already been stressed in section 10.4.8 in connection with the measurement of rainfall rates. Good results in the typhoon tracking and associated flood forecasting roles are also critically dependent on good maintenance and calibration. Tang (1976) calibrated some radars located in those countries which were members of the WMO/ESCAP Typhoon Committee (sect) and found that, on average, the effective range of the tested radars was only one half of their designed maximum range. Some radars were found to be operating so that they would have a range of only one third of the designed maximum.

It is not always possible for even an experienced observer to judge the performance of a radar by inspection of the PPI display alone. Even if there are permanent echoes normally visible at ranges of 60 km or more their reflectivity may change with wetness, the seasons and propagation conditions. It is therefore necessary to have a strict routine for preventive maintenance and instrumental calibration if full value is to be obtained from a radar and if it is to perform adequately in the typhoon warning role.

Tang (1976) reported that one radar he tested was operating with a performance 21.6 dB lower than the designed value. The receiver sensitivity was down by 20.0 dB and the peak power output was down by 1.6 dB. A storm at 180 km range having a rate of rainfall to 60 mm/h would appear on such a radar to have a rainfall rate of only 4 mm/h. The effects of a 20.6 dB fall in performance when tracking a mature typhoon near maximum range and a weaker tropical storm closer in, are illustrated in Fig. ~~10.21a~~ 10.5(13). The pictures were obtained using a Plessey 43S radar which is more powerful and is sited higher than many others (Table ~~10.5~~ 10.4(3)). Fig. ~~10.21a~~ 10.5(10) implies that in many cases a fall in radar performance of about 21 dB would prevent a typhoon or tropical storm from being detected until it was close to the station. An example of errors due to inadequate calibration of radar azimuth is given in sect 10.7.1 and Fig. 10.7(3)

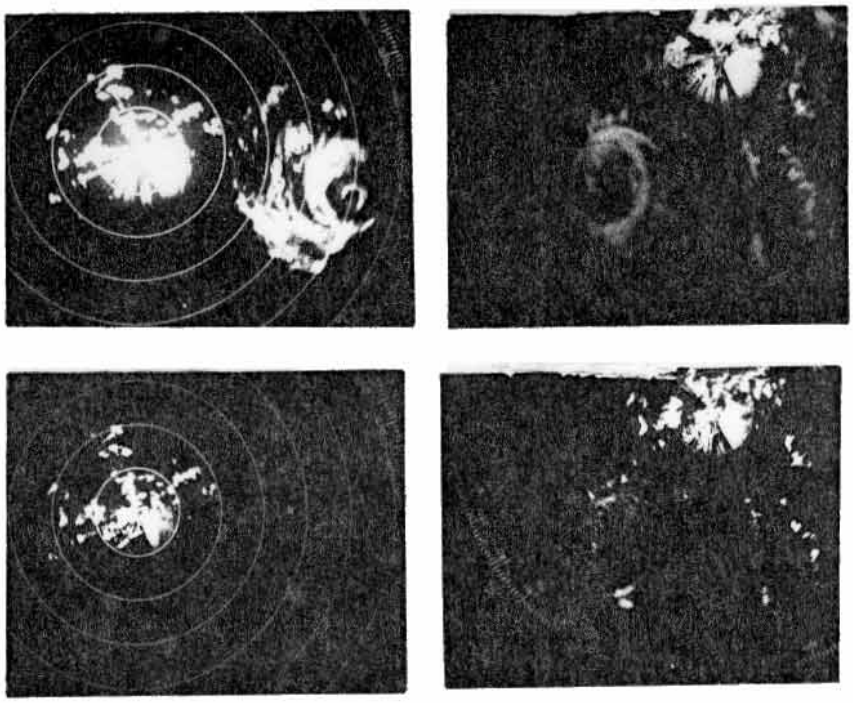

10.5 (13)

Fig. ~~10.21a~~. Tropical storm Doris and typhoon Elsie displayed normally on the Hong Kong radar (top) and with 20.6 dB attenuation (bottom) at 0915 GMT on 5 October 1976 and 0936 GMT on 13 October 1976 respectively. Tropical storm Doris passed 150 km to the west of the radar and typhoon Elsie 50 km to the south and the maximum rainfall rates (15s mean) recorded near the radar station during the passages were 191 and 150 mm/h respectively.

Meteorologists in charge of warning centres must maintain good liaison with maintenances staff to ensure that the radar is available for use in severe weather occasions. Routine maintenance and calibration should not be undertaken if there exists a potential threat from a tropical cyclone or if heavy rain is occuring or expected. It is also necessary to protect maintenance personnel. They should not be exposed to radar radiation intensities which exceed 100 W/m^2 averaged over any 6-min period. For a 100 mm radar with 2^o beam width and 500 kW power this level of exposure will occur in the stationary beam at a distance of about 58 m. Maintenance personnel should be tested for colour blindness, a condition which occurs in about 8% of European males (much less in females) but which can be lethal in radar work where cables are often colour coded. Precautions are also necessary to avoid fires triggered by radiation or by equipment malfunction. Aoyagi et al (1981) give a good summary of the precautions which should be taken to ensure that a radar station and its personnel are able adequately to fulfil their tropical cyclone warning role.

10.6 Tropical Cyclones as seen by Radar

10.6.1 The model

The banded structure of their rain-bearing clouds (Fig. ~~10.30~~ 10.7(5) and ~~10.31~~ 10.7(6)) is characteristic of all tropical cyclones whilst the presence of a rain-free eye with a complete or partial eye wall is further characteristic of those of severe tropical storm and typhoon intensity. Wexler (1947) first recognised that hurricane rainbands were spiral in shape while Hiser and Freseman (1956) found them to be well represented by logarithmic or equi-angular spirals, centred on the eye, and having crossing angles between the spiral and a concentric circle of 10^{o}, 15^{o} or 20^{o}; the smaller the crossing angle, the more nearly circular is the spiral. Other features sometimes seen on the radar presentation of tropical cyclones are the "rainshield" and the "precursor band". The former is a region of general ascent in which rainbands are embedded in a more extensive area of less intense rain. Such regions can be seen in Figs. ~~10.30~~ 10.7(5) to ~~10.32c~~ 10.7(10). The precursor band is a line of intense echoes found well clear and ahead of the outer spiral bands. This band does not have the shape of a spiral and is often missing or transient.

10.6.2 Spiral rainbands

In a mature typhoon, spiral rainbands originate at the eye wall and grow at their tails or outer ends as they move away from the storm centre as illustrated in Fig. ~~10.22~~ 10.6(1). The bands propagate outward at 5-15 m/s in a direction perpendicular to their longitudinal axis (Senn and Hiser 1959). The individual rain cells of which the bands are comprised move in approximately circular paths around the eye and so cross rainbands from their inner sides to their outer sides. The speed of individual echoes as they approach a band is generally greater than when they move away (Staff Members 1969). The bands are usually oriented between the isobars and the surface wind. New cells form mainly at the tail or outer ends of the rainbands while old cells dissipate at the head or inner end of the bands. In this way the bands tend to remain in the same sector throughout their lives as shown in Fig. ~~10.22~~ 10.6(1). On some occasions however, when a band comprises some part of the eye wall, convective cells there do not dissipate but increase in number so that the band grows by both the head and tail and progresses some distance around the eye as indicated by the dashed lines in Fig. ~~10.22~~ 10.6(1). The outer, newer cells are

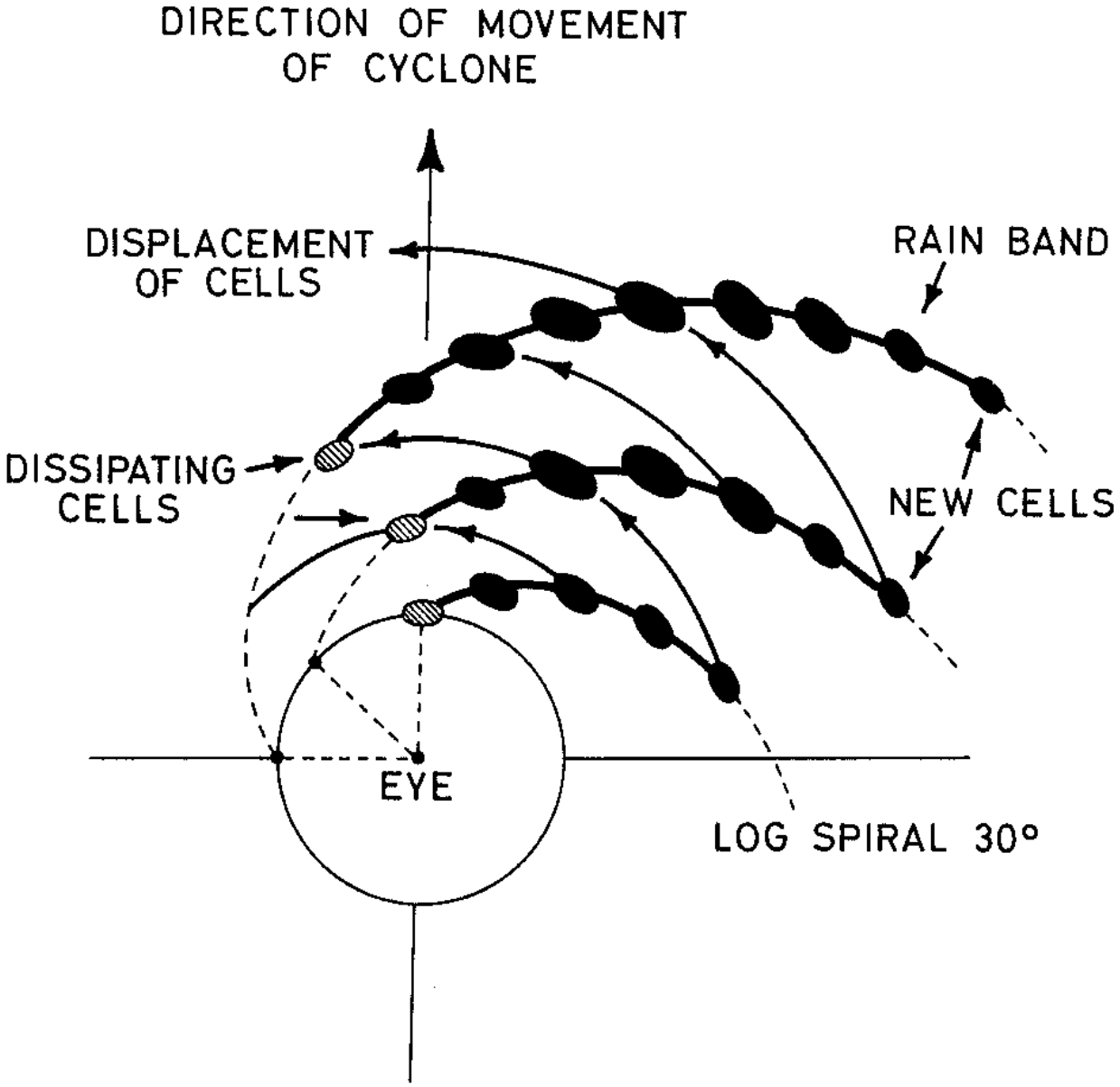

Fig. ~~10.22~~ 10.6(i). A model of the displacement of rainbands and their cells relative to the eye of a tropical cyclone (After Tatehira 1961).

strongly convective and present a well-defined discrete shape on the radar screen whereas, the older cells nearer the centre, often appear more diffuse and continuous as is characteristic of returns from rain which falls from stratiform cloud (Ligda 1955). However, strongly convective cells are also found in this inner region and particularly in the eye wall. The lifetime of the individual cells is relatively short, being on average about 35 minutes. The lifetime of spiral bands is very variable and can range from about 20 minutes (Senn and Hiser 1959) to about one day. It frequently happens that one region of a tropical cyclone is favourable for the formation of convective bands whilst convection is suppressed in other areas. Spiral bands then persist for long periods in the active areas and dissipate rapidly elsewhere. This was first noticed by Malkus et al (1961).

Having made these introductory generalisations it should be noted that there is a great variation in the shape and nature of rainbands as seen from time to time in any one tropical cyclone, or between different cyclones. The radar photographs in this book bear witness to this fact. Compare, for example, Fig. 4.3 and Fig. 10.7(5) ~~10.30~~ which are from the same radar. Furthermore, most of the published investigations on the nature and movement of echoes in tropical cyclones have been made at latitudes north of 25°N, in typhoons as they approached Japan or in hurricanes as they approached the U.S.A. Spiral bands in tropical cyclones away from the effects of land and in low latitudes have not yet been adequately studied. One would expect changes in the behaviour of the rain cells with changes in cyclone intensity and environmental conditions but, our knowledge is currently inadequate to permit a full description of the bands and their cells in terms of the many environmental factors. With these reservations in mind we will discuss the limited information on rainbands and their constitutent cells which has been gleaned in the last two decades and which has fairly general applicability.

The number and distribution of rainbands and their crossing angles vary with the intensity of the tropical storm or typhoon. Watanabe (1964) found that as the intensity of a cyclone increased so did its rainfall and the number of spiral bands while their crossing angle markedly decreased giving the typhoon a more circular form as shown in Fig. 10.6(2) ~~10.23~~. He attributed the changes to the reduction in directional shear of the wind in the vertical as the storm intensified and the cyclonic vortex reached

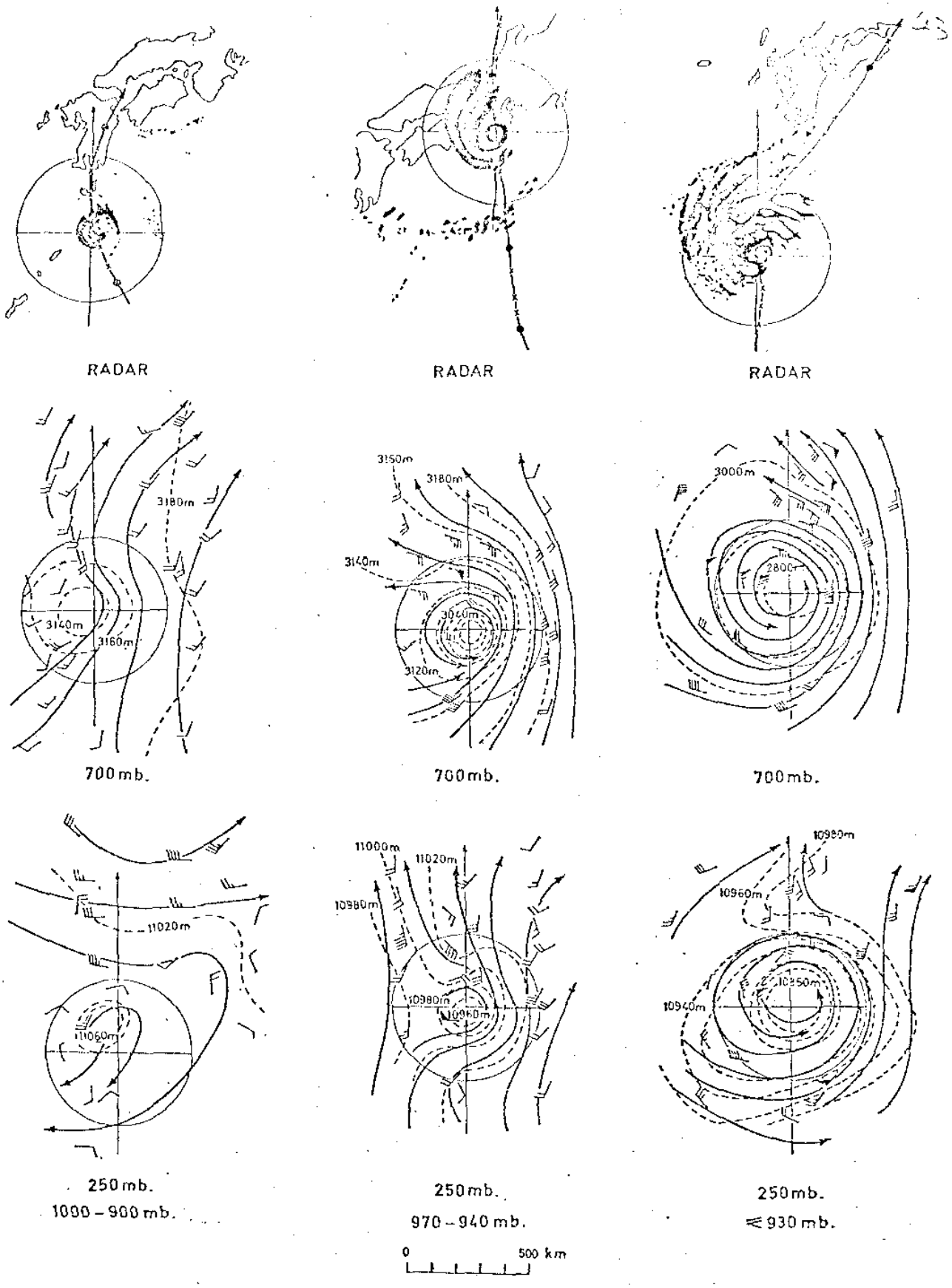

10.6(2)

Fig. ~~10.23~~ Typical rain patterns and associated wind and pressure fields at 700 and 250 mb in typhoons of low, medium and high intensity (reading from left to right) illustrated by actual conditions in typhoon Vera 1962, Thelma 1962 and Nancy 1961, respectively. (After Watanabe 1964)

to great heights. In deep typhoons, with central minimum pressure below about 950 mb, the inner spiral bands have such small crossing angles that they frequently become circular and form a second "eye wall" such concentric bands are shown in Figs. ~~10.29~~ 10.7(4) and ~~10.31~~ 10.7(6).

Spiral bands in the outer regions of tropical cyclones frequently depart from the logarithmic form such that their crossing angles increase at larger radii. Indeed, spiral bands can depart from the classical form in all areas of some tropical storms and lesser typhoons where they may run into one another as shown, for example, in Fig. ~~10.8~~ 10.4(5)(b). Very long 'feeder' rainbands of length 1 500 km or more can sometimes be seen on radar (and on satellite pictures eg. Fig. 4.2) but they depart considerably from the logarithmic shape in their outer regions. They most frequently originate in the outer parts of a tropical cyclone in the eastern sectors and curve around towards the equator to extend into the W and SW inflow. Rockney (1956) first reported these very long bands of heavy rainfall which he called "streamers." They are also seen in the Bay of Bengal cyclones (Raghavan et al 1980).

A sudden increase of surface wind speed and heavy rain should be expected as a rainband moves over a station. The squalls can be severe and sustained for long periods as the rainband remains nearby. Indeed, the wind speed sometimes does not fall again during the continued approach of the cyclone eye.

10.6.3 The rain shield

During the life of a tropical cyclone, spiral rainbands may become more numerous in one particular sector where, in the inner regions, they broaden and merge into one another to form a widespread area of rain which is known as the "rain shield". In other sectors of the storm rainbands are much less numerous or even entirely absent (Fig. ~~10.32~~ 10.7(7)). A rain shield is not always present, neither is it always to be found in the same sector. It is frequently said (eg. Aoyagi et al 1980) that tropical cyclones most frequently have a rain shield in the right-front and right rear quadrants as was reported to be the case in Atlantic hurricanes (Senn 1966b). However, when typhoons are observed without significant attenuation the location of the rain shield is more variable as illustrated in Figs. 10.4(5), 10.6(2), 10.7(1), 10.7(7) and 10.7(8). If the sensitivity of the radar receiver is reduced or iso-echo circuits used, then it is usually possible to delineate spiral bands of somewhat heavier rain within the rain shield (Fig. ~~10.8~~ 10.4(5)). The bright-band phenomenon (sect 3.6.1) can often be observed in the rain shield (Rockney 1956) indicating that ascending currents are less than 1 m/s and that thunderstorms will be less frequent in this area.

10.6.4 Precursor bands

Sometimes the first echoes to be seen by radar, well in advance of an approaching storm, are sharply defined, intense convective echoes which form a long, narrow squall line known as a "precursor band". When present, these bands precede the first spiral bands by 100 - 500 km and occasionally more. There may be more than one band each separated from the others and from the spirals by about 100 km. Precursor bands are located in the front two quadrants of the cyclone and lie across its track. They appear nearly straight or much less curved than the nearest spiral bands.

Those precursor bands over the sea and several hundred kilometres ahead of the spiral rainbands are usually outside the storm's cyclonic circulation. The constituent echo cells move in approximately the same direction as the storm centre but at a somewhat faster speed. Those precursor bands located closer to the cyclone centre may be just within the storm circulation so that their echoes have a tangential component of motion. Precursor bands can be associated with tropical cyclones of any intensity and they have been found as far as 750-1000 km ahead of hurricane centres (Donaldson and Atlas 1964) but in the South China Sea, the bands are seldom further than 750 km ahead of the centre of tropical storms or typhoons. The sharp edged echoes found in these bands are often the source of lightning. They are also associated with a sudden enhancement of surface wind speed like that which occurs during the passage of spiral bands. Fig.10.6(3)shows precursor rainbands about 300 km from the centre of typhoon Rose 1971. Satellite views of precursor bands are shown in Fig. 11.

p 48d

Although precursor bands form part of the model storm as seen on radar they are much less frequently observed than current texts indicate. Indeed, the bands are more frequently absent than present, a situation clearly shown by the infrequency of precursor cloud lines on satellite pictures. → p.48

(a)

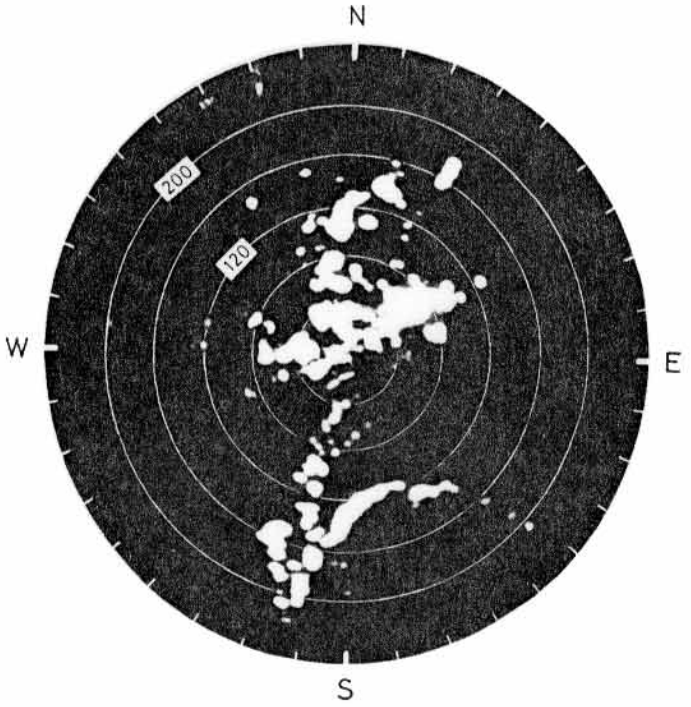

(b)

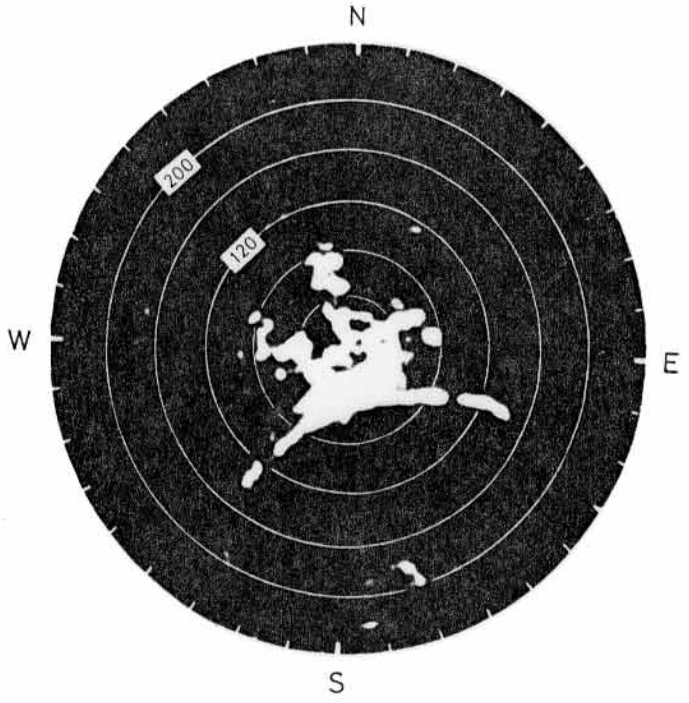

10.6 (3)

Fig. ~~10.24~~. In (a) a weakening precursor band is shown running out from the Hong Kong radar station on a bearing of 190° in the NW sector of typhoon Rose at 0600 GMT on 15th August 1971 as Rose was moving WNW at about 5 m/s.

In (b), taken 6 h later, Rose was moving on a NNW course at about 3.6 m/s. A new precursor band lies across the track from WSW to ESE south of the radar station on the first range ring (40 n mile, 74 km). Some eye-wall echoes are visible at a range of 220 n mile (407 km) on a bearing of 175°. The photographs are from a 16 mm time-lapse film.

Although precursor bands form part of the model storm as seen on radar they are much less frequently observed than current texts indicate. Indeed, the bands are more frequently absent than present, a situation clearly shown by the infrequency of precursor cloud lines on satellite images. Radar photographs illustrating case studies in the literature, whether from the Caribbean, Japan, India or Australia seldom show all the features of the model and the photographs in this book are, in this respect, typical.

10.6.5 Lifetime and movement of echo cells

The lifetime of echoes which comprise spiral bands was found by Senn and Stevens (1965) to be longer in the left quadrants, to average about 35 minutes overall and to depend upon the echo diameter such that larger echoes had a longer lifetime than smaller ones. The average diameter of the echoes was about 10 km. The results, in Table 10.6(1) ~~10.7~~, were derived from radar time-lapse films of typhoon Wendy 1958 and Shirley 1968 which, respectively, passed close to and over Hong Kong (Liu and Lai 1969). They show that, on average, echoes over the sea and in rainbands tend to be longer lived than those occuring over land or between rainbands.

Table 10.6(1) ~~10.7~~. Lifetime of radar echoes

Position	Surface	Lifetime			Number of cases
		Average	Extremes		
			Minimum	Maximum	
		min	min	min	
On a Rainband	Sea	47.3	36	57	12
	Land	20.8	10	30	11
Between Rainbands	Sea	35.5	25	53	12
	Land	27.4	10	40	18

Ligda (1955) determined the velocity of individual convective echoes in a Florida hurricane and found that they correlated well with the storm winds at 700 mb. He coined the term "spawind" for wind velocities

found in this manner. Many other investigators have subsequently examined the relationship between echo velocities and winds in hurricanes and typhoons and obtained varying results. Spawinds have been reported as agreeing best with the winds near the surface, the winds at 700 mb or the average of the winds near the surface and 9 km, the last being frequently equivalent to the 700 mb wind. Watanabe (1964) suggested that the velocities of echoes at different stages in their lifetime are determined by winds at different levels. Subsequently, Senn and Stevens (1965) observed that, in general, echoes tend to move more slowly as they get older. One of the difficulties in determining the relationship between echo movement and winds is that very few simultaneous radar pictures and wind measurements are available. Black (1971) overcame this difficulty by using aircraft to measure both echo speeds and wind speeds in hurricane Debbie 1969. He found that the movement of the echoes agreed best with the wind flow near cloud base. Most of the echoes he studied were in the mature or growing stage.

Black suggested that because new convective echoes are from growing clouds, containing up-currents probably greater than 10 m/s, they move at all levels with the momentum of the air flowing into them near cloud base. The boundary of the echo then moves with a speed approximating that of the low level winds as long as strong updrafts are maintained. When the updrafts eventually weaken, through dilution by mixing with environmental air, the echoes, at any particular level, move with a speed closer to that of their environment. At this stage, falling precipitation would be expected to move with nearly the speed of the wind at the precipitation generating level and the echo would then be of the more diffuse kind. New hard echoes from rapidly growing convective clouds should therefore tend to move more in accordance with the fast low-level wind flow whilst older, more diffuse echoes should tend to move in accord with the weaker winds at higher levels, in agreement with the findings of Senn and Stevens (1965).

Senn and Stevens (1965) traced several thousand small, discrete echoes in five hurricanes and found large systematic differences in their movements in the different sectors of the hurricanes. In addition, they

found echo cells to be smaller and to move faster over land. By night hurricanes were more compact and symmetrical and their echo speeds were slower. Slowest echo speeds were found in the right front quadrant and the fastest in the left rear while all echo speeds increased as the hurricanes moved faster. Inward moving echoes in the front quadrant had higher speeds than outward moving eachoes and the situation generally reversed in the rear of the storms, especially in the left rear. They also found significant differences in the relationship between winds and echo speeds in different sectors of the storms. Echoes in the right front quadrant moved more slowly than winds at low and middle levels but with crossing angles similar to the winds near 4 km. Echoes in the right rear quadrant had speeds close to those of the low and middle-level winds but greater inward crossing angles. In the left quadrants the speed and direction of the echoes was closest to that of the winds near the 450 m level. Echo motion in and very near to the eye wall was nearly circular, a finding which agrees with those of other authors including Jordan (1960) although he studied echoes in the layer between 6 and 9 km.

Aoyagi et al (1980) state that "A general rule of thumb for echo velocity measurements from land based radar is that the surface winds will be 50 - 70 percent of (the) speeds determined from echo motion" - This is a satisfactory rule for rough and ready, real-time observations averaged over the cyclone and different types of convective echoes. However, if the radar image is enlarged and used with some time-lapse device on only those echoes which are small discrete, newly formed, strongly convective,near the eye wall and over the sea then, the spawinds will be found to approach the velocity of the wind at cloud base ($\sim$500 m). The spawind echo can be expected to move a little slower than the wind at cloud base because: 1) the former is a layer average and 2) it is usually a time average over typically 10 - 15 min and 3) there will be components of inflow at cloud base relative to the echo and 4) there is a transfer of momentum upwards which, for ascent in discrete columns, will be attenuated by entertainment. Consequently, good eye-wall spawinds are a little closer to the sustained surface wind than is the free wind at 500 m. Under the specified conditions the sustained surface wind over the ocean is typically 85% - 90% of the spawind. For example, the eye wall shown in Fig. 10.7(9) ~~10.32b~~ for 0600 GMT was ideal for determining spawinds as it contained more than the usual number of small discrete cells.

The fastest cells were moving at 34 m/s as the eye crossed a number of ships and anemometers (Bell 1979). Observed surface winds were about 31 m/s with gusts to 42 m/s. On this occasion therefore, sustained eye-wall surface winds reached 91% of the spawind speed.

From the evidence so far available, the relationship between the movement of echoes and the winds in a tropical cyclone appears to depend on the age of the echoes, on their position in the storm circulation and probably on the stage of development of the tropical cyclone. The larger echoes may also be subject to propagation effects, such as are known to affect the motion of thunderstorms; in this case spawinds may differ from the wind at every level and from the mean wind over the layer containing the precipitation. However, if observations are restricted to newly-formed, small, discrete, strongly convective cells within about 20 km of the eye wall of a mature tropical cyclone then, for practical purposes, it can be considered that they move with a velocity which is close to that of the wind near cloud base. The sustained surface wind speed will then be about 90% of that of the spawind or less, according as to how nearly conditions meet the specified criteria.

10.6.6 Tilt of echoes

RHI photographs from radars which have narrow beams often show that, in tropical cyclones, some echoes tilt with height. This is due to the shear of wind through the layer containing the echo. It should be noted that it is only the component of tilt along the radar beam that is seen on RHI. For a given shear, the tilt will depend on the stage of development of the echo column because strong updrafts are tilted less than weaker ones. Shear and tilt of echoes depend both upon the stage of development of the tropical cyclone and on the quadrant in which the echoes are located. Significant tilt of RHI precipitation columns in the mature hurricane Debbie 1969(Black et al 1972) occurred mainly below 9 km. Most echoes leaned slightly into wind and radially outward as they increased with height. This is consistent with the model tropical cyclone in which the upper winds have less tangential speed and a greater outward component, than those near the surface. The average tilt of an echo column 6 km high amounted to 2 km horizontally, equivalent to an angle of 20° to the vertical. On the basis of certain reasonable assumptions about the precipitation particles and their fall speed it can be calculated that the average tilt is equivalent to a wind shear of about 3 m/s per 4.6 km of

height. The greatest tilt observed was 45°. Senn (1966a) found average tilts and shears in Betsy 1965 to be almost double those in Debbie, this difference was attributed to the fact that, at the time of the observations, Betsy had been intensifying.

10.6.7. The height of radar echoes

The determination of the height of the top of a volume of precipitation particles is not always a simple matter. Complications arise from atmospheric refraction, curvature of the earth's surface and the differing distributions and sizes of precipitation particles but the main source of uncertainty is due to the radar beam having a finite width in the vertical plane. Corrections for the curvature of the earth's surface and standard refraction are usually made electronically as, for example, in Fig. ~~10.25~~ 10.6(4) where the height-marker line (at 16.82 km) curves downwards with range. Because of the large uncertainties which can arise from beam-width effects it is not advisable to measure the heights of echoes at distances beyond about 200 km.

The axis of a beam can be well above the top of a highly reflective target which may nevertheless return sufficient energy via the lower portions of the beam to be detected; the echo top will then appear to be about a half-beam width above its true height. A typical beam of 2^{o} width (i.e. between half-power points) will have a depth of about 6 km at a range of 180 km and could therefore exaggerate, by about 3 km, the height of intense precipitation echoes at this range. On the other hand, the precipitation may be so light that the entire beam must be intercepted in order to return a detectable signal; in this case the radar top will be lower than the true height by about half a beam width. In general then, the indicated height of precipitation areas will vary with the shape of the precipitating volume, the sizes and distributions of the precipitation particles, the type of radar used and its distance from the precipitation. In the case of intense, strongly reflective, growing cumulonimbus clouds in typhoons and elsewhere most of these factors are unimportant and it is only necessary to subtract one half of the beam width at the echoing range to get the height of the top of the echo to within 500 m or thereabouts, depending on range.

Although about 80% of the total power in a radar beam lies between the half-power points, there is, in most radars, sufficient power in the side lobes to permit the detection of strongly echoing targets at close

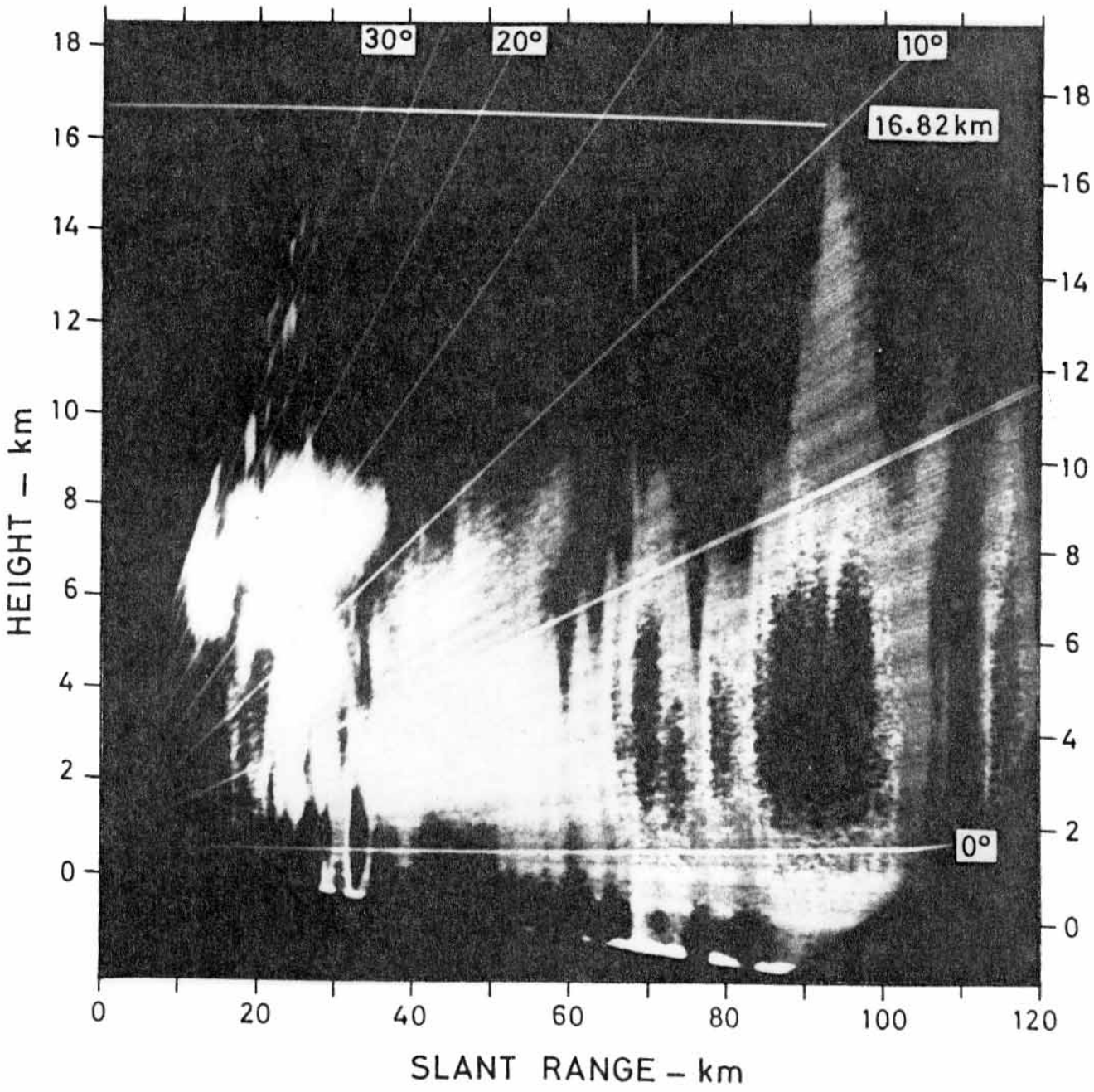

10.6(4)
Fig. ~~10.25~~. A cross section of cumulonimbus clouds as seen on the RHI display of the 43S radar using the iso-echo facility. The dark core of the clouds correspond to rainfall rates greater than 100 mm/h, the bright surrounds to 13 to 100 mm/h, the next brightest to 1-13 mm/h and in the black outer areas the rainfall is less than 1 mm/h.

range. Because the significant side lobes are usually found a few degrees off the main beam axis, side-lobe echoes will appear at an exaggerated height. However, side-lobe echoes can often be identified because they appear on RHI displays as tall thin protruberances from the main-beam return. In Fig. ~~10.25~~ 10.6(4)(6) the black core within the echo at 70 km range indicates that the reflectivity factor there exceeds 2×10^5 mm^6/m^3 (Fig. ~~10.6~~ 10.4(3) shows that this is equivalent to a rainfall rate in excess of 100 mm/h if $Z = 200R^{1.6}$). This strong target gives rise to returns from four side lobes, the first of which is seen protruding from the top of the main echo at an elevation of about 7°, and the next appears as an isolated echo at about 11.5° elevation near a height of 14 km. The other two returns, at 16° and 19° elevation, occur at heights beyond those recorded in the photograph. Unless side-lobe returns are recognised they can lead to radar tops being over-estimated by several kilometers; fortunately, it is possible to identify them. If the main beam of a radar is above an intense column of precipitation so that the latter is illuminated only by side lobes then, both the radiation incident on the column and the gain of the aerial (e.g. the Plessey two-way 43S) will be greatly reduced from that in normal operation. In a typical radar this reduction below main beam sensitivity amounts to about 54 dB. Therefore, if the receiver sensitivity is decreased so that the displayed intensity of the target is nowhere more than 54 dB above the minimum detectable signal (equivalent to a target reflectivity factor of 69 dBZ) then returns from this storm via side lobes will not be detectable. The radar height indicated in this reduced sensitivity mode is due to the main beam alone and will tend to be below the true top of the precipitation by an amount usually less than 1.5 km (Battan 1973). Enough has been said to indicate that reports of radar tops should be treated with caution unless the full circumstances are known. A more detailed discussion of this subject, with references, will be found in Battan (1973).

The visual tops of rain-bearing clouds may be higher than that of the precipitation column within them and therefore higher than the corrected radar top. When a large tropical cumulonimbus is in the growing stage, corrected radar and visual observations of cloud top height are usually quite close, but during the decay phase the large precipitation elements fall from the top of the cloud so that the radar top is then found below the cloud top by an amount depending on radar range and characteristics.

Hill and Lewis (1974) compared the heights of cumulonimbus tops (> 14 km) near Singapore as measured from special aircraft flights and by radar. They found that, at distances up to 150 km, most cloud tops were within 2 km of the radar top corrected for curvature of the earth's surface and atmospheric refraction in a standard tropical atmosphere. Smaller differences were found for growing clouds. Corrections for the beam width and side lobes were not applied because Donaldson (1964) showed that for radars with characteristics similar to theirs (Plessey 43(S)) the uncorrected radar tops would not be consistently in excess of true tops as long as the maximum reflectivity factors were less than about 10^6 mm^6/m^3 (equivalent to 60 dBZ, see Table 10.6 (2) and the above discussion on Fig. 10.6(4)(a)) - as was the case in their observations. For cloud tops between 12 and 19 km in the U.S.A., Kantor and Grantham (1969) found radar (WSR 57) tops (corrected for earth curvature, refraction and beam width) to be 1.2 km below cloud tops on average, with a root mean square difference of 2 km. Within the imposed range limit of 185 km they found no significant increase in the height errors with distance from the radar. These and other unpublished observations suggest that for intense growing tropical cumulonimbus clouds, corrected tops measured by 100 mm radars will be close to the visible top. For weaker and dissipating cumulonimbus clouds the precipitation top may be as much as 6 km below the visible cloud top.

Radar tops in tropical cyclones are usually highest in the eye wall. Photographs of the RHI of a 30 mm radar aboard a reconnaissance aircraft in hurricane Daisy (1958) were studied by Jordan et al (1960). One of these classic photographs taken from a height of 5.79 km show the eye-wall echoes extending to heights of 21.3 km (Fig. 10.6(5)(a)) corresponding to 19.8 km after correcting for one half of the 1^o beam width. Away from the eye-wall clouds echo tops are lower and remarkably even - probably as a result of the warm upper outflow (sect 10.8.3). This is illustrated by Fig. 10.6(6)(b) which shows the eye-wall echo in typhoon Hope (1979) reaching to 10.29 km with tops further out being at 8 km or less. The eye-wall echoes in Hope were remarkably low for such an intense typhoon (P_c less than 950 mb) and prevented the complete eye wall from being seen on radar at ranges in excess of 278 km (Bell 1980). Fig. 10.6(4)(b) shows echo tops to 16.82 km in the outer circulation of the weak tropical storm Ida (1980). The height of echo tops is not a reliable measure of cyclone intensity (sect 10.7.2).

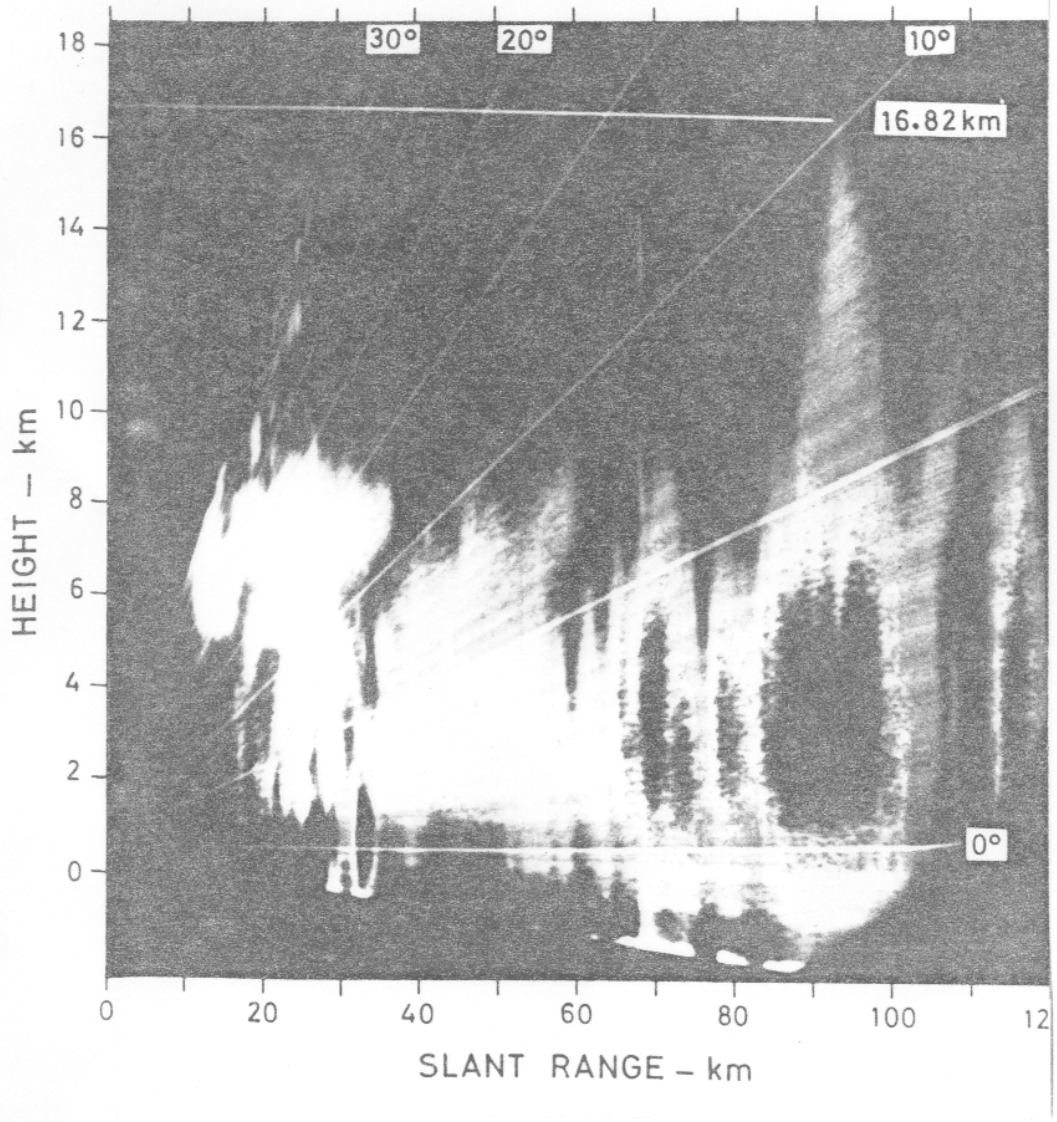

(a)

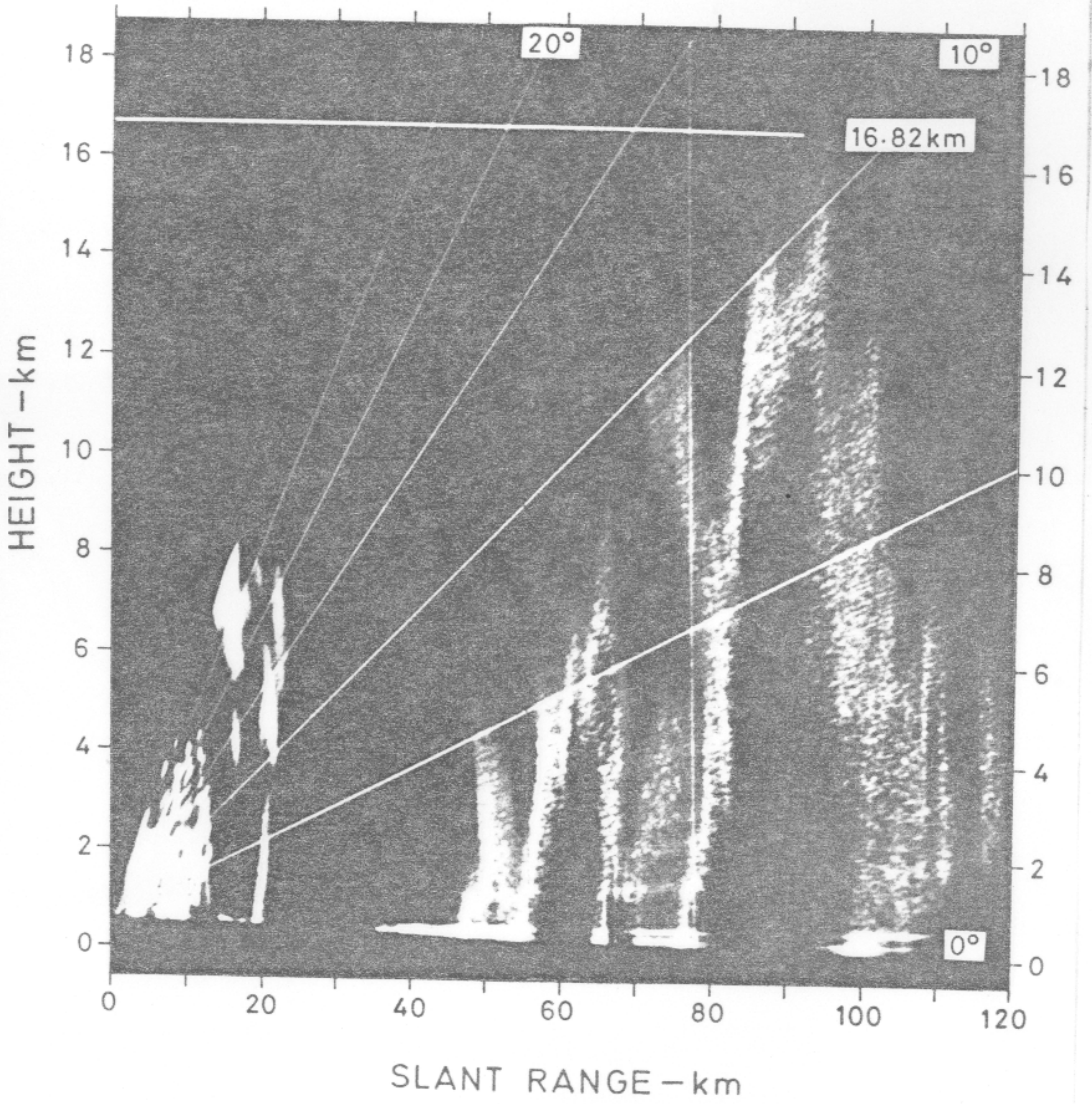

(b)

Fig. 10.6(4) The photographs show (a) a thunderstorm over the sea to the WSW of Hong Kong at 2319 GMT on 7 August 1975 and (b) a cumulonimbus 470 km to the west of the centre of severe tropical storm Ida which was centred 440 km ESE of Hong Kong at 1522 GMT on 10 July 1980. This echo had a reflectivity factor greater than 57 dBZ.

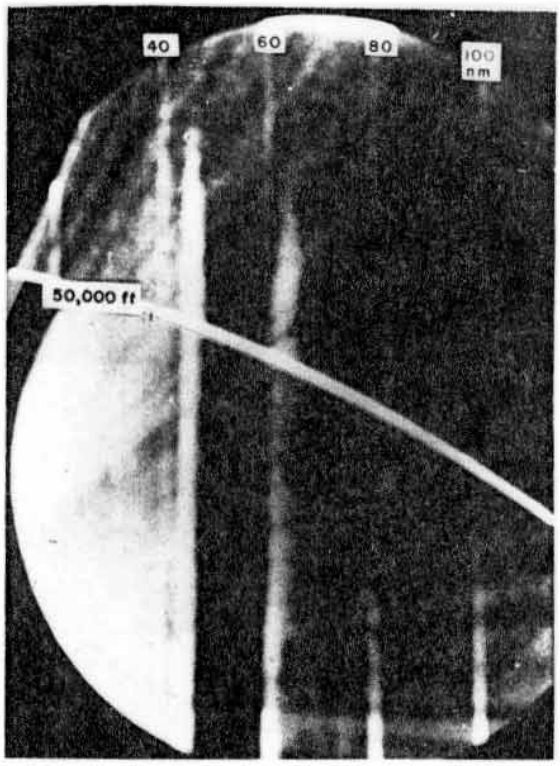

Fig. 10.6(5) RHI presentation of the eye-wall echoes in hurricane Daisy on 27 August 1958 from a 30 mm radar on board a U.S. Navy VW-4 reconnaissance aircraft flying at 5.79 km. The eye diameter was 17 km and the central pressure 935 mb. The left eye-wall echo top shown at 21.3 km (70 000 ft) is near 19.8 km when corrected for radar beam width (from Jordan et al 1960)

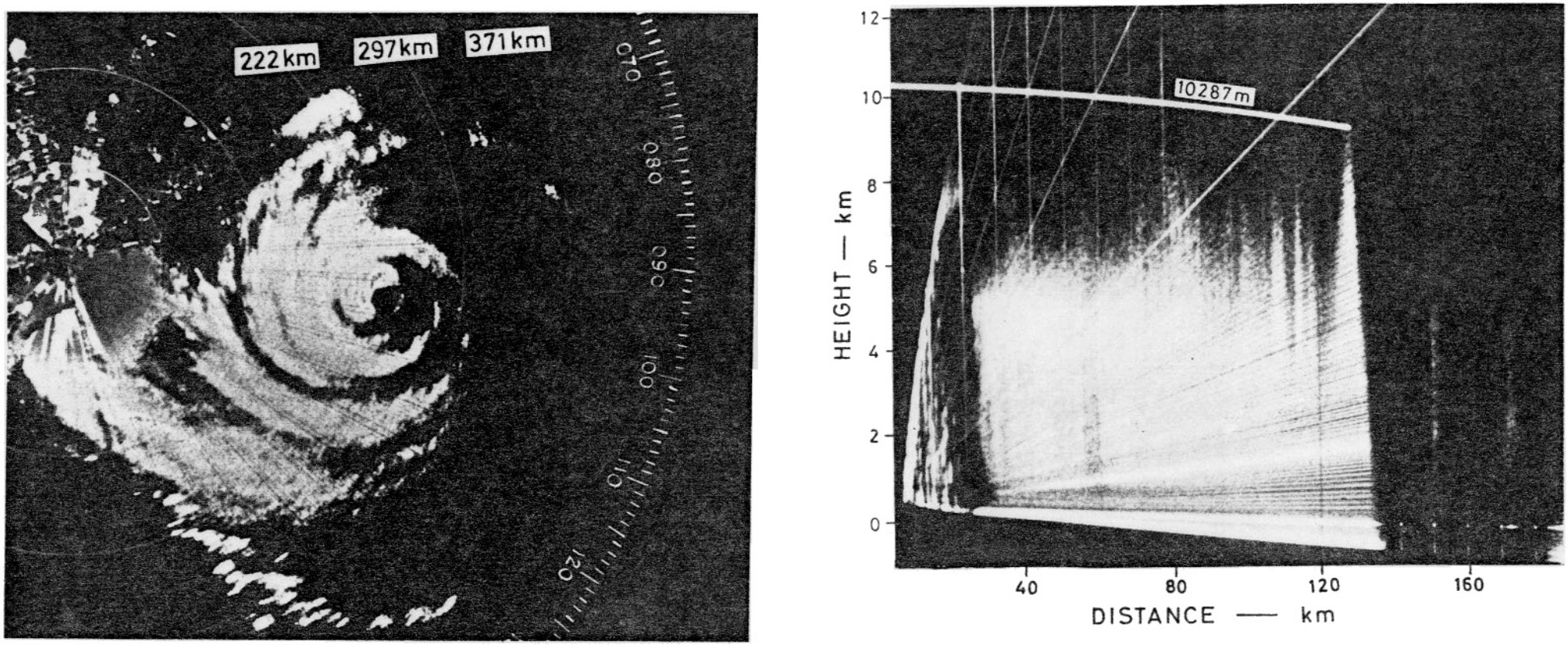

Fig. 10.6(6) . Typhoon Hope east of Hong Kong as seen by a Plessey 43S radar. (a) at 2357 GMT on 1 August 1979. The black areas in the eye wall correspond to rainfall rates greater than 100 mm/h. The RHI cross-section taken two hours later shows weak returns from the weaker, concentric eye wall on either side of the clear eye at 160 km. (From Bell 1980)

10.7 Tracking Tropical Cyclones by Radar

10.7.1 Locating and tracking the eye

Radar enables the centre of a mature, destructive typhoon, within range, to be accurately tracked and often indicates when one develops, intensifies or weakens. However, radar has limitations when used on weaker tropical cyclones the centres of which may not be well defined on radar. The well-defined eyes shown in radar photographs in textbooks and articles on typhoons and hurricanes are, for most stations, the exception rather than the rule, and the complete model radar presentation of the previous section is seldom seen. Somervell and Jarrel (1969) share this experience and state that, except for the case of deep typhoons, typhoon reconnaissance crews report similar findings (sect 14.5.5). Frequently, the eye wall is not clearly depicted especially when it is centred at a range beyond about 250 km or contains only weak, shallow convective activity. On these occasions the positive identification of the eye requires patient, continuous observation and careful interpretation. Indeed, eye position reports should never be given after a brief "spot" observation but only after a period of careful, continuous observation has established the movement of echoes around the eye. The eye wall of tropical cyclones as seen by radar undergoes rapid changes in shape and structure and may completely disappear at times and, to add further difficulties, the chance juxtaposition of rain bands and rain cells can form "false eyes" which are rain-free areas surrounded by rain-bearing clouds and which are not near the true centre of the storm. For these reasons, the reporting of the location and movement of the centre of tropical cyclones as determined from radar observations should only be undertaken by those who have had appropriate training or experience.

If the eye-wall cloud of a mature typhoon contains sufficient snow or rain at an altitude of 10 km (where the temperature will be around $-25^{\circ}C$) it will be detected by a radar sited near sea level when at a range of about 400 km. However, it is necessary to detect part of the eye wall on the far side of the eye to confidently locate the storm centre which will then be at a range of 370 km or less. Greater ranges of detection are possible if the radar is sited on high ground. To track a typhoon, the bearing and distance of its centre, as indicated on the radar PPI display, is plotted on a large-scale chart from which the latitude and longitude of the centre can be read to a tenth of a

degree. It is usual to plot positions of the centre at intervals of one hour; infrequently, they lie along a smooth path indicating the steady progression of a well defined eye but more often the positions, known as "fixes", are found to wander eratically about a mean track. These short term changes of speed and direction of movement of the eye arise from both uncertainties in locating the centre on the PPI and from short term variations in its direction of movement but they do not necessarily reflect changes in the movement of the storm as a whole. However, these small variations become important as the typhoon approaches the coast for they indicate where the eye may make a landfall. At greater distances offshore the expected place of land fall of the storm, as deduced by extrapolating the movement of the eye between hourly radar fixes, will tend to move to and fro along a coast as each observation is received and, for this reason, a smoothed track and speed derived from fixes made over a period of at least 3 hours are normally used as the basis for issuing warning bulletins. Slow moving tropical cyclones can be particularly erratic in their movement as illustrated by the path of tropical storm Susan 1972 shown in Fig. 10.7(1). The resulting small change in position of the eye over a few hours between observations is often comparable to the uncertainty of the radar fix and it is then possible to deduce only that the storm is slow moving. Hourly radar plots of the centre of typhoon Rose 1971 are shown in Fig. 10.7(2) together with seven fixes made by reconnaissance aircraft. Rose was a mature typhoon with a well defined eye and a speed of about 3 m/s and its radar track was steadier than most.

When fixes on a tropical cyclone centre are available from two or more radar stations it is found that they often differ by distances of 20 km or so. These differences arise partly from inaccuracies in the setting up and calibration of the radars and partly from differing judgements on the exact location of the centre of the eye as seen on the PPI displays. It has been noted (Senn & Hiser 1961) that when the far side of the eye wall cannot be seen, then the estimated range of the centre is frequently less than the true range, irrespective of the direction of movement of the storm. Also, the reported azimith or bearing of a storm centre will be in error if the rotation of the aerial and of the PPI scan get out of synchronisation, a condition which may occur in some radars when the aerial is not protected by a dome and suffers severe wind buffeting.

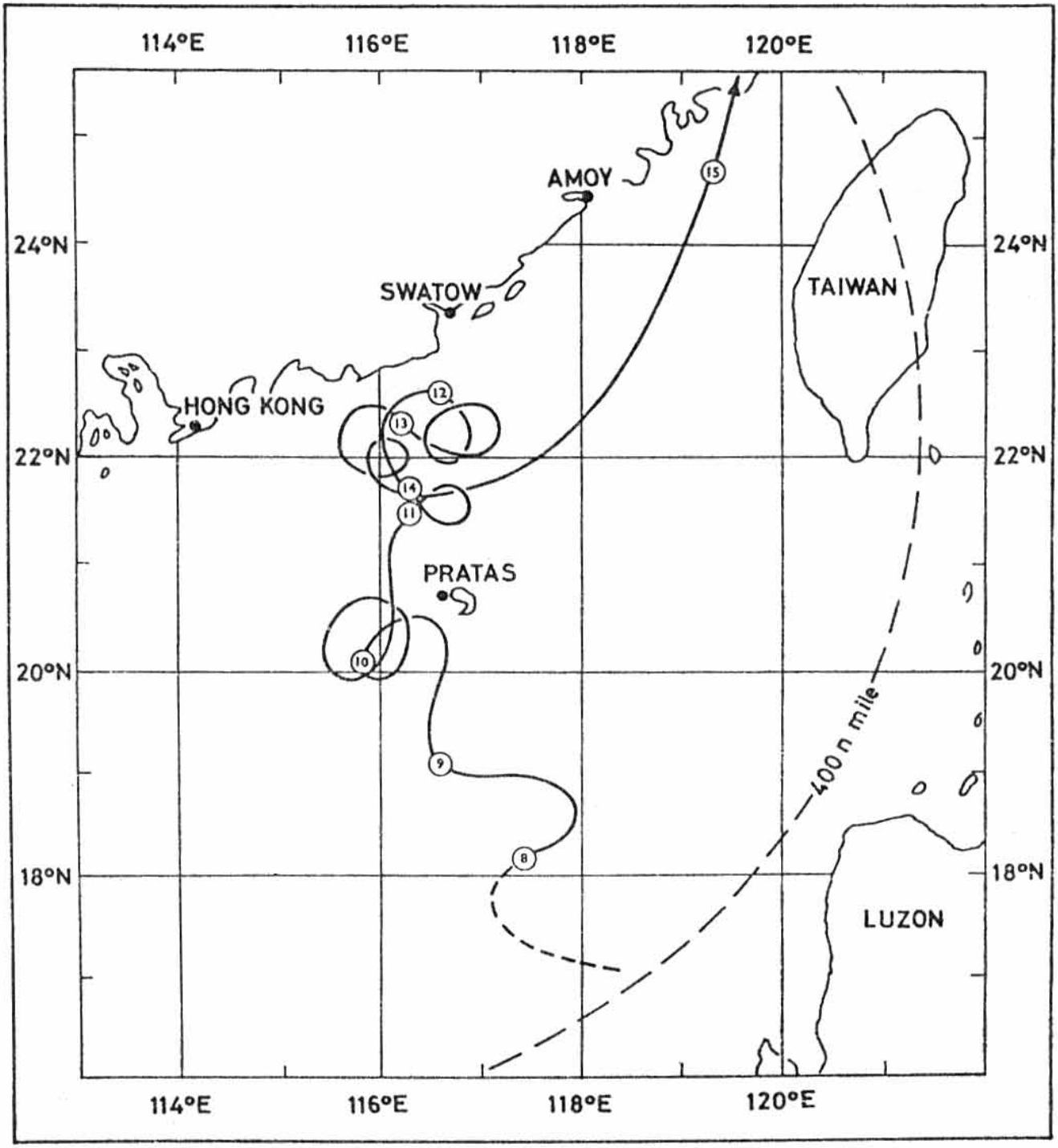

10.7(1)
~~10.6(5)~~

Fig. ~~10.26~~ The track of tropical storm Susan in July 1972. The date is shown in the position circles for 0000 GMT. No other tropical cyclone has remained within 200 n miles of Hong Kong for such a long time since records began in 1884.

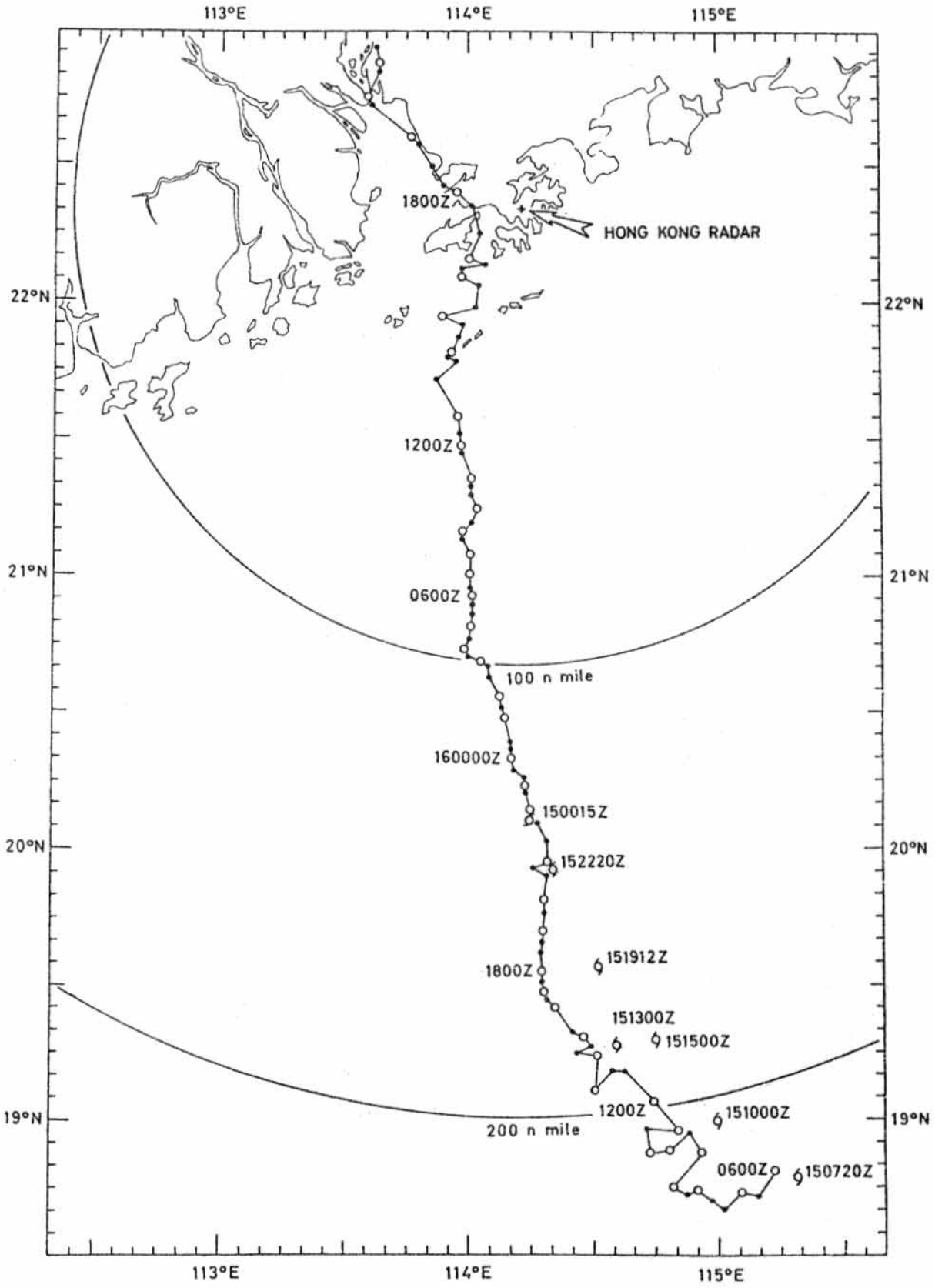

10.7(2)

Fig. ~~10.27~~ The track of typhoon Rose in August 1971 as indicated by hourly positions determined by the Hong Kong 100 mm radar. Seven fixes made by U.S.A.F. reconnaissance aircraft are indicated by the symbol ϕ with the time given on their right. The difference between the aircraft and radar fixes were probably due to the radar bearings being 1.6° too large - see text

Careful and frequent checking of the radar range and bearing of known targets is necessary to ensure reliable fixes. It has been shown that when instrumental and subjective errors are corrected two or more radars are capable of showing a reasonable well-defined radar eye to be in a "single and accurate location" (Conover 1961). Bell (1977) has drawn attention to the good results which can now be achieved in the routine tracking of typhoons and Fig. ~~10.28~~ 10.7(3) illustrates this point. In this example the eye of typhoon Elsie was well defined on both radars and was less than 20 km in diameter as shown in Fig. 10.7(4). Any differences in location must therefore be attributed to instrumental factors. By using solar radiation and the few permanent echoes which could be located with sufficient precision, it was found that the Hong Kong bearings were too large by 1.6° (a feature also suggested by the aircraft fixes in Fig. ~~10.27~~ 10.7(2)). Correction for this error brings the positions reported by the two radars into closer agreement. The more complete presentation shown by the Hong Kong Plessey 43S radar is mainly attributable to it being more powerful (Table ~~10.6~~ 10.5(1)) and sited higher (568 m above sea level) than the Kaohsiung WSR-57 radar (350 m above sea level). The central pressure in typhoon Elsie as reported by the last aircraft fix, near Basco Island at 0923 GMT on 12th October, was 913 mb.

At ranges near 440 km and latitudes of 20° or so, the errors arising from the use of rhumb lines - as on Mercator's Projection - instead of the appropriate great circles can amount to as much as 0.75° in azimuth or 5.6 km in storm position.

If the eye wall is not well developed, as often happens, then it is difficult to accurately locate the centre of the eye on the PPI. However, if well developed spiral bands are visible they can sometimes be used to derive an estimate of the position of the cyclone centre. Most texts recommend that an overlay of an appropriate logarithmic spiral - the one for 10°, 15° or 20° crossing angle as best fits - should be laid on the PPI and adjusted for a good fit to a chosen rainband. The centre of the typhoon will then lie under the origin of the spiral as shown in Fig. ~~10.30~~ 10.7(5). However, I have seldom found this method to be of practical value because, at times when the spirals make a good fit with the rainbands, the storm centre is usually so well defined as to be readily determined without the use of overlays. In addition, it is my experience, and that of Imai (1964), that the crossing angle of the best fitting spiral can vary from 0° to 40° according to the intensity of the storm and, in addition, when bands merge together it is difficult to be objective about the best fit.

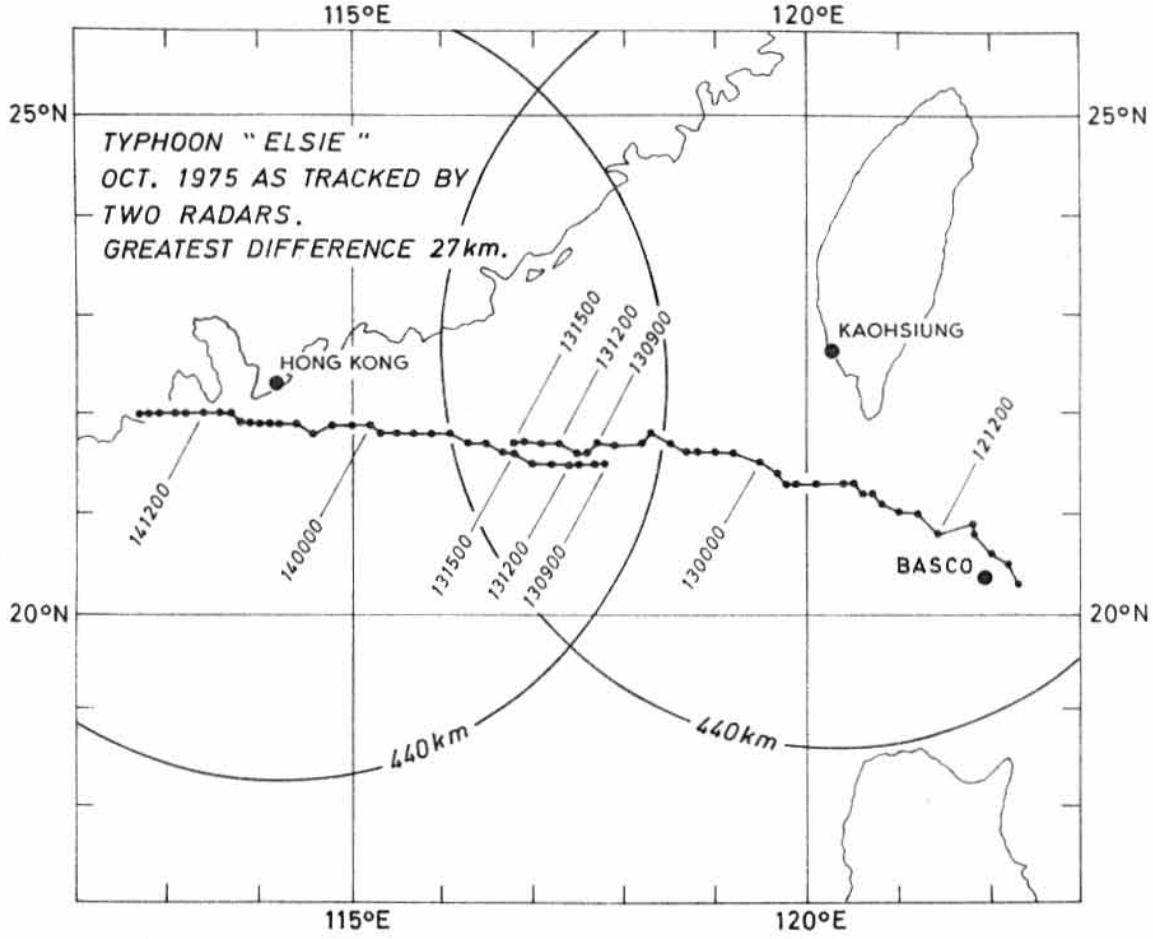

Fig. ~~10.28~~.10.7(3) The track of typhoon Elsie as reported operationally and independently from indications on the Hong Kong and Kaohsiung 100 mm radars. (From Bell 1977).

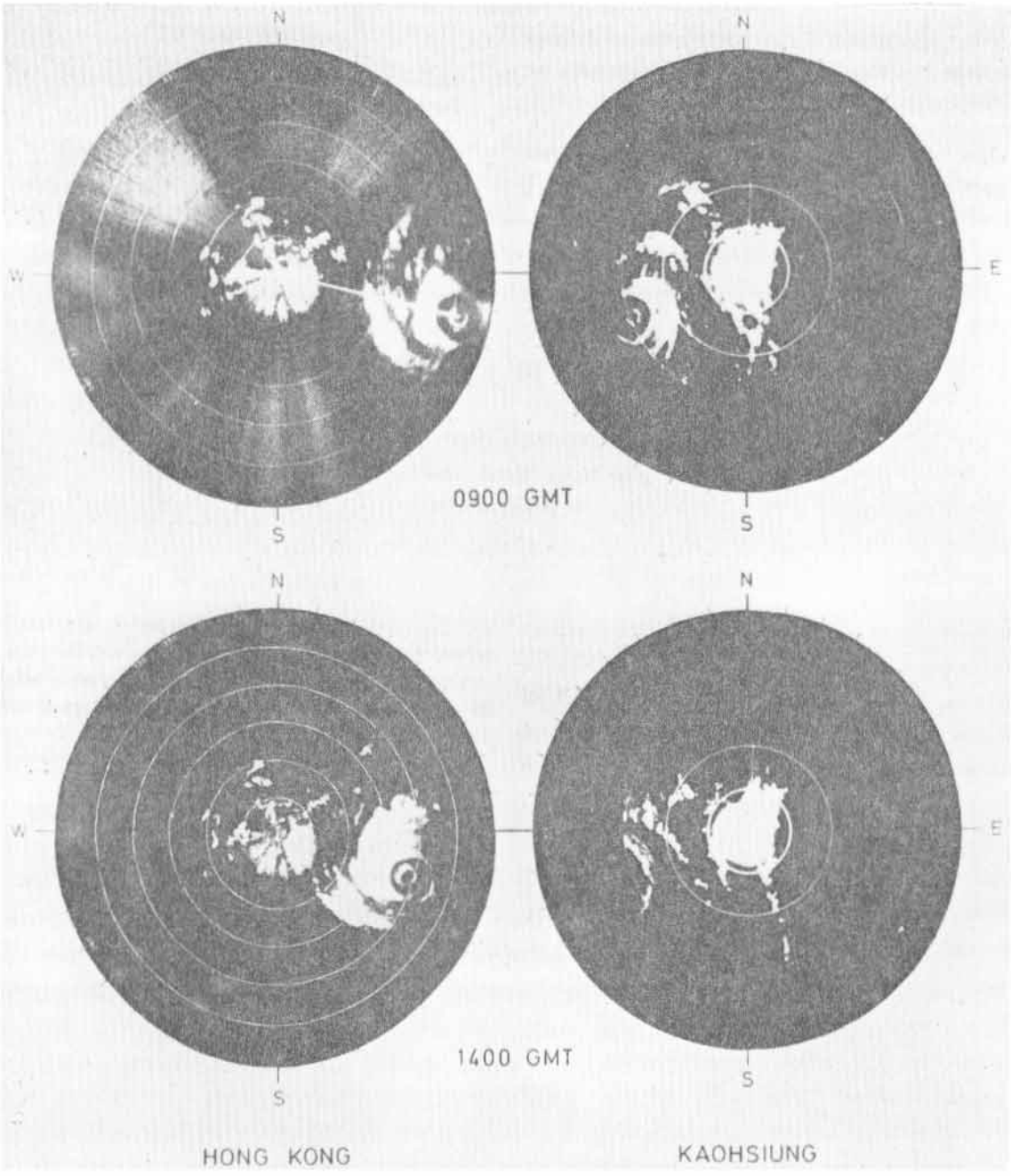

10.7(4)
Fig. ~~10.29.~~ Typhoon Elsie 1975 as seen simultaneously on the Hong Kong and Kaohsiung radars at the beginning and end of the overlap period shown in Fig. 10.7(3). Range rings are at 74 km intervals in the Hong Kong 43S radar display and of 93 km intervals in the Kaohsiung WSR57 display. (From Bell 1977).

Raghavan et al (1980) found similar difficulties in fitting spirals to tropical cyclones in the Bay of Bengal. They note that the visible arcs of spiral bands are usually less than 180° and that outer bands have larger crossing angles than those nearer the centre. They found that fitting spirals to rainbands extending over less than 180° of arc gave rise to large errors in fixing the cyclone centre.

The interested reader can better appreciate these difficulties by tracing the 10° spiral from Fig. 10.7(5) onto transparent paper and trying to fit it to rainbands in other radar photographs. The method may sometimes be useful when the centre of a well organized typhoon is just beyond radar range; a spiral overlay fitted to an extensive and well defined rainband may then give a useful indicatior of the location of the centre. Jordan (1963) applied this method to photographs c hurricane rainbands and found a median error of about 40 km between the position c the storm centres located by the use of a spiral overlay and those indicated in th official post-analysis storm track. Larger errors should be expected under operational conditions.

In intense typhoons the inner rainbands are numerous, almost circular in shape and diffuse into one another (Fig. 4.3) so that it is difficult to follow any one band. When a band can be traced in such storms it will be found to be "wound up" and to be fitted best by a spiral of less than 10°. Indeed, in mature typhoons near their peak intensity the circular nature of the rainbands frequently leads to the formation of concentric bands [often referred to loosely as "double eyes" (sects 4. and 10.6.2)] in the inner regions of the typhoon as in Fig. 10-7(6). In some deep typhoons three such concentric rainbands may be observed as in typhoon June 1975 (Holliday 1976). Circular rainbands indicate that the parent typhoon is intense and most probably has a central pressure of less than 950 mb. In tropical depressions and lesser tropical storms, the rainbands often do not conform to the shape of logarithmic spirals but rather contain straight sections, sharp bends or angles and frequently run into one another as illustrated in Fig. 16. —. The use of overlays on such rainbands can produce misleading results and is not recommended. In short, spiral overlays should only be used to determine the centres of well organized typhoons and severe tropical storms. Their use should be further restricted to those occasions when spirals can be fitted with reasonable confidence and objectivity, to discrete inner rainbands which extend over an arc of more than 180°.

Unless spiral rainbands clearly indicate an incontrovertible eye position it is better to watch small,

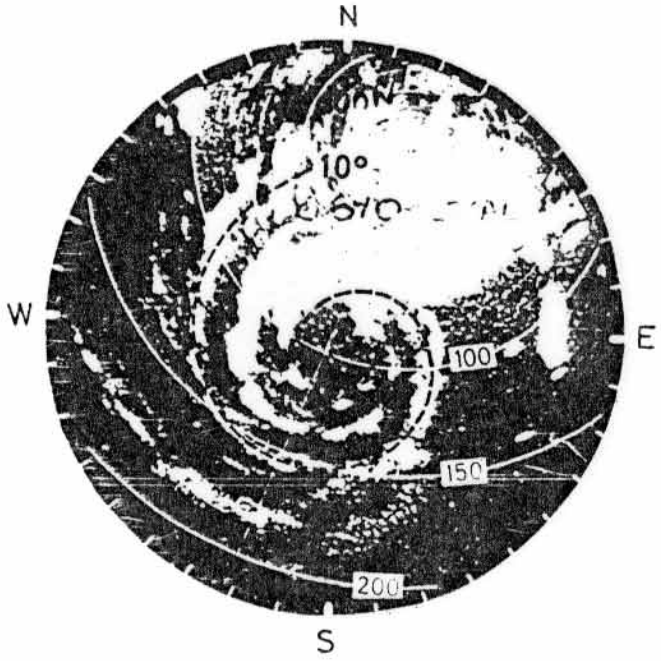

10.7(5)

Fig. ~~10-3~~0. Typhoon Alice 1961 as seen on 18th May at 2110 GMT by a high power 230 mm radar sited 958 m above sea level at Hong Kong. A 10^{8} logarithmic spiral has been superimposed on a rainband. The central pressure was 981 mb and as the eye passed over Waglan Island, sustained wind speeds of 26 m/s with a gust to 36 m/s were recorded - a little less than typhoon intensity. Range rings are shown in nautical miles.

10.7(6)

Fig. ~~10-3~~1. Typhoon Elsie as seen on the Hong Kong 100 mm radar at 1800 GMT on the 13 October 1975. Range rings are at [illegible]74 km intervals

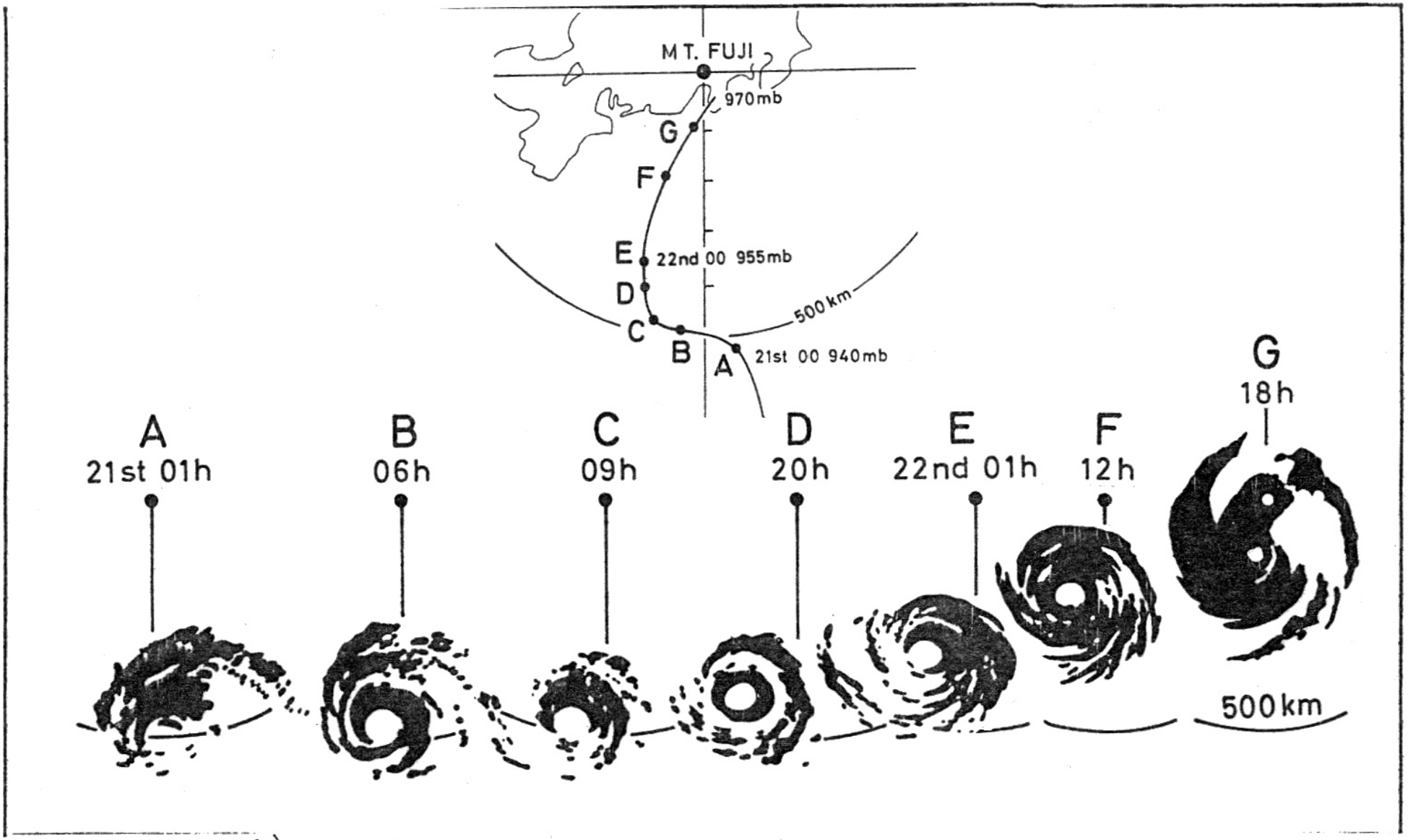

(10.7(7)

Fig. ~~10-32~~ Typhoon Lucy August 1965 as shown on the Mt. Fuji radar. The track of the typhoon and its location when each of the radar photographs was taken is shown at the top of the diagram. (After Tatehira and Itakura 1966).

individual echoes near the estimated centre of the storm and determine their movement. The most useful echoes are those nearest the embryonic eye wall; they tend to be transient in nature as individual convective cells form or grow to heights above the radar horizon. The difficult task of following these echoes,which move slowly on the screen,can be greatly facilitated if a time-lapse film (or equivalent video-tape or digital record) of the PPI is replayed. This increases the apparent speed of the echoes thereby permitting the centre of rotation to be more readily determined. In addition, this method of observation clearly identifies the many echoes or bands which grow in length in a direction opposed to the wind and may appear stationary or even to move against the wind. Unless these echoes are identified they can lead to erroneous estimates of wind velocity. This retrograde apparent motion is caused when large cumulus clouds in a rainband grow upwards into the radar beam in an upwind sequence. As each cloud top appears on the PPI upwind of the last one, it gives rise to an apparent echo motion in a direction opposite to that in which the individual clouds are moving. The impression is accentuated if the downwind head of the band dissolves as it moves into an area which will not support convection.

From the previous paragraph, the great assistance of a time-lapse video recorder in tracking the centre of a tropical cyclone and estimating its intensity will be apparent. Furthermore, its use greatly reduces the chances that a false eye position will be reported. The Hong Kong, prototype, time-lapse device records pictures at selected time-intervals - 15 minutes is found to be the most useful - and these can then be replayed in time-lapse mode for selected periods - usually 2 to 3 hours. Not only is the direction of movement of an echo readily apparent but the speed of those which are well defined and persistent can be quickly derived. In a 2-hour replay, 8 successive positions, at 15-minute intervals, may be seen for a few minutes as an afterglow. Fig. ~~10.32a~~ 10.7(c) shows the real-time presentation of severe tropical storm Agnes 1978 as an afterglow while the presentation 2 hours earlier is superimposed at full intensity. The eye wall in the left hand picture is clearly moving to the left(west) and the storm is intensifying as indicated by the increased area of afterglow echoes relative to that 2 hours earlier. In the right hand photograph - taken 3 days and 9 hours

2300 GMT 26 July 1978
Aerial elevation 1.5°

0830 GMT 29 July 1978
Aerial elevation 0°

10.7(8)

Fig. ~~10.32~~a. The bright, recorded radar displays of severe tropical storm Agnes are shown superimposed on the fainter, afterglow displays two hours later. Agnes is shown moving W on the 26 July, and weakening and moving NE on the 29 July. The central pressures and maximum winds are 980 mbar, 31 m/s and 973 mbar, 21 m/s respectively. Range rings on the Hong Kong radar are at intervals of 74 km.

later - the storm has returned after reversing its direction of movement, and the eye wall echoes are there seen to move towards the NE covering 50 km in two hours, a speed of 6.9 m/s, and to have become less extensive. The storm was rapidly weakening at this time. Such video-tape, time-lapse recordings are superior to film not only because they are immediately replayable but also because the information can be displayed at any chosen scale or section or fed to a computer for further analysis.

Finally, the difficulty that may sometimes arise in locating a centre from one presentation is illustrated by two examples. In Fig. ~~10.32b~~ 10.7(9) the centre of rotation of the echoes in the middle picture is in the lower bulge with the small isolated eye echo moving westward. Photographs taken 3 hours earlier and 9 hours later are also shown. The rain-free area where convection is suppressed rotated cyclonically around the eye at a slower speed than the wind. Echoes moving into the area fade away. The area of suppressed convection can be seen to the right of the eye marker in the left photograph but it has almost disappeared in the photograph on the right taken 9 hours later. The suppression of echoes over one half of the same storm is dramatically illustrated in Fig. 13. . In Fig. ~~10.32c~~ 16.7(10) the centre of the apparent large eye in the left photograph was tracked until it was realized that the eye was further north as indicated by the complete eye wall shown in the right hand photograph. The error could have been avoided by tracking the small echoes further to the west in the left-hand picture.

10.7.2 Indicators of intensity

Apart from locating the centre of tropical cyclones, radar also gives some indication of their intensity and of the amount and intensity of rainfall they contain. Over the oceans, in the tropics, rainbands usually occur when low level convergence takes place and if they show any systematic curvature then it is highly probable that they form part of the low-level inflow into a developing tropical depression. This can be the first indication that a tropical depression is developing (sect 16.—). During the early formative hours, individual echoes from rain cells appear on the screen in increasing numbers, mostly along lines defined by existing echoes. All these echoes grow from cumulus clouds which, from aerial observations, are known to exist in bands before they reach the precipitation stage. If the bands, as seen on the PPI, become more organized and adopt a spiral form then it usually indicates that intensi-

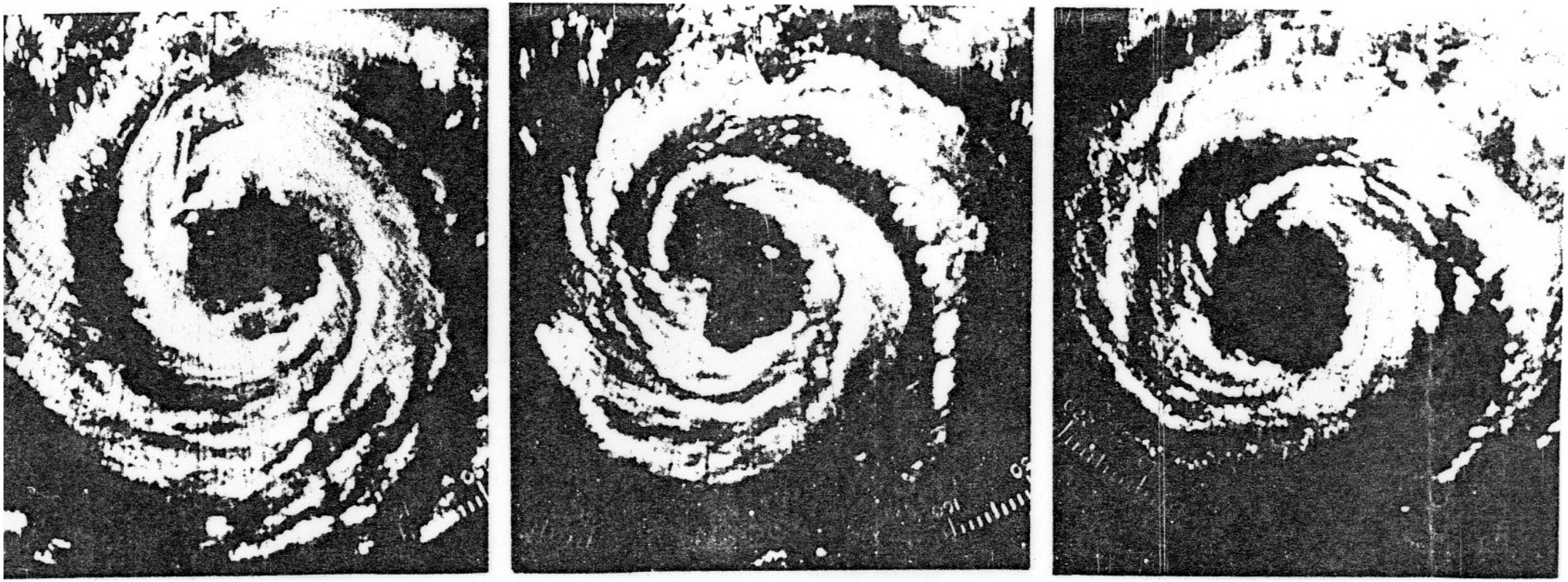

0600 h GMT 0900 h GMT 1800 h GMT

Fig. ~~10.32~~ 10.7 (9) b. Severe tropical storm Agnes as seen on the Hong Kong radar on 26 July 1978. The echo-free area to the E of the eye at 0600 h rotated to the NE by 0900 h to give the appearance of a false eye. The radar is located at the cross, top centre, and the range to outer bearing scale is 220 km.

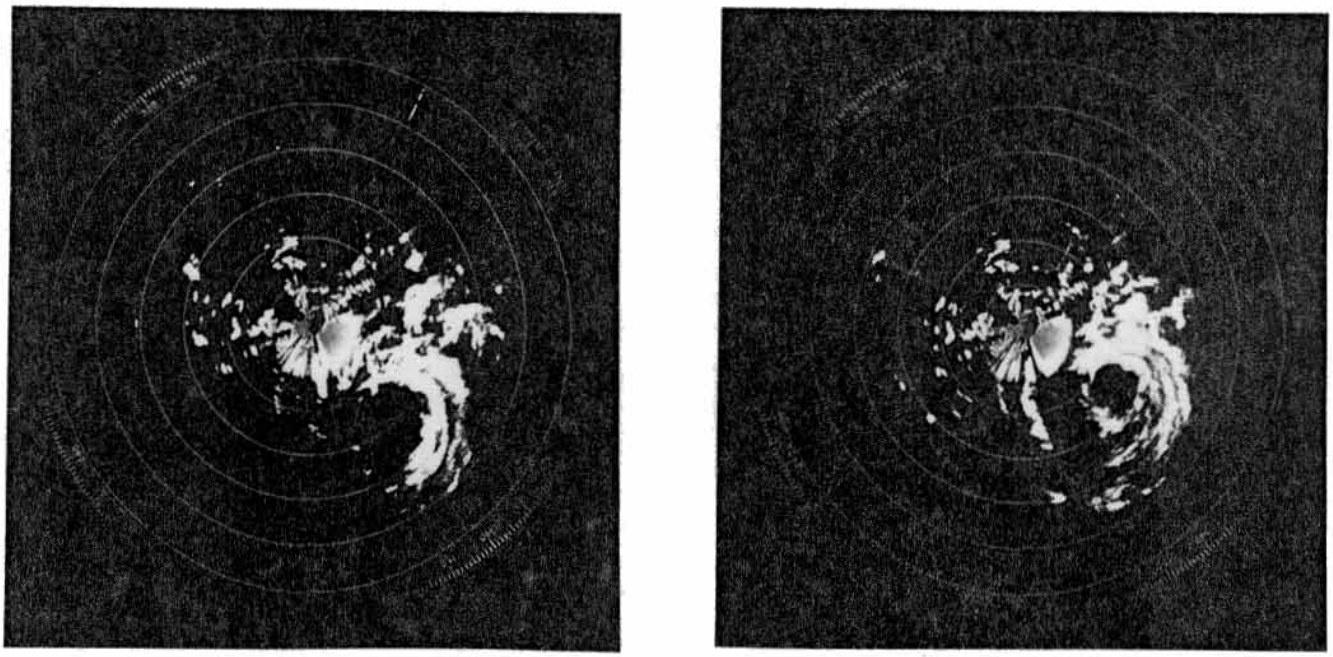

10.7(10)

Fig. ~~10.32c~~. The apparently large eye (~150 km) of severe tropical storm Georgia as seen (left) by the Hong Kong radar at 0800 GMT or 23 May 1980. Three hours later (right) the south west eyewall reforms indicating that the eye is about 75 km in diameter and centred ~40 km further north. Range rings are at intervals of 74 km.

-fication has taken place. Should the storm continue to intensify a clear central eye and eye wall will form when the strongest winds reach about 20-25 m/s. As typhoon intensity is approached the spiral bands become more numerous and appear to "wind up" to present a more circular and symmetrical appearance and, the eye diameter usually tends to decrease unless it has been small from its first appearance (sect 4.). Further deepening usually leads to the formation of concentric ring rainbands (Fig. 10.7(b)) at or near the time of lowest pressure. A persistent decrease of eye diameter over a few hours is three times more frequently followed by an intensification of maximum winds than by their weakening (see sect 13.). However, the case needs to be differentiated from those in which the eye shrinks because of the intrusion of dry, cold air (Fig. 6.). The latter cases are weakening storms although high winds may persist in the eye wall region for some hours. Shrinking eyes, increasing echo intensities and rising echo tops all suggest intensification however, the use of these features to compare the intensities of different storms is totally misleading. For example, Table 4. shows that a given eye diameter can be associated with a wide range of minimum pressure

During weakening over the sea, the above sequence is reversed. The eye wall disappears, echoes appear in the eye and the rainbands become less numerous, less curved and more diffuse and loose their tightly organized regiment ation, especially in the inner regions of the storm. Some of these features are apparent in Fig. 10.32a showing the weakening (right) and intensifying (left) severe tropical storm Agnes and in the weakening typhoon Elsie (Fig. 6.5.3).

Overland the weakening process, as seen on radar, is somewhat different. Imai(1963) showed that when a typhoon approaches the coast of Japan the diameter of the eye begins to decrease about two hours before landfall, and completely disappears an hour or two after reaching land. He showed that the filling of the eye with rain cloud begins at low levels and takes about 20-25 minutes to reach above 3 km. Similar effects are noticed at Hong Kong when typhoons and tropical storms cross the coast of China. The reasons for the disappearance of the clear eye have been discussed in sect . The filling of the eye with rain clouds is usually complete before a distance of 50 km is traversed over land. However, when intense fast-moving storms cross low-lying land extensively flooded by rain and storm surge, the eye and associated hurricane force winds may persist for a longer period. For example, when hurricane Camille 1969 crossed the Mississippi coast near New Orleans, it was travelling at 8.3 m/s and moved 180 km inland in 6 hours before the eye became difficult to identify on the radar screen (Bradbury 1971). At that time, winds of about 32 m/s with gusts to 45 m/s were experienced but were down to about 18 m/s when all vestige of the radar eye was gone (Anon 1969). In contrast

the intense typhoon Viola 1969 lost its eye as soon as the centre crossed the coast and reached the rough terrain of South China; wind speeds overland quickly fell to moderate values (Fig. 3.19) although gales were still being reported offshore.

An experienced radar observer can make a fair estimate of the maximum winds in a tropical cyclone from its general appearance on the PPI. Determining the speed of new "hard" echoes in the eye wall will provide an even better estimate of maximum surface wind speeds (sect 10.6.5).

A diurnal variation in the intensity of tropical-cyclone radar images is frequently observed. The echoes tend to become more intense and better organized around the time of day break. This intensification is real and shows in rainfall averages taken from many tropical cyclones (sect 6.3.8). There is a consequent and subsequent change in the cirrus outflow which can be seen on satellite images (sect 11.).

will travel. Senn (1960 b) showed that in 31 observations on 20 [illegible] the rain shield was spread over the right front quadrant on 29 occasions. On the other 2 occasions it was mainly in the right rear quadrant. Tatehira and Itakura (1966) noticed that the rainbands close to the eye of typhoon Lucy 1965 were often more numerous and crowded in one particular sector than elsewhere and that they remained there for several hours. Since the individual echoes in rainbands rotate around the eye, through about 45° to 90° per hour, the persistence of this extensive rain area, or rain shield, in one sector implies that conditions there are favourable for generating or intensifying rain clouds. The relative location of this area changed markedly as the direction of movement of typhoon Lucy changed (Fig. 10.7(7) ~~10.32~~). In Stage A the crowded sector is to the N W of the eye while it is to the N E in stages C to E; the rainbands were nearly equally distributed around the eye in stage B where the curvature of the track changes sense. In other words, the typhoon moved towards the area where the rainbands close to the eye were most crowded. It was suggested that this feature had not been previously detected because sea-level radars cannot "see" equally well the rain clouds in all storm sectors. The diameter of the eye of Lucy shrank markedly just before recurvature, at position C. It is usually found that individual, well defined echoes tend to move in almost circular paths around the centre as, for example in cyclone Tracy (Australian Bureau of Met.1977) reflecting the low-level wind flow. Therefore, these movements cannot be used to determine the movement of the tropical cyclone (sect 12.).

Echoes in precursor bands outside the storm circulation tend to move with a speed slightly greater than that of the parent tropical cyclone centre and if its direction of movement changes, then the precursor bands, if they are to remain precursors, must change location. In Fig. ~~10.24~~ 10.6(3)(a) (a) the north-south oriented precursor band ahead of typhoon Rose 1971 (moving WNW) weakened and disappeared to be replaced by a precursor band extending over the N.E. and N.W. sectors Fig. ~~10.24~~ 10.6(3) (b) This change occurred as the typhoon made an abrupt change of course from WNW to NNW (Fig. ~~10.27~~ 10.7(2)).

Such well-defined re-arrangement of echoes and their good correlation with storm movement are exceptional. More frequently the signs are hard to read without the assistance of hindsight, and the storm does not always move as indicated by the echo distributions. In addition the observer cannot always be sure that he is seeing all the rain. Accordingly, it cannot yet be said that these methods have been developed to a stage where they have positive forecasting value. Raghavan et al come to the same conclusion from their study of Bay of Bengal cyclones. Nevertheless, a forecaster should be on the alert for a possible change in the direction of motion of a tropical cyclone if the area of crowded rainbands near the eye or the precursor rainband move from one sector to another or if the velocity of the echoes in the precursor rainband show a marked change. Recent findings from satellite observations (sect 11.) are relevant to this problem of predicting storm motion from storm structure.

Dunn et al (1955) noted that the track of the radar eye in Atlantic hurricanes often veered to the left upon landing. Imai (1963) noted a similar deflection in typhoons which crossed the coast of Japan. The phenomenon has been attributed (Dunn et al 1955) to the winds in that part of the storm which is over land being more retarded by friction than those over the sea (see sect 12.2.3). The track of the radar eye of typhoon Rose 1970, Fig. ~~10.27~~ 10.7(2) shows a similar turn to the left at the China coast. However, radar eyes frequently cross coasts without changing significantly their direction of motion so the effect cannot be relied upon. More case studies are required to determine what proportion of tropical cyclone eyes are deflected on crossing a coast and to see if those which are deflected can be identified before landfall. Trochoidal+ or wave like

+ A trochoid is a curve generated by a point in the plane of one curve that rolls on another. A particular case is the cycloid - the path of a point on a wheel which rolls on a straight line.

oscillations in the track of the eye of a tropical cyclone are sometimes observed by radar. These oscillations have periods between 6 and 48 hours and they are described in sect 12.2.2.

10.8 Some Radar Phenomena and Tropical Cyclones

10.8.1 Sea clutter

Tropical cyclones are born and live over the ocean. Radars for tracking them must therefore survey as large an expanse of sea as possible. Radar energy incident on a smooth sea surface is partly absorbed and partly reflected, after the manner of light reflected by a mirror. When such regular reflection takes place, known as "specular" reflection, no energy will be returned to the radar and the sea surface will not be "seen" on the PPI. However, when the surface is disturbed some fraction of the incident radar energy is scattered in all directions and the amount so scattered increases with sea surface roughness. At some state of sea the energy back scattered towards the radar will be sufficient to be detected and will then appear on the PPI display as "sea clutter". Rough seas will cause the clutter to be seen wherever the sea is illuminated by the radar and this is limited in range, of course, to the radar horizon. Strong sea clutter can obscure returns from ships and rain clouds and it confuses the PPI presentation when tropical cyclones are being tracked for, at such times, the sea will be very rough and the sea clutter severe. Returns from the sea can be eliminated if the radar beam is elevated so as not to impinge on the sea surface. However, in this condition, distant rain echoes normally detected will be below the radar beam and not seen. Therefore, when tropical cyclones approach a station, it is usual to effect a compromise by elevating the radar beam progressively so that the storm centre is always clearly visible; nearby rain echoes will then be seen as well as the reduced sea clutter permits but the more distant rain echoes will be lost or will not be seen so well.

The intensity of the returns which form sea clutter depends upon many factors such as, the angle that the incident beam makes with the horizontal, the wavelength, power, sensitivity, pulse length and other characteristics of the radar, the polarization of the radiated energy, propagation conditions, the state of the sea and the wind speed and direction.

Most of the instrumental factors which improve the capability of a radar in the tropical cyclone detection role also increase the sea clutter. A site near the coast results in a large area of sea surface receiving radar energy, a higher site increases this area and also increases the

angle at which the beam is incident on the surface when looking at distant storms, these factors increase both the area and intensity of sea clutter. Increasing the power of the transmitter or the sensitivity of the receiver increases the sea clutter and causes it to be detected at lower sea states and to greater ranges until limited by the radar horizon. However, the intensity of the sea clutter decreases linearly with the radar wavelength so that using a radar wavelength of 100 mm give less sea clutter, other factors remaining unchanged, than shorter waves of 30 or 50 mm. Also, the plane of polarization can be chosen so as to greatly reduce the intensity of the returned sea clutter in certain circumstances. With lightly disturbed seas and vertically polarised radiation of 100 mm wavelength, the returns from the sea will be 100 to 1 000 times (20 to 30 dB) greater than with horizontal polarisation (Skolnik 1962). As the sea becomes rougher the difference between intensity of the clutter for the two states of polarisation decreases and becomes negligible for seas with waves 1 to 2 m high.

Although the sea clutter performance of radars with horizontal polarisation is good for light to moderate seas, it is not yet certain whether it is necessarily best for use in the tropical cyclone detection role because there have been no reported polarisation experiments in typhoon conditions. Newell and Geotis (1955) found that in the precipitation melting zone, horizontal polarisation produced returns about 40% greater than those obtained with vertical polarisation. When a melting band is present in a tropical cyclone the use of horizontal polarisation would be advantageous on this additional ground. It is also probable that the numerous raindrops of near maximum size ($D \sim 6$ mm) falling in the preferred oblate form in the intense rainfall in tropical cyclones might also give an enhanced return with horizontal polarisation (sect 10.2.2). It would therefore seem that the use of horizontal polarisation for tracking tropical cyclones is to be preferred on three grounds, but experimental confirmation is required. Seliga and Bringi (1978) measured the returns from Illinois thunderstorms and obtained returns for horizontal polarisation (at λ = 100 mm) which were up to 6 dB greater than those from the vertical mode

In the absence of significant swell, the presence of sea clutter indicates that the wind speed offshore is at least fresh and at many stations clutter first appears when mean winds are approaching the speed for which warnings for small craft are issued (11 m/s). However, the exact speed at which sea

clutter appears on a given radar depends upon its characteristics and settings, its siting, the sea state and on the direction of the wind. Sea clutter returns are 3 to 10 times (5 to 10 dB) greater when looking into wind than when looking downwind. The sea state is not uniquely defined by wind speed but depends upon other factors such as fetch, swell, tide, currents and air to sea temperature differences. Hiser et al (1967) using a 100 mm radar sited 33 m above sea level at Miami, found that sea clutter extended to ranges of about 65 km which was well beyond the station's normal radar horizon of 24 km. Off Miami, north easterly winds blow counter to the Gulf Stream and so develop rougher seas than do southerly winds of the same speed; sea clutter usually appears there with northeast winds of 8 - 10 m/s and with south or southeast winds of 10 - 13 m/s. The reason for the extended range of sea clutter reported by Hiser et al is not known but is probably due to anomalous propagation in low level ducts over the sea. Figs. 10.33(b) and 10.34(a) show that in tropical cyclone situations, the higher radars at Mount Fuji (3 776 m) and Hong Kong (568 m) show sea clutter out to their normal radar horizons of about 250 km and 95 km, respectively. (sect 10.3.2)

The outer edge of the sea clutter associated with tropical cyclones is usually very irregular Fig. 10.33(b). During the fine spell which usually occurs in the early stages of the approach of a tropical cyclone towards Hong Kong, patterns often appear in the sea clutter. They frequently intensify and take on irregular shapes, often of zig-zag form and the clutter may weaken or disappear at shorter ranges as in Fig. 10.34(a). The reason for this phenomenon is not definitely known but when it occurs, nearby upper-air soundings show conditions to be favourable for anomalous propagation. The patterns disappear if the beam is elevated about 2° as in Fig. 10.34(b). Note that, on both the occasions illustrated in Fig. 10.34 the wind over the sea clutter was light with a northerly component and pre-storm swell was running. The effect is particularly well developed when a typhoon is to the east of Hong Kong in the early afternoon and so causes hot dry air from the interior of China to move out across the cooler waters of the South China Sea (Peterson 1976). The air picks up water vapour and is cooled in the lowest layers to form an inversion - ideal conditions for setting up gradients of water vapour and density which give rise to anomalous propagation ducts (sect 10.3.2) → p 62a.

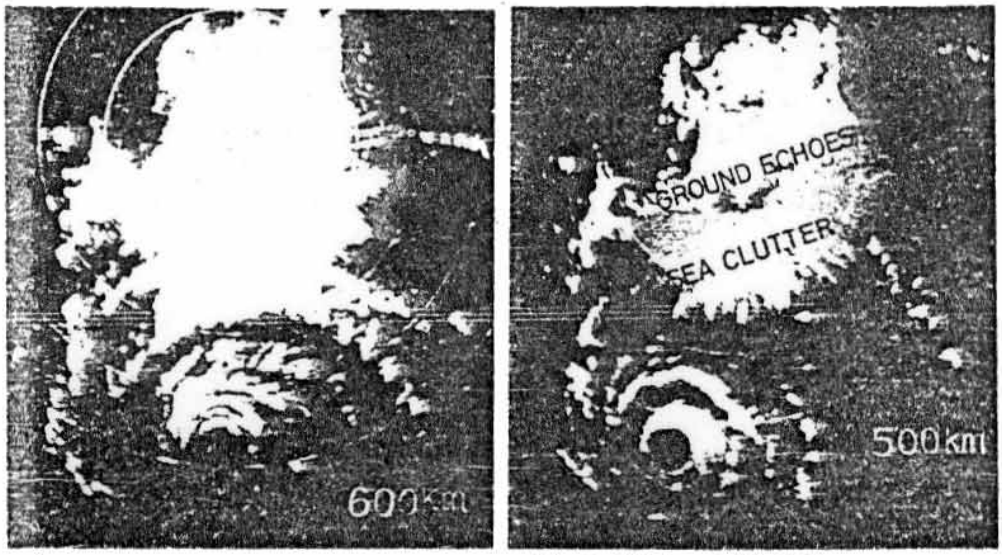

(a) 03 JST August 21, 1965.
Elevation -1.7 .

(b) 16 JST August 21, 1965.
Elevation -1.7 .

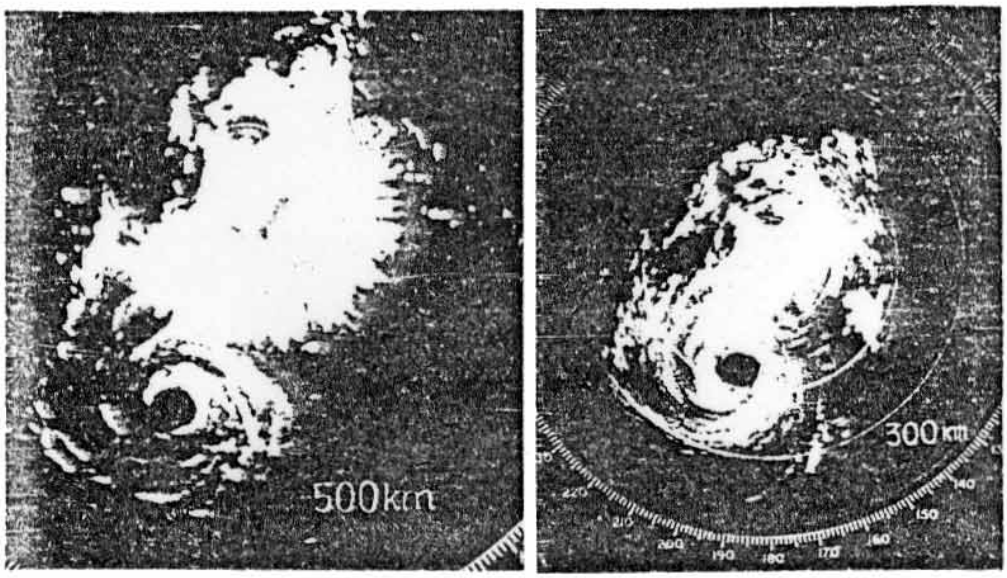

(c) 01 JST August 22, 1965.
Elevation -1.7 .

(d) 14 JST August 22, 1965.
Elevation -0.5 .

10.8(1)

Fig. ~~10.53~~. Photographs of the Mt. Fuji radar PPI when tracking typhoon Lucy 1965. Range rings are at intervals of 100 km (From Tatehira and Itakura 1966).

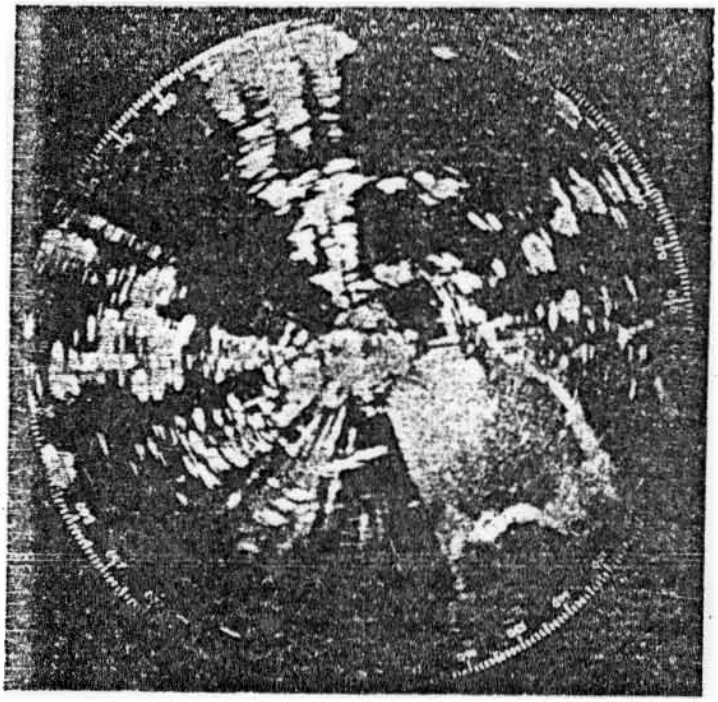

(a)

10.2(2) 24

Fig. ~~10.33~~ Anomalous sea clutter patterns seen to the S.E. of Hong Kong during the approach of tropical cyclones. The sharp edge to the clutter on a bearing of 155° is caused by Kowloon Peak which intercepts the radar beam at low elevations. The range ring is at 74 km (40 n. miles).

a) On 14 July 1970 at 2152 GMT when tropical storm Ruby was centred about 485 km S.E. of Hong Kong. The wind over the sea was light northerly and the swell was from the east with a height 1-2 m and period 6 s.

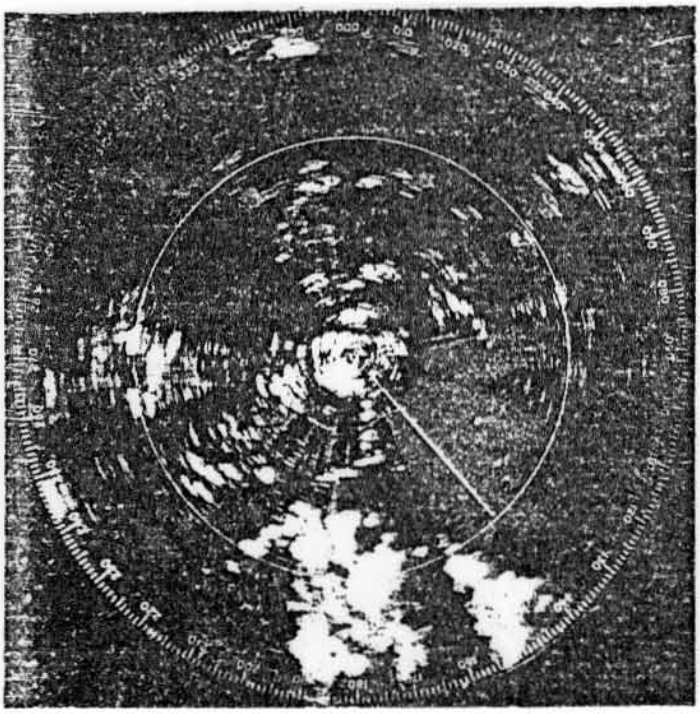

(b)

b) On 19 August 1967 at 0213 GMT when tropical storm Kate was centred about 730 km S.E. of Hong Kong. The radar beam had been elevated 2° above the horizontal just prior to the photograph so that the "after glow" of the sea clutter was still visible; note its intensification in the arc marked by the indicator line. The wind over the sea was light northeasterly and the swell was easterly with a height of about 1 m and period 6 s.

The mechanism is enhanced by the subsidence taking place in the fine weather area ahead of the tropical cyclone (see Fig. 5.3.1(2)). During the approach of typhoon Viola, in July 1969, sea clutter extended as far as 130 km from Hong Kong or more than twice as far as usual. Sometimes there are clear areas or skip zones between nearby sea returns and those from further afield. This phenomenon is illustrated in Fig. 10.8.(2c) for the case of a tropical depression for they are equally as effective as typhoons in causing anomalous propagation.

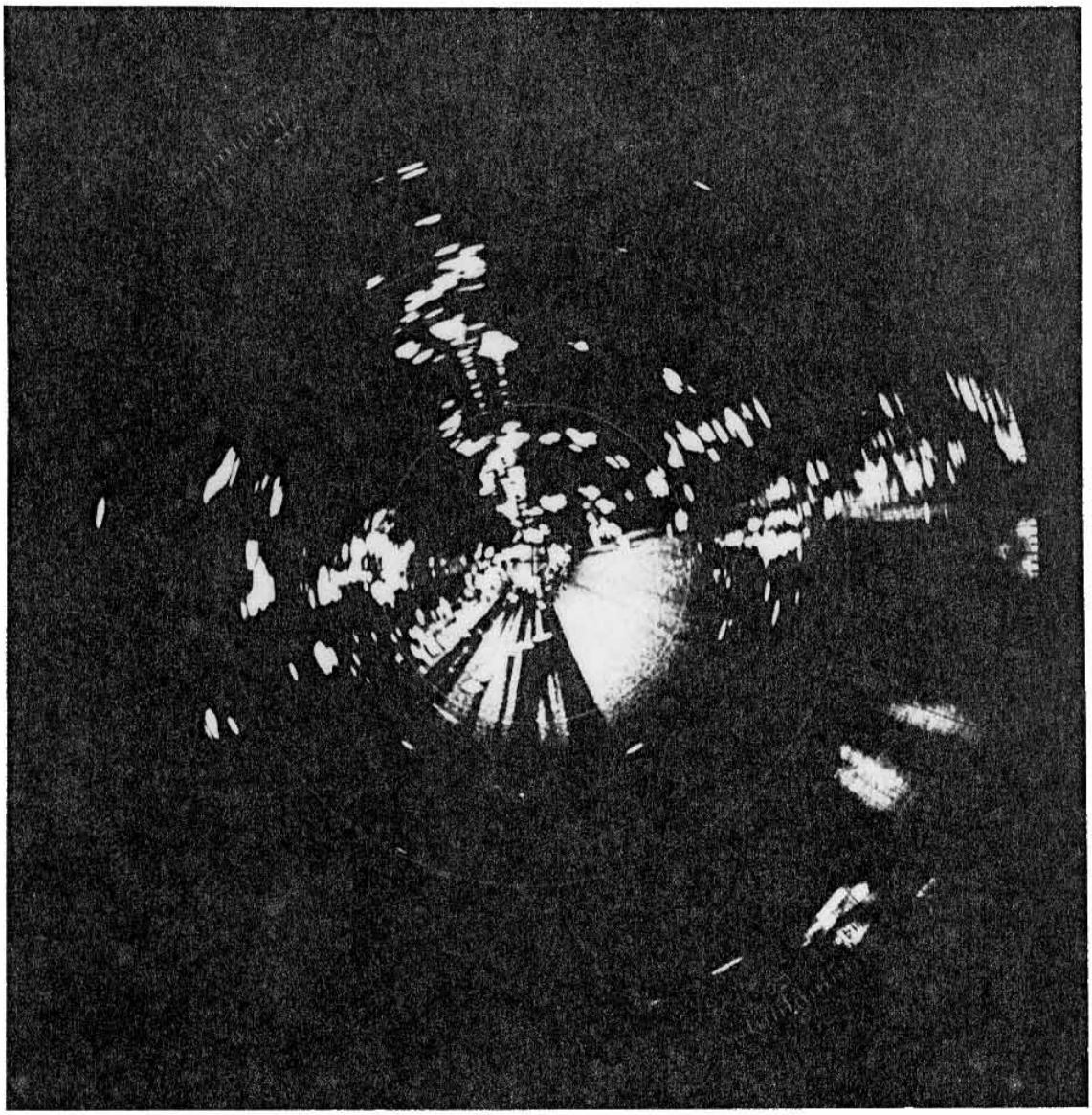

Fig. 10.8(2c). Sea clutter can be seen to the southeast of Hong Kong extending as far as the first range ring (74 km). More distant returns between the second and third range rings (148 and 222 km) are also seen to the east and southeast of the Hong Kong radar. Note also the multiple echoes from ships and hills. The photograph was taken on 12 September 1980 when a tropical depression was centred over the northern part of the South China Sea.

U.S. Navy meteorologists, flying typhoon reconnaissances in VW-4 Constellation aircraft equipped with 100 mm radars, found that, although sea clutter was generally intense near the centre of typhoons and tropical storms, the eye region would often show up as an area with little or no sea clutter. This was attributed to the presence of light or calm winds at the surface in the eye. The phenomenon was used to identify the centres of tropical cyclones which were otherwise ill-defined (Senn & Hiser 1961). Similarly, Tatehira and Itakura (1966) concluded that the absence of sea clutter in the western half of the eye of typhoon Lucy 1965 Fig. 10.8(1)(d) was due to the calm centre of the wind vortex being displaced to the west of the eye centre as defined by rainclouds. (See sect 9.1).

The exact causes of sea clutter are not yet known and are the subject of research using radar waves of different frequencies and polarisation together with Doppler radars to identify the speed of movement, along the line of sight, of scattering elements. Sea spray plays an important role because drops of sea water scatter energy like raindrops. However, by itself a sea spray theory does not explain the polarisation effects or the difference in intensity between upwind and downwind observations. Neither can it account for the velocity of some of the scatterers as determined by Doppler radar. Other theories include diffraction effects caused by a regular sequence of sea waves, specular reflection from waves which present suitable aspects and a 'facet' theory, in which facets or patches on the sea surface are assumed to scatter like an array of inclined plates. It should be noted that if specular reflection were to occur from individual waves they would have to be separated by at least half a radar pulse length if they were to be resolved. For example, the wave length would have to be greater than 300 m if the waves were to be resolved by a radar with a 2 μs pulse (600 m).

Pidgeon (1968) concluded from his Doppler radar experiments that vertically polarised waves are scattered from just below the sea surface whereas horizontally polarised waves were returned from the surface itself. He was led to this conclusion because the vertically polarised waves were returned from scatterers having a velocity appropriate to the

'orbital' velocity of water within the crests of waves. Enough has been written to show that the subject is complex, suffice it to say that there is more than one effect contributing to the scattering of radar energy over the sea.

10.8.2 Anomalous propagation

In the previous section we attributed both the occasional extension of the sea-clutter horizon and the irregular sea clutter affects noted ahead of tropical cyclones, to anomalous propagation. Because strong winds cause turbulent mixing it would be unlikely that extensive areas with strong gradients of refractive index could exist in tropical cyclones and anomalous propagation of radar waves there would not therefore be expected. However, there have been reports of anomalous propagation near tropical cyclones and Senn (1967) has shown that about 33% of the hurricane soundings which he studied, indicated that some anomalous propagation could be expected. It is probable that this figure is higher than would be found in tropical cyclones over the oceans away from land influences.

Rockney (1956) reported that, although the eye wall is normally first detected at a range of about 270 km, in hurricane Betsy 1956 it was clearly defined at a range of 375 km by a high power 32 mm radar although powerful 100 mm radars nearby were unable to detect the eye wall at all. He attributed this to an isothermal layer at 3 km wherein there was a moisture inversion that caused ducting of the 30 mm waves (but not the 100 mm waves) to within about 240 km of the eye; beyond this the duct was broken down by the hurricane circulation and propagation became normal. Senn and Hiser (1961) agree that the exceptional ranges of detection achieved by 32 mm radar both in Betsy 1956 and in Daisy 1958 were due to the refractive conditions. Ducting takes place only if the wavelength is less than some critical value determined by the steepness of the gradient of the refractive index within the duct and its depth. Short waves are trapped by shallower ducts than long waves. The frequency with which ducting occurs at different wavelengths depends on both the siting of the radars and the local climatology. Hiser (1957) reported that a 50 mm radar with a $3\frac{1}{2}^{\circ}$ conical beam, sited at the University of Miami, consistently showed less anomalous propagation than a nearby 100 mm radar with the same beam width. Raghaven et al (1980) detected a spiral band of a deep depression over the Bay of Bengal when it was at a range between 600 - 700 km. They were using a 100 mm radar located at Madras and the depression occurred during the 22-29 November 1976. The storm destroyed the favourable propagation conditions as it moved closer to the radar.

It is difficult to tell whether or not sub-refraction or upward bending is taking place ahead of a distant tropical cyclone. It is possible, of course, to recognise super-refraction if a tropical cyclone or sea clutter is seen at much greater distances than usual, ~~but this does not occur very often~~. Radar operators should therefore be on guard for anomalous propagation when tracking tropical cyclones although current experience indicates that it is unlikely to cause a serious loss of performance at such times. Nevertheless, more detailed information on the gradients of refractive index in the low levels around tropical cyclones is required to enable a more thorough determination to be made of the characteristics and frequency of occurrence of anomalous propagation there.

10.8.3 The melting band

The appearance of enhanced radar returns from regions in which snowflakes are melting, the melting band was first predicted by Ryde (1946) from theoretical considerations. Its formation has been discussed in sect 3.6.1 and illustrated in Fig. 3.13. A similar bright band was detected in the first hurricane to be scientifically studied using radar (Wexler 1947). The formation of these bands is restricted to regions where there are updrafts of about 1 m/s or less (at greater speeds snowflakes will rise) and since the inner portions of hurricanes and typhoons are comprised of a significant proportion of cumulo nimbus clouds, which contain strong upcurrents, the frequent appearance of the bright band there was surprising. Early observations were at relatively high latitudes and it was at first thought that the bright band was a consequence of changes in the structure of hurricanes and typhoons as they became extratropical. However bright bands have since been observed, quite frequently, in hurricanes and typhoons in the tropics. For example, Senn (1966a) described airborne

radar observations in hurricane Betsy 1965 which showed bright band returns in all parts of the storm. At the time of the observations Betsy was about 4 degrees of latitude north of Puerto Rico (18.5°N) and had a central pressure of 970 mb. It is now generally considered that the bright band forms in tropical cyclones because some rain there falls from stratiform clouds. In addition, some of the embedded cumulonimbus clouds may also contain regions in which updrafts have velocities of less than 1 m/s because such areas are found even in thunderstorms.

Snowflakes begin to melt as they fall through the freezing level but they do not become water drops until they have fallen some distance through warmer air. The top of the melting band therefore indicates the height at which the temperatures is 0°C although it will be brightest just below this level. The relatively warm air found in the inner regions of cyclones causes the 0°C level there to be higher than in the undisturbed atmosphere and to increase in height as the eye wall is approached. The corresponding variation in the height of the top of the melting band in individual storms can usually be seen on RHI. In addition, the melting band can sometimes be seen to be relatively high in, and near, strong spiral bands (Fig. 10.8(3) ~~10.35~~) which, as Gentry (1964) showed, are warmer than their environment.

Senn (1966a) found the height of the bright band in hurricane Betsy 1965 to be between 4 300 and 4 600 at moderate ranges from the centre and to rise to 5 200 to 5 800 m in, and near, the eye wall. In hurricane Debbie 1969 (Black et al 1972) the melting band was found to be about 600 m greater than that 185 km from the centre. One quarter of the RHI photographs taken in Debbie showed a bright band. Similar conditions have been observed in other hurricanes. The height of the 0°C level in the West Indies in the undisturbed atmosphere is about 4 724 m while in the Western Pacific it is some 400 to 500 m higher. Strong typhoons have warmer cores than weaker ones and, in general, the 0°C level in the former will be higher than in the latter as also will be the top of any melting bands which may be present. In the inner regions of intense typhoons, the 0°C level is over 7 000 m (sect) but no RHI photographs defining a bright band in such intense storms have yet been published.

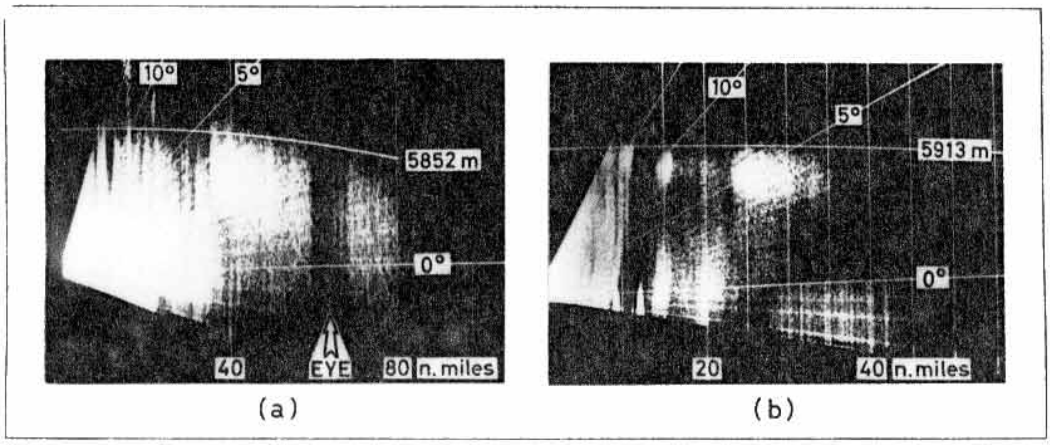

Fig. ~~10.35~~ 10.8(3). Photographs of the 100 mm Plessey 43S radar RHI at Hong Kong in tropical storm Ruby on 16 July 1970 at 0550 GMT. (a) view through the eye of the storm which was overland at a range of 63 n mile on a bearing of 042°. (b) view through rainbands over the sea on a bearing of 172°. The sensitivity of the radar was reduced to 1/40th of normal (16 db) in (a) and to 1/316th (25 db) in (b). The 0°C level at Hong Kong was 5 550 m at midnight GMT on the 16 and sea level pressure at the storm centre at 0600 GMT was 992 mb. Range markers at 40 n mile (74 km) in (a) and 5 n mile (9.3 km) in (b).

When tropical storm Ruby 1970 was decaying over land 116 km northeast of Hong Kong the RHI photograph in Fig. ~~10.35~~ 10.8(5) was taken on a bearing through the eye of the storm. The 0 °C level can be seen sloping downwards towards the eye; a phenomenon usually observable in decaying storms over land for reasons given in sect . In the rainbands over the sea, more distant from the centre, the top of the melting band was still high and can be seen in Fig. ~~10.35~~ 10.8(3)(b) to be higher still in the rainband about 20 n mile (56 km) south of the station. When these photographs were taken the sensitivity of the radar was reduced so that returns from snow above the freezing level would not be seen, in this way the top of the melting band is more clearly defined but note that even in this relatively weak and dissipating tropical cyclone it is about 200 m higher than that given in the previous paragraph for hurricane Betsy.

Tropical cyclones over the China Sea to the south of Hong Kong sometimes show the bright band and sometimes not. Even weak storms can be variable in this respect. For example, typhoon Carmen 1974 and severe tropical storm Doris 1975 showed no bright band but typhoon Irma 1974 showed a good one (the eye was just over land at the time); these storms had cloud tops near 7.6 km. Typhoon Elsie 1975 showed no bright band as can be seen from Fig. 10.8(4).

In summary, it appears that the bright band can be found in weakening tropical cyclones in which the areas containing strong convection are decreasing and in those parts of stronger tropical cyclones in which convection has weakened. However, in the inner regions of steady state typhoons, where convection is strong, as in Fig. ~~10.35~~ 10.8(3)a, a bright band will not be found.

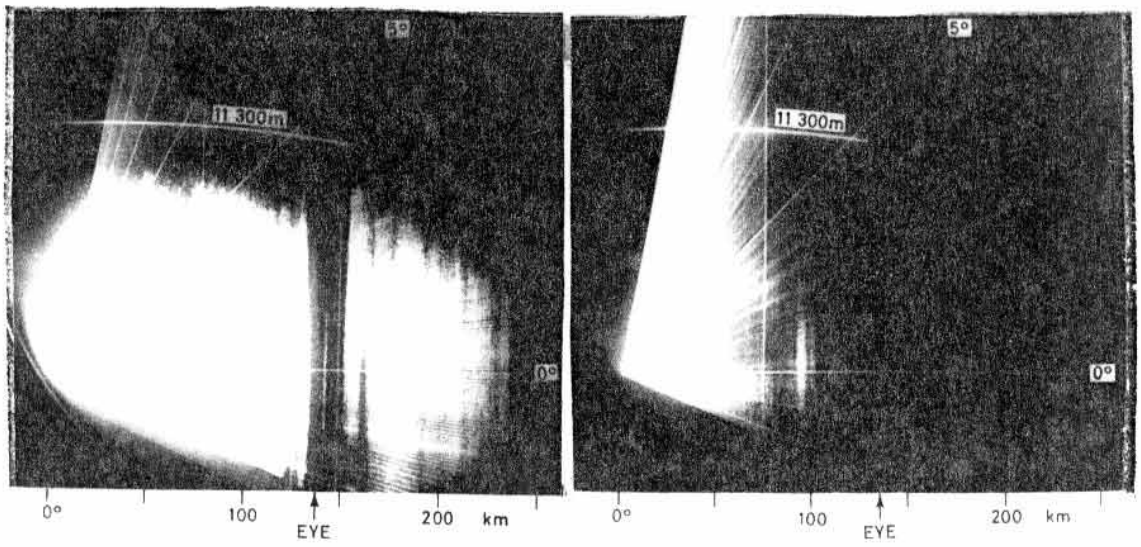

10.8(4)

Fig. ~~10.35a~~ RHI presentations of the eye of typhoon Elsie at 2215 GMT on the 13 Oct 1975 when it was about (140 km) on a bearing of 113° from the Hong Kong radar. The line indicating the top of the highest echo is at 11.3 km. In the picture on the right the radar sensitivity has been decreased by 36.6 dB (i.e. by a factor of 1/4 500) to show the absence of a bright band. The rainfall intensities in the convective columns were in excess of 65 mm/h. A PPI presentation of Elsie is shown in Fig. ~~10.31~~.

10.7(6)

10.8.4 Doppler radar

Conventional meteorological radars are called "non-coherent radars" because no account is taken of the phase of the returning waves with respect to those transmitted. However, these phase relationships contain information on the velocity of scatterers along the line of the radar beam. Radars which are phase sensitive are called "coherent" and make use of the Doppler principle - familiar from school physics in connection with the fall in pitch (frequency) of the whistle of a passing express train. Doppler radars can be continuous wave or pulsed although both the theory and construction of pulsed radars are more complex than in the case of continuous wave radars.

Following Atlas (1964) we can consider a point target at a range r from the radar, there will be $2r/\lambda$ wavelengths in the out-and-return path. Each wavelength corresponds to a phase change of 2π so that the phase position of the target will be $4\pi r/\lambda$. If the target has a radial motion v with respect to the radar, its position in terms of phase will change continuously and proportionately. Phase changes in time are represented by an angular velocity ω such that

$$\omega = 2\pi f = 4\pi v/\lambda \qquad (10.8(1))$$

or

$$f = 2v/\lambda \qquad (10.8(2))$$

where f is the Doppler frequency shift caused by the radial velocity v. If $\lambda = 0.1$ m then the Doppler shift is given by

$$f = 20v \qquad (10.8(3))$$

and is seen to amount to 20 Hz for each increment in radial velocity of 1 m/s. In the meteorological context, shifts will range from zero to say 3 000 Hz - one millionth of the transmitted frequency f = 3 000 x 10^6 Hz. In continuous wave radars, f is readily obtained by combining the returned waves with those from the transmitter so obtaining "beats" but the process is more involved when pulses are used.

It can be arranged that only those signals showing a Doppler shift, i.e., returns from targets with a radial velocity are displayed. This facility is known as "moving target indicator" (MTI) and can be used to eliminate permanent echoes due to stationary objects. In Fig. 10.5(2)(a), the clutter from hills and sea returns cannot be differentiated from the typhoon rain clouds whereas, in the MTI equipped radar used to produce Fig. 10.5(2)(b), the clutter from stationary targets without Doppler shift is eliminated leaving only clearly-defined rain clouds.

There are some limitations in the use of Doppler radars which arise from ambiguities in range and speed and the existence of "blind speeds". In order to measure a frequency f_1 its intensity must be sampled at the rate of at least $2f_1$. For example, if a pure sine wave was sampled at its own frequency then the amplitudes found would remain equal, as if the signal were steady. A signal must be sampled both near its maximum and minimum intensities. In a pulse radar the frequency (actually the phase) in each pulse is sampled and so the sampling frequency equals the prf; the highest Doppler shift which can properly be identified is therefore

$$f_{max} = prf/2 \qquad (10.8(4))$$

and from eqn (10.7) the maximum radial velocity detectable will be

$$v_{max} = (prf)\lambda/4 \qquad (10.8(5))$$

Signals returned with f greater than prf/2 will appear falsely at a frequency f - n (prf/2) where n is an integer, and at equivalent false velocities. With a typical 100 mm radar with prf = 275/s, f_{max} will be 137.5 Hz and the corresponding speed 6.9 m/s.

On the reasonable assumption that raindrops will be swept along with a velocity very close to that of the wind in which they are embedded then, the Doppler shift from raindrops can be used to measure the radial component of winds. To measure wind speeds up to 100 m/s unambiguously in this manner would require a special radar with a prf of 4 000/s ; such a high prf would limit the maximum unambiguous range because time is needed for a pulse to go out to maximum range and return at the speed of light c before the next pulse so that the unambiguous range is given by

$$r_{max} = c/2\ (prf) \qquad (10.8(6))$$

For the typical radar with prf = 275/s, r_{max} equals 545 km but for a special radar with a high prf of 4 000/s the maximum unambiguous range would be only 37.5 km - much too short to be of use in the typhoon warning role. The maximum range and maximum unambiguous radial velocity are related such that

$$v_{max} = \lambda c/8r_{max} \qquad (10.8(7))$$

Echoes received from ranges greater than r_{max} will be falsely indicated at $r - nr_{max}$ where n is an integer. It should also be noted that targets moving across the beam at right angles have no radial velocity r and they will not be detected until they have moved far enough to have ameasurable

radial component of velocity v which, with most modern equipments, is about 1.5 m/s. Typhoon rain clouds are usually detectable even when moving across the beam because they contain turbulent elements with velocities other than that of the cloud as a whole, for this same reason a whole spectrum of Doppler shifts will be returned from the many scatters in a rain cloud and much valuable information can be derived from its characteristics.

In the U.S.A. Brown et al (1975) described the use by the National Severe Storms Laboratory of two modified 100 mm FPS-18 radars to measure wind speeds in tornadoes. These radars have a maximum unambiguous range of 115 km and an unambiguous Doppler interval of $\pm$ 34.2 m/s and $\pm$ 35.6 m/s respectively. Since Doppler radars can only measure velocities along the line of sight the two radars are used together and sited 41 km apart to enable the complete wind field to be determined over an area of about 100 x 160 km. Such radars would be of great value in tropical cyclone areas.

The primary requirement of Doppler radar, in the typhoon warning role, is that it should give an indication of the maximum wind speeds near the centre when it is at a range of 100 km or more. The ambiguities can be overcome in this application because the target is near continuous in space and the speed will increase as the eye is approached and the approximate wind speeds will be known. The rain on either side of the eye will be moving directly towards or away from the radar giving large Doppler shifts of both signs. If necessary, instrumental arrangements can also be made to help resolve the ambiguities. For example, the prf can be made adjustable and successive pulses can be "labelled" or coded to permit their indentification on return. Doppler radar would yield not only the maximum wind but also the approximate radius of the ring of maximum winds. Knowledge of both these factors is essential for the prediction of storm surges by numerical methods (14.) and for the identification of potentially disastrous tropical cyclones.

It is remarkable that at the time of writing (1978) no Doppler probing of tropical cyclone wind velocities has been made and no such radar forms part of a tropical cyclone warning system. This

sad state of affairs is primarily due to the initial high cost of Doppler radars yet they are no more expensive than similar radars long in use in other fields. The ratio of potential benefits to first cost of such an installation in vulnerable areas, regularly threatened by tropical cyclones, is great. The WMO Tropical Cyclone Project (sect) proposed that studies on the design of Doppler radars for use in the tropical cyclone role should be encouraged and Baynton (1977) responded to this call.

Because low level hurricane force winds can be much reduced at heights above 6 km he concluded that the radar beam should see the eye-wall rain below this level. This implies that the range will normally be limited to 300 km at which distance a one-degree beam will be 5.24 km wide and fill the height range 5.29 $\pm$ 2.62 km. A one-degree beam was chosen 1) to get good resolution of velocities and in particular to match the distance over which extreme eye-wall winds will be found at 300 km range and 2) to yield an adequate return from exceptional storms which have high winds in association with only light rain. For this latter reason also, a 1 MW transmitter power with a long 4 μs pulse was specified. A one-degree beam at the chosen wavelength of 107 mm requires a large aerial of diameter 7.7 m which will need protecting in a costly dome. The aerial should have a gain of about 41 dB and the receiver a sensitivity of -108 dBm so that the minimum detectable reflectivity would be 11 dBZ (about 0.2 mm/h) which should be adequate for all threatening storms. At the specified wavelength of 107 mm and prf of 500 per second equations (~~10.20~~ 10.8(5)) and (~~10.21~~ 10.8(6)) yield a maximum unambiguous velocity of $\pm$ 13.38 m/s.

A coherent Doppler radar system is specified together with a mini computer to process the Doppler information and to control the display of velocities on a coloured television monitor in standard PPI format. Provision is also made to expand the scale of the display to magnify certain features. The standard T.V. monitor display can resolve 256 x 256 elements and assign 15 colours to them. For clarity of display Baynton proposed to use only seven colours each corresponding to one seventh of the unambiguous velocity. Outside this range the

colours repeat themselves in the same order but they can be followed and the ambiguity resolved in the context of the pattern. This is shown in Fig. 10.8(3) ~~10.36~~ in which the wind field associated with the Hughes (1952) mean typhoon (Fig. 5.) has been used to illustrate the velocities to be expected and their display.

Some errors and limitations of the method can be foreseen. The whole of the central region of the tropical cyclone will not always contain rain. Black areas will then appear and break up the continuity of the display shown in Fig. 10.8(5) ~~10.36~~. This effect may cause some colours to be skipped. Colours will also be missed if the wind shear in the horizontal exceeds about 2 m/s/km. It is expected that these difficulties of interpretation will usually be easily overcome. At ranges beyond about 100 km wind speeds will need to be increased - by up to 6% - as in sect 10.6.5 to estimate surface winds. The fact that the beam samples a volume of several km^3 introduces some smoothing of the peak wind speeds as does the colouring method used in the display. Baynton estimates that in extreme cases this may lead to an underestimation of peak winds of about 12% for a typhoon at 200 km range. Because the strongest winds in a tropical cyclone are found to the right of the track (Fig.) the most accurate estimates of storm intensity are obtained when the angle between the storm track and its bearing from the radar is small. The most accurate readings are thus obtained on storms approaching the radar directly. For passing storms the most accurate readings will be obtained before closest approach.

Radar systems of the type described but operating on a wavelength of about 50 mm have already been used successfully in storms of temperate latitudes (Baynton et al 1977). Winds of up to 70 m/s have been observed although the maximum unambiguous velocity was only 14.6 m/s. The cost of the radar for use in tropical cyclones as specified by Baynton (1977), will be high - large aerial, high power, large dome - but it is nevertheless hoped that some such radar will soon be built and its utility tested in typhoon conditions.

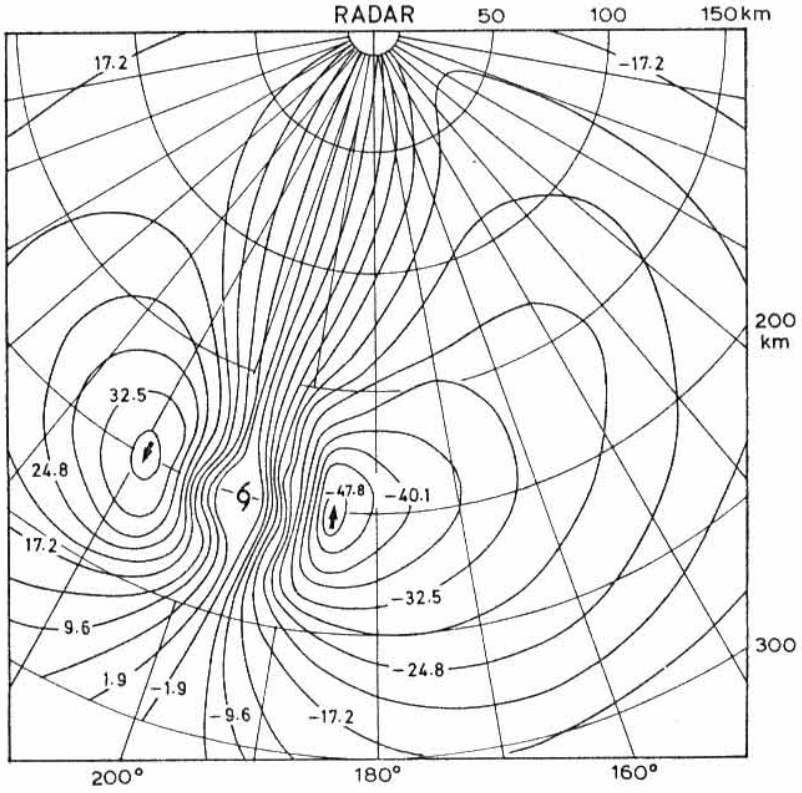

(a)

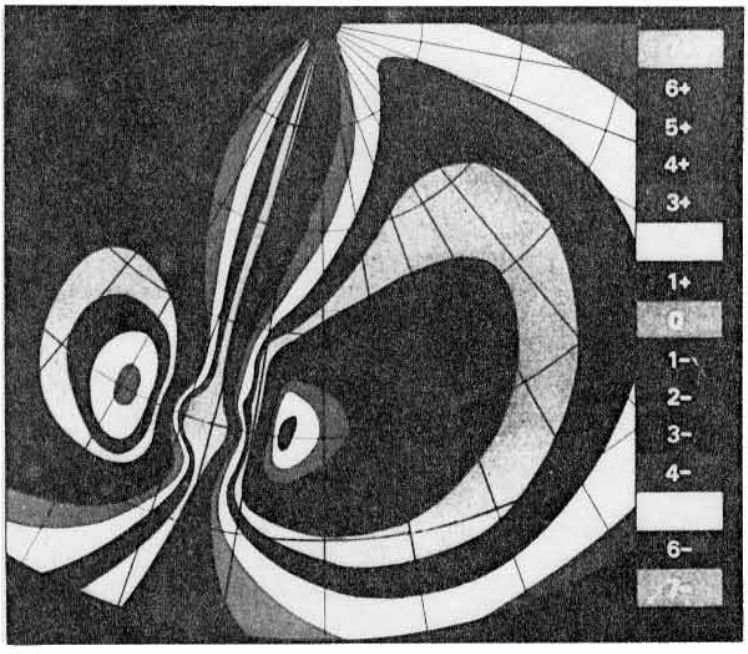

(b)

Fig. ~~10.36~~ 10.8(5). The distribution of wind speed (a) away from the radar (positive) for the case of the mean typhoon of Fig. 5. . In (b) the same wind field is shown as it would appear, colour coded, on a television screen. (After Baynton 1977)

10.8.5 Ground clutter

The detection and measurement of meteorological targets is often complicated by unwanted echoes of non-meteorological origin which come from the ground, mountains and sea. The problem is particularly severe for radars operating in the tropical-cyclone warning role as they are often on elevated sites to obtain maximum range (sect 10.8.1).

There is a difference between returns from meteorological targets of rain drops and those from ground targets. This difference permits the two signals to be identified and separated. Ground echoes change little in intensity over short periods of time whereas echoes from rain drops within the target volume fluctuate randomly from pulse to pulse due to the Doppler shifts arising from the relative motion of the randomly distributed particles. The returns from rain clouds therefore have an alternating current (AC) or variable component which can be separated from the steady or mean signal due to rain alone or to both rain and ground clutter. This method of separating the returns is particularly attractive because the mean power of the precipitation echo is approximately proportional to the variance of the amplitude of the linear-detected echo signal irrespective of the intensity of the ground clutter in the same echoing volume (Tatehira and Shimuzu 1978). It is therefore possible to remove ground echoes and still obtain a measure of the intensity of the precipitation echo.

When the signal from precipitation is linear-detected in the radar receiver, the amplitude probability distribution (P(X)) of the precipitation return signal can be expressed as a Rayleigh distribution[+] (Marshall and Hitschfeld 1953). Since the amplitude X has a dimension of voltage at the output of the receiver, its variance σ^2 and mean square value $\overline{X}^2$ have a dimension of electric power. Therefore, the variance σ^2 and the mean square value of the amplitude $\overline{X}^2$ can be considered as the AC power and mean power respectively. From the Rayleigh distribution it can be shown that the ratio of the AC power σ^2 to the mean power $\overline{X}^2$ of precipitation signals is constant and equal to 4.66 (6.68 dB). When the

[+] $P(X) = \frac{X}{\sigma^2} \exp\left(-\frac{X^2}{2\sigma^2}\right)$ from which $\overline{X}^2/\sigma^2 = 1/(1-\pi/4) = 4.66$

precipitation echo is superimposed on ground clutter, the probability density distribution of the amplitude changes from the Rayleigh distribution to the Rayleigh-Gaussian distribution and it can then be shown (Tatehira et al 1978) that the variation of the ratio of the AC power of the linear-detected composite signal at the receiver output to the mean power of the precipitation echo is as shown in Fig. 10.8.(6). This ratio is seen to range from 3.01 dB to 6.68 dB. The maximum error in the estimation of the mean power from precipitation is therefore at most 1.84 dB if estimated from a ratio of 4.85 dB.

In practice, the echoes from ground targets do change slowly and slightly ($\sim^{+}$ 1 dB) with time due to the movement of vegetation, changes in propagation path and pulse to pulse variations. For this reason ground echoes are not completely eliminated but only greatly ($\sim$35 dB) suppressed. The ground echo can be further suppressed (to about 50 dB) and the accuracy of estimation of rainfall rate in the presence of strong clutter further improved if the 0.7th power of the linear-detected echo is used as the input to the filter processor (Tatehira and Shimuzu 1980).

Storm warning radars have been modified in Japan and Hong Kong to operate on the above principle and Fig. 10.8(7) shows how effectively ground clutter can be removed in typhoon conditions. As explained in sect 10.8.1, returns from the sea surface have an unsteady component. Therefore, sea clutter cannot be entirely suppressed by this technique.

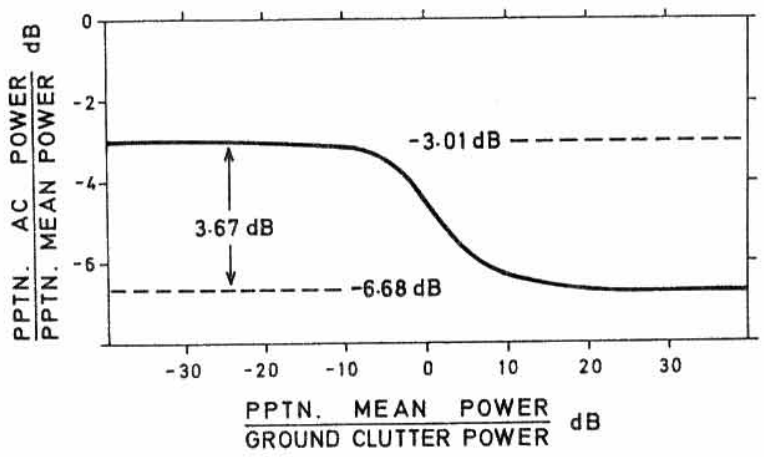

Fig. 10.8.(6). Ratio of AC power in a linear-detected precipitation echo to the mean power of the echo, as a function of the power of ground clutter relative to that of precipitation (after Tatehira and Shimizu 1978).

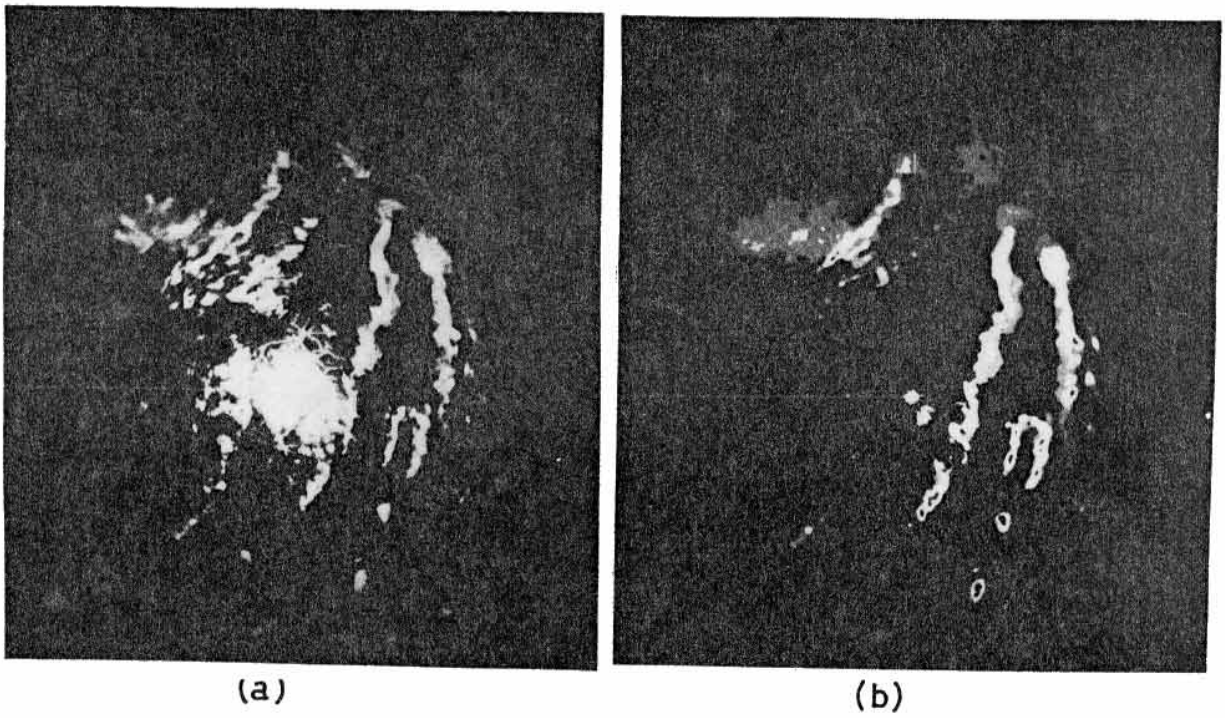

Fig. 10.8.(7). PPI pictures taken with the Tokyo radar at 0048 JST during the passage of tropical storm Ken on 5 September 1979 (Elevation: 0.0°, Range marks: every 50 km).

(a) Precipitation echo superposed on ground clutter in conventional log-characteristic

(b) Estimated mean power of precipitation echo in gray-scale (Gray: Equivalent rainfall intensity of 1-4 mm/hr, White: 4-16 mm/hr, Black: more than 16 mm/hr) (From Tatehira and Makino 1980)

10.9 Radar Developments

10.9.1 Sky-wave radar

Experiments have been made with radars operating at high radio frequencies, usually about 20MHz (λ = 15 m), so that the beam may be reflected by the "ionosphere" (sect 15.) and so travel many thousands of kilometres around the earth. The frequency chosen is a compromise between the need to use a frequency high enough to permit a reasonable beam width to be obtained yet low enough to enable the F layer of the ionosphere (around 300 km) to reflect the waves in the oblique mode in daylight hours. These frequencies are too low, of course, to detect rainclouds but they are back scattered by the sea surface and it is possible, by using Doppler techniques, to infer the sea state many thousands of kilometres away and over large areas. Such observations will indicate when and where tropical cyclones form. If the radar were to be sited on an island in the mid-Pacific then the formation and approximate location of tropical cyclones over a very large area, of radius more than 4 000 km, could be determined. Such distances can be attained with one reflection at the ionosphere but observations have been made out to 6 000 km by double reflections or "two hop " paths.

The principle that permits these oceanographic observations to be made was first discovered by Crombie (1955) when he directly observed a disturbed sea surface with high frequency radio waves. He found that for radio waves of length λ the sea waves acted as a diffraction grating sending back a large signal from those sea waves of wavelength $L = \lambda/2$ moving radially from the transmitter. The speed of such a wave is

$$C = \sqrt{\frac{g}{2\pi} L} \qquad \text{~~(10.22)~~ } 10.9(1)$$

where g is the acceleration due to gravity. Sea waves moving at this speed produce a Doppler shift f such that

$$f = \frac{2C}{\lambda} = \frac{2}{\lambda}\sqrt{\frac{g}{2\pi}\cdot\frac{\lambda}{2}} = \sqrt{\frac{g}{\pi\lambda}} \qquad \text{~~(10.23)~~ } 10.9(2)$$

For a wavelength λ = 14.3 m and g = 9.81 m/s^2 eqn ~~(10.23)~~ 10.9(2) yields a frequency shift of 0.475 Hz. Sea waves of length $\lambda/2$ are always present, because the sea wave spectrum is continuous, so that this sharply defined Doppler frequency, known as the Bragg reasonance frequency, is determined only by gravity and the radio frequency, and is independent of the sea state. However, the amplitude of the signal is a measure of the sea wave spectrum.

Although the Doppler spectrum of the returned signal is dominated by the Bragg line there are also some other weaker lines and a lesser continuous background of radio frequencies the spectrum of which can be used to derive the sea wave spectrum. It is possible to vary the radio frequency and so scan the sea waves by determining the amplitudes of the relevant Bragg lines. However, this cannot be done when ionospheric paths are used.

Ward (1969) extended the range of these observations by using the ionosphere so developing a "sky wave radar". He used a very large aerial in order to produce a beam width of 12^{o}. However, it is possible to use the radio-astronomer's method of aperture synthesis. Using ordinary radio receivers and two television-type Yagi aerials which can be moved relative to each other, an effective beam width of about 2^{o} can be obtained from 4 minutes of observation. Ionospheric Doppler radar currently suffers from noise due to travelling ionospheric disturbances. This limits the resolution with which the Doppler spectrum can be resolved to $\pm$ 0.01 Hz. To minimise these effects observations are made near local noon when the ionosphere is most nearly steady but it may prove possible to monitor independently the reflection regions in the latitudes of interest and so correct for their effects.

Maresca and Barnum (1979) used a wide-aperture radar to locate hurricane Eloise 1979 over the Gulf of Mexico some 3000 km west of their radar site in California. The radar beam 0.5^{o} wide at 15 MHz was produced by an array of aerials 2.55 km long. The Doppler spectra of the energy backscattered from the ocean was obtained simultaneously and immediately. Spectra at five different azimuths and at a range covering the core region of the hurricane are shown in Fig. 10.9(1) (~~1~~). Each spectrum represents a spatial average from the returns from ocean gravity waves in an area 63 km in range and 25 km in azimuth. The principle direction of the first-order Bragg resonance waves (8-9 m long) is inferred from the power ratio of approaching and receding waves. Because the waves are short it is assumed that they are coincident with the local wind direction.

The relative amplitudes of the first-order echoes (the two maxima) changes in Fig. 10.9(1) (~~1~~) from approaching to recedeing directions in less than 100 km. By shifting the azimuths and ranges a wind chart can be produced. In this way Maresca and Barnum (1979) located

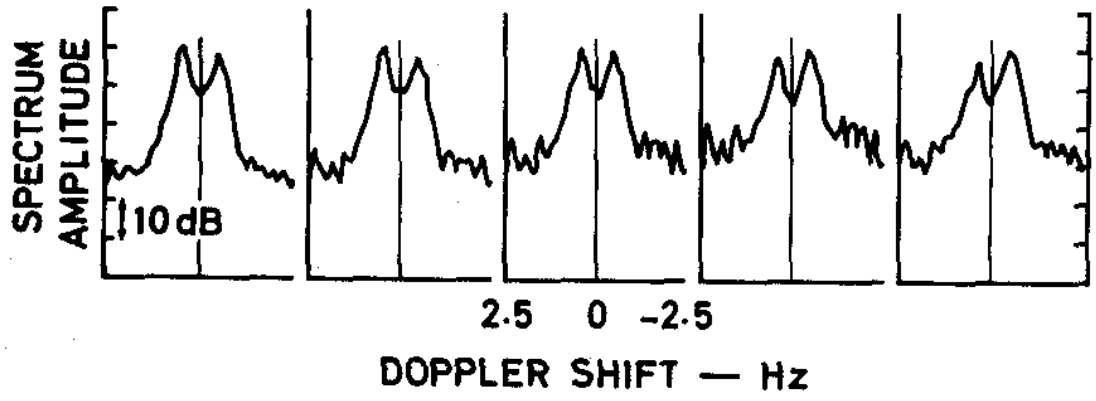

Fig. 10.9(1)(H). Doppler spectra obtained from an incoherent average of two coherent 12.8 s skywave-radar measurements. Each spectrum is an average of the Doppler spectra obtained from 21 different ranges spaced 3 km apart. The Doppler spectra shown are spaced $\pm$ 0.25° in azimuth from the middle spectrum which is near the centre of hurricane Eloise. The returns are from an area of ocean 100 km in azimuth and 60 km in range. (Adapted from Maresca and Barnum 1979).

Eloise 1979 to within 35 km of the official position. In 1977 hurricane Anita was tracked for four days and the 17 skywave-radar fixes were within 18 km of the National Hurricane Centre's smoothed track positions. Estimates of the surface wind speed can be infered from radar estimates of rms wave height and radial distance from the storm centre using a wind-wave prediction model (sect 14.). On a limited sample the estimated speeds were with 10% of those determined by conventional means.

Even at its present state of development, ionospheric radar produces valuable information over the tropical oceans to supplement satellite observations of cloud cover.

10.9.2 Displaying target movement

It was mentioned earlier that it is often not possible to be sure of the location of a centre of a tropical cyclone displayed on a PPI until the movement of the associated rain clouds has been determined and that this can be facilitated by some time-lapse facility. The use of cine film and video-tape time-lapse devices was discussed. It is however possible to use computers directly both for recording displays and for determining echo movement. The rapid progress in the development array processors and their decreasing cost per unit of performance will result in this method of recording being futher developed in the future. In this technique PPI video signals are suitably digitised and fed to an array processor where they are mapped and processed before transfer to the mass memory system of a computer. From here on, many manipulations of the data are possible.

Comparisons within a computer of two PPI images separated by some minutes can be used to determine the movement of discrete echoes which may then be displayed as vector arrows at the appropriate position on a PPI. The orientation of these vectors would indicate both the maximum wind speed and any centre of circulation. The method has been demonstrated for thunderstorm and shower movement but has not yet been adopted to the tropical cyclone case.

10.9.3 Other radar devices

Some other radar devices relevant to the study and forecasting of tropical cyclones have already been demonstrated. These include special radar altimeters for use in reconnaissance aircraft and on satellite to determine wave heights and so to derive surface wind speeds (sect 11.) and the use of synthetic aperture radars on the same platforms to determine sea states (Fig. 14.16). It has also been suggested (Simpson 1974) that aerial reconnaissance of typhoons could best be achieved by flying around an octagon at a distance of about 90 km from the storm centre with a sideways looking C-band Doppler radar. This radar would scan in a vertical plane (using a phased array rather than a nodding aerial) enabling a three dimensional picture of the distribution of rain in the whole storm to be determined. In addition, Doppler information would be retrieved to permit the computation of wind speeds - both vertical and horizontal - by methods pioneered by Lhermite (1972).

Radars purchased in the nineteen eighties for tracking tropical cyclones should have some device for storing the received signals and a mini-computer to process them. The computer should have the necessary software to control the aerial in elevation so that a large volume of the atmosphere is scanned in the time taken for the aerial to move a few revolutions in azimuth. The processing system should then provide details of signal intensities at selected attitudes to provide a display known as "Constant Altitude PPI" or "CAPPI". Vertical cross sections should also be available as required. The processing system should also be capable of integrating the echo intensities over discrete areas and periods of time for flood forecasting purposes and provide a time-lapse facility for facilitating the determination of echo velocities and for making Doppler measurements. Finally, the system should have softwave for a forecasting algorithm - based on the cross-correlation of individual points of two CAPPI displays separated by a short interval of time - so that objective forecasts of the echo pattern can be produced by extrapolation.

REFERENCES

Anon 1969. Hurricane Camille (Preliminary Report). U.S. Weather Bureau, Washington D.C.

Aoyagi, J., Kodaira, N, Barclay, P., Lewis, B.M., 1981. "Weather Radars for Monitoring Tropical Cyclones", W.M.O. Geneva.

Atlas, D. 1964. Advances in radar meteorology in "Advances in Geophysics" 10, 317-478, Academic Press, New York.

Atlas,D., and Chmela,A.C. 1957. Physical-synoptic variations of drop-size parameters. Proc. 6th Weather Radar Conf., Amer. Meteor. Soc., Boston, 4, 21-29.

Atlas, D., Kerker, M. and Hitschfeld, W. 1953. Scattering and attenuation by non-spherical atmospheric particles. J. Atm. Terr. Phys. III, 108-19.

Atlas, D. and Ulbrich, C.W.,1977. Path-and Area-Integrated Rainfall Measurement by Microwave Attenaution in the 1-3 cm Band J. Appl. Met., 16, 1322-1331.

Austin, P.M., Geotis, S.G., Cunning, J.B, Thomas, J.L Sax, R.I., and Gillespie, J.R. 1976. Raindrop size distributions and Z-R relationships for GATE. 10th Tech. Conf. on Hurricanes and Tropical Meteor., Amer. Met. Soc.

Australian Bureau of Meteorology, 1977. Report on Cyclone Tracy 1974. Aust. Govt. Pub. Service. Camberra.

Battan, L.J. 1973, "Radar Observation of the Atmosphere" The University of Chicago Press, Chicago and London, p.324.

Baynton, H.W., Frush, C.L., Serafin, R.J., Hobb, P.V. Houze, R.A. and Locatelli, J.D. 1977. Real-time wind measurements in extratropical cyclones using Doppler radar. J. Appl. Met. 16, 1022-1028.

Baynton, H.W., 1979. The case for Doppler Radars along our hurricane affected coasts. Bull Amer. Met. Soc., 60, 1014-1023.

Bell, G.J. 1969. The monsoon trough near the south China coast. Proc. Conf. on summer monsoon of S.E. Asia. 83-105. U.S. Navy Wea. Res. Facility Norfolk, Virginia.

Bell, G.J. 1977. Comments on "Cape Hatteras Radar Observations of Hurricane Gladys" Mon. Wea. Rew. 105, 550-552.

Bell G.S. 1980. Typhoon Hope, August 1979. Mar. Wea. Log. 24, 7-14.

Black, P.G. 1971. Use of echo velocities to evaluate hurricane modification experiments. 1970 Project Stormfury Ann. Rep. Miami Florida.

Black, P.G., Senn, H.V. and Courtwright, C.L. 1972. Airborne radar observations of eye configuration changes, bright band distribution and precipitation tilt during the 1969 multiple seeding experiments in hurricane Debbie Mon. Wea. Rev., 100, 208-217.

Bocks, J.S. 1967. A brief statement on winds that damaged the radar station at Hua Lien, Taiwan in November 1967. Manuscript & private communications.

Bradbury, D.L., 1971. The filling over land of hurricane Camille. S.M.R.P. Res. Paper No. 96 University of Chicago.

Brown, A.R., et al 1975 NSSL dual-Doppler radar measurements in tornadic storms: a preview B.A.M.S. 56 524-526

Conover, L.F. 1961. Evaluation of the eye fixes obtained by radar for hurricane Donna, September 1960. Rep. No. 50. Nat. Hurricane Res. Project, Weather Bureau, Washington D.C. 85-100.

Cotton, W.R., and Gokhale, N.R. 1967. Collision, coalescence, and breakup of large water drops in a vertical wind tunnel. J. Geophys. Res., 72, 4041-4049.

Crombie, D.D., 1955. Doppler spectrum of sea echo at 13.56 Mc/s. Nature 175, 681-682.

Cunning, J.B. 1976. Comparison of the Z-R relationships for seeded and nonseeded Florida cumuli. J. Appl. Met., 15, 1121-1125.

Cunning, J.B. and Sax, R.I. 1977. A Z-R relationship for the GATE B-scale array. Mon Wea Rev, 105, 1330-1336.

Diem, M., 1966, Rains in the ~~artic~~ arctic, temperate, and tropical zone, Sci. Rept., Meteorologishes Institut Technische Hochschule, Karlsruhe, Contract DA-91-591-EUC-3634, 93.

Donaldson, R.J., Jr. 1964, A demonstration of antenna beam errors in radar reflectivity patterns. J. Appl. Met., 3, 611-623.

Donaldson, R.J., and Atlas, D. 1964. Radar in tropical meteorology. Proc. Symp on trop. meteorol. Rotorua. New Zealand Meteorological Service Wellington 423-473.

Dunn, G.E., Davis,W.R., and Moore,P.L. 1955. Hurricanes of 1955. Mon. Wea.Rev.,83, 315-326.

Gentry, R.C. 1964. A study of hurricane rainbands. Rep. No. 69. Nat. Hurricane Res. Project, Weather Bureau Washington D.C.

Herman, B.M. and Battan, L.J. 1961. Calculations of Mie back-scattering of microwaves from ice spheres. Quart. J. Roy. Meteor. Soc. 87, 372, 223.

Hill, F.F. & Lewis, R.P.W., 1974. The distribution and frequency of high cumulonimbus tops near Singapore as measured by 10-centimetre radar (Part I). Met. Mag. 103, No.1219, February 1974.

Hiser, H.W. 1957. Comparisons between a 10 cm and a 5 cm wavelength radar for meteorological purposes. Proc. 6th Weather Radar Conf. Amer. Meteor. Soc. Boston. 253-259.

Hiser, H.W., Andrews,G.F., & Courtwright,C.L., 1967. Relations between radar sea clutter and existing local weather conditions. Final Report, Radar Meteor.Lab., University of Miami.

Hiser,H.W. and Freseman,W.L. 1956. Final Report on U.S. Navy Contract No as 55-620-d, Univ. of Miami.

Holliday, C. 1976. Typhoon June - most intense on record. - To be printed.

Imai, I. 1963. Filling of typhoon eye by landing. Proc. 10th Conf. on Weather Radar. Amer. Meteor. Soc., Boston 214.

Imai, I. 1964. Use of radar for typhoon observation in Japan. Proc. Symp. on Trop. Meteorology. Rotorua. New Zealand Meteorological Service. Wellington. 474-483.

Jordan, C.L. 1960. Spawinds for the eye wall of hurricane Daisey of 1958. Proc. 8th Conf. on Weather Radar. Amer. Meteor. Soc., Boston. 219-226.

Jordan, C.L., 1963. The accuracy of center positions of hurricanes as determined by the spiral overlay technique. Proc. 10th Conf. on Weather Radan Amer. Meteor. Soc. Boston. 202-207.

Jordan, C.L., Hurt, D.A. and Lowery, C.A., 1960. On the structure of hurricane Daisy on 27 August 1958. J. Met. 17, 337-348.

Kantor, A.J. and Grantham, D.D. 1969, Effect of range on apparent height and frequency of high-altitude radar precipitation echoes, Mon. Wea. Rev., 97, 429-431.

Kashimoto, T. and Veda, H. 1967. Weather radar on the summit of Mt. Fuji. Mitsubishi Denki Engineer. Tokyo.

Kerker, M., Langleben, P., and Gunn, K.L.S., 1951, Scattering of microwaves by a melting, spherical ice particle, J. Met. 8, (424)

Kessler, E and Atlas, D, 1956, "Radar synoptic analysis of hurricane Edna, 1954", Geophysical Research Papers, no.50, Bedford, Mass: Air Force Cambridge Res. Labs.

Lewis, B.M., Radlein, R.A., and Jorgensen, D.P. 1976. Comparison of rainfall distributions obtained from digitized 10-cm radar data and a rain gauge network for hurricane Eloise, 1975. Proc. Conf. on Hydrometeorology, Amer. Met. Soc., Boston, Mass.

Lhermitte, R.M., 1972. Real-time processing of meteorlogical Doppler radar signals. 15th Radar Met. Conf, AMS, Boston, 364-367.

Ligda, M.G.M. 1955. "Analysis of the motion of small precipitation areas and bands in the hurricane of August 23-28 1949". Tech. Note No.3,Dept. of Meteorology, Massachussets Institute of Technology.

List, R. and Gillespie, J.R. 1976. Evolution of raindrop spectra with collision-induced breakup. J. Atmos. Sci.,33, 2007-2013.

Liu,P.,and Lai,M.H. 1969 Radar observations of typhoons Shirley and Wendy. Manuscript Royal Observatory Hong Kong.

Malkus, J.S., Ronne, C and Chaffee,M. 1961. Cloud patterns in hurricane Daisy. Tellus 13, 8-30.

Maresca, J.W. and Barnum J.R., 1979. Remote measurement of the position and surface circulation of hurricane Eloise by HF skywave radar. Mon. Wea. Rev., 107, 1648-1652.

Marshall, J.S. and Hitschfeld, W., 1953. Interpretation of the fluctuating echo from randomly distributed scatterers. Pt. I. Canadian J. Physics 31, 962-964.

Marshall, J.S., and Palmer, W.M.K., 1948, The distribution of raindrops with size. J. Met. 5(4), 165-166.

Mason, B.J., 1971, "The Physics of Clouds". Oxford University Press, London & New York.

Mason, B.J. and Ramanadham, R. 1954. Modification of the size distribution of falling raindrops by coalescence, Quart.J.R. Met. Soc., 388-394.

Maynard, R.H. 1945. Radar and weather. J. Meteor., 2, 214-226.

McTaggart-Cowan, J.D. & List, R. 1975. Collision and breakup of water drops at terminal velocity. J. Atmos. Sci., 32, 1401-1411.

Merceret, F.J., 1974a, On the size distribution of raindrops in hurricane Ginger, Mon. Wea. Rev., 102, 714-716.

Merceret, F.J., 1974b, A note on the vertical distribution of raindrop-size spectra in tropical storm Felice, Met. Mag., 103, 358-360.

Mueller, E.A. and Sims, A.L., 1966a, The influence of sampling volume on raindrop size spectra, Proc. 12th Conf. on Radar Met., Norman, Okla., 135-141.

Mueller, E.A. and Sims, A.L., 1966b, Investigation of the quantitative determination of point and areal precipitation by radar echo measurements. Ill. State Water Survey, Final Rept., Contract DA 28-043 AMC 00032(E), 110.

Newell, R.E., and Geotis, S.G. 1955. Meteorological measurements with a radar provided with variable polarization. Dept. of Meteorol. Weather Radar Res. Tech. Note No 8. Massachussets Institute of Technology.

Oguchi, T. & Hosoya, Y., 1974. Differential attenuation and different phase shift of radio waves due to rain: Calculations at microwave and millimeter wave regions. J. Rech. Atmos., 8, 121-127.

Pidgeon, V.W. 1968. Doppler Dependence of Radar Sea Return. J. Geophys. Res., 73, 1333-1341.

Probert-Jones, J.R. 1962. The radar equation in meteorology. Quart. J.R. Met. Soc., 88, 485-495.

Raghavan, S., Rengarajan, S. and Varadarajan, V.M., 1980. Some experiences of radar observation of cyclonic storms in the southern Bay of Bengal. Mausam, 31, 81-92.

Rockney, V.D. 1956. Hurricane detection by radar and other means. Proc. Trop. Cyclone Symp, Brisbane Bureau of Meteorology, Melbourne. 179-197.

Ryde, J.W. 1941 Echo intensities and attenuation due to clouds rain, hail, sand and dust storms. Rept. No. 7831 General Electric Co. Wembley England.

Ryde, J.W., 1946. The attenuation and radar echoes produced at centimetre wavelengths by various meteorological phenomena. Meteorological factors in radio-wave propagation, p.169. Phys. Soc. & Roy. Met. Soc.

Scott, W.D. and Dossett, C.K., 1972, Annual Rept. 1971 Project Stormfury N.O.A.A., Miami, Florida. (165)

Seliga, T.A. and Bringi,V.N., 1976. Potential use of radar differential reflectivity measurements at orthogonal polarizations for measuring precipitation. J. Appl. Met.,15, 69-76.

Seliga, T.A. and Bringi,V.N., 1978. Preliminary results of differential reflectivity measurements in rain. 18th Conf on Radar Met. A.M.S.,

Senn,H.V. 1966a Precipitation shear and bright band observations in hurricane Betsey 1965. Proc. 12th Weather Radar Conf. Amer. Meteor. Soc. 447-453.

Senn, H.V. 1966b Radar Hurricane Research. Final Rep. Contract No CWB-11266, Radar Meteorol Section, University of Miami.

Senn, H.V. 1967. Theoretical radio refraction in hurricanes Proc. 5th Tech. Conf. on Hurricanes and Trop. Meteor. Caracas Venezuela.

Senn, H.V. and Hiser, H.W. 1961. Effectiveness of various radars in tracking hurricanes. Rep. No.50. Nat. Hurricane Res. Project, Weather Bureau, Washington D.C. 101-114,

Senn, H.V. and Hiser, H.W. 1959. On the origin of hurricane spiral rain bands. J. Met. 16, 419-426.

Senn, H.V., and Stevens, J.A. 1965. A summary of emporical studies of the horizontal motion of small radar precipation echoes in hurricane Donna and other tropical storms. Report No. 74 Nat. Hurricane Res. Lab. Washington D.C.

Simpson, R.H. 1974. On the design and evaluation of tropical cyclone seeding experiments. Proc. WMO Tech Conf on Typhoon Modification WMO - No. 408, Geneva.

Simpson, R.H., Ahrens, M.R. and Decker, R.D. 1963. A cloud seeding experiment in hurricane Esther, 1961. Rep. No. 60 Nat. Hurricane Res. Project Weather Bureau Washington D.C. (20).

Skolnik, H.I. 1962 "Radar Systems". Mc Graw-Hill Book Co. New York.

Somervell, W.L. & Jarrell, J.D. 1969. Tropical Cyclone Evasion Planning. Tech. Paper No. 16-69 Navy Weather Res. Facility. Norfolk. Virginia.

Staff Members 1969 Precipitation bands of typhoon J. Met. Soc of Japan, 47, 298.

Stout, G.E. and Mueller, E.A., 1968, Survey of relationships between rainfall rate and radar reflectivity in the measurement of precipitation, J. appl. Met., 7, 465-473.

Tang, C.H., 1976. Performance test, r-f trouble shooting and preventive maintenance of a meteorological radar. Tech. Note WMO/ESCAP Typhoon Committee Secretariat.

Takahashi, T., 1978. Raindrop size distribution with collision breakup in an axisymmetric warm cloud model. J. Atmos. Sci., 1549-1553.

Tatehira, R. 1961. Radar and meso-scale analysis of rainband in typhoon - case study of typhoon Helen. J. Meteor. Res, Tokyo 13, 264-279.

Tatehira, R. and Itakura, H. 1966. Radar observations of typhoon Lucy by Mt. Fuji radar. Proc. 12th Conf. on Radar Meteorology, Amer. Meteor. Soc. Boston. 432-435.

Tatehira, R. & Shimizu, T., 1978. Intensity measurement of precipitation echo superposed on ground clutter. Proc. 18th Conf. on Radar Meteorology, A.M.S., Boston.

Tone River Office 1975. Radar pluviometer used for rainfall determination along the basin of the Tone river. Tone River Dam Co-ordinated Control Office Ministry of Construction, Tokyo, Japan.

Wantanabe, K. 1964. Radar spiral bands and the typhoon structure. Proc. Symp. on Trop. Meteorol. Rotorua. New Zealand Meteorological Service. Wellington 484-491.

Ward, J.F., 1969. Power spectra from ocean movements measured remotely by ionospheric radio backscatter. Nature 223, 1325-1330.

Wexler, H., 1947. Structure of hurricanes as determined by radar. Ann. N.Y. Acad. Sci., 48, 821-844.

Willis, P.T. and Merceret, F.J. 1977. Comments on "Evolution of raindrop spectra with collision-induced breakup". J. Atmos. Sci., 34, 1144-1149.

Wilson, J.W. and Pollock, D.M. 1974. Rainfall measurements during hurricane Agnes by three overlapping radars. J. Appl. Met., 13, 835-844.

Woodley, W.L. 1970. Precipitation results from a pyrotechnic cumulus seeding experiment. J. Appl. Met. 9, 242-257.

W.M.O 1981 Weather radar for monitoring tropical cyclones. W.M.O. Geneva